

Solar energy absorption mediated by surface plasma polaritons in spectrally selective dielectric-metal-dielectric coatings: A critical review

Atasi Dan,^a Harish C. Barshilia,^{b,*} Kamanio Chattopadhyay,^{c, d}

Bikramjit Basu^{a, c,*}

^a Materials Research Centre, Indian Institute of Science, Bangalore-560 012, India

^b Nanomaterials Research Laboratory, Surface Engineering Division, CSIR-National Aerospace Laboratories, HAL Airport Road, Kodihalli, Bangalore 560 017, India

^c Interdisciplinary Centre for Energy Research, Indian Institute of Science, Bangalore-560 012, India

^d Materials Engineering, Indian Institute of Science, Bangalore-560 012, India

Abstract

The effective use of solar energy has become significantly important due to unnatural weather changes and fossil fuel exhaustion. Concentrating Solar Power (CSP) technology is a promising approach to harvest solar energy in the form of heat using solar selective absorber coating. These coatings are expected to absorb maximum incoming solar radiation ($\alpha \geq 0.95$) and prevent loss of the absorbed energy as infra-red radiation ($\varepsilon \leq 0.05$). Efficiency of the absorber coating can be evaluated by a metric called “Solar selectivity (α/ε)”. In recent years, a number of effective attempts have been made to achieve remarkable selective property and high temperature stability of the absorber coating using the concept of Surface Plasma Polaritons (SPPs). The SPPs have the capability to capture solar energy by confining electromagnetic field in the metal-dielectric interface. Solar absorption, with the help of SPPs, can be maximized by tailoring the optical constants of the metal and dielectric. In this review, we have described different types of solar absorber coatings with particular emphasis on dielectric-metal-dielectric (DMD) -based absorber coatings. We have presented a brief

overview to comprehend physics of DMD coatings. This review additionally highlights some of the case studies based on the DMD -based absorber coatings with the high temperature stability and their importance in the context of CSP technologies.

Keywords: Solar energy, Concentrating solar power, Solar selective absorber coating, Surface plasma polaritons, Dielectric-metal-dielectric stack

*** Corresponding Authors**

Email: harish@nal.res.in (Harish C. Barshilia)

bikram@mrc.iisc.ernet (Bikramjit Basu)

1. Introduction

It is widely accepted that the use of fossil fuels like petroleum, natural gas and coal gives rise to serious environmental concerns with their essential energy usage abilities [1]. All stages of fossil fuel usage have severe impact upon the environment, from recovery to storage and end use. There are alternative sources of energy being developed to replace the use of fossil fuels. Solar energy, a source of a clean environmental friendly energy and the largest available carbon-neutral energy source, can be considered as a potential solution to the environmental pollution as well as the world energy crisis. Every day, almost 400 trillion kWh energy from the sun touches surface of the earth in the form of electromagnetic radiation [2]. It does not disrupt the environment or create a threat to the eco system the way fossil fuels do.

The solar energy can be harnessed by two approaches, as passive solar technique and active solar technique. Main features of a well-deigned passive solar systems are structures, design and position, which can be optimized to use solar energy [3, 4]. Active systems use mechanical and electrical equipments to utilise the solar radiation into a more usable form, such as heat or electricity [5, 6]. The most well-known active solar techniques are

1 photovoltaic panels and solar-thermal electric energy systems [7]. Though solar photovoltaics
2 have attracted significant attention within the energy community, solar thermal energy
3 systems recently have become prominent in the field of power generation, as such technology
4 has proven its performance in production of clean, secure and low cost energy. These Solar
5 thermal systems are also characterized by its simplicity in the manufacturing process, scale
6 up potential, low technical and financial risk [8]. Unlike photovoltaic technologies, solar
7 thermal plants have the scope to store the heat energy for some period to facilitate a
8 successful continuous and year round supply of electricity. Solar thermal plants are usually
9 equipped with the thermal energy storage (TES) and backup systems (BS) to provide
10 electricity in the night hours or during cloudy days when the sun is not available [9]. Among
11 the solar thermal technologies, concentrating Solar Power (CSP) is one of the most mature
12 technology which has shown a great promise for the future and is currently being deployed
13 worldwide. According to available technology road map of International Energy Agency
14 (IEA), the CSP systems, by 2050, could provide 11.3% of global electricity with 9.6% from
15 solar power and 1.7% from backup fuels (i.e., fossil fuels and biomass) [10].

16
17
18
19
20
21
22
23
24
25
26
27
28
29
30
31
32
33
34
35
36
37 The first commercial CSP plant was constructed by Luz International Ltd. with a
38 capacity of 354 MW in Mojave Desert, California in the period of 1984 – 1991 [11].
39 However, efforts to duplicate similar plants suffer a setback as the reduction in fossil fuel cost
40 dismantled the policy framework of CSP systems. A new era of CSP began in 2006 when the
41 first central receiver tower plant, PS10, was commissioned with an overall capacity of 11MW
42 in Sevilla, Spain [12]. This achievement led to the approval of California Energy
43 Commission in September, 2010, for the construction of four more solar thermal power
44 plants in California, USA, with an overall capacity around 1000 MW. The solar energy
45 experts have estimated that CSP systems with about 118 GW could be installed by 2030 and
46 1504 GW by 2050 in the USA [13]. Numerous commercial projects for solar thermal plants

1 have been taken up in Europe as well. The European Solar Thermal Electricity Association
2 (ESTELA) estimates that the total installed capacity could reach up to 1000 GW by 2050
3 [14]. The government of India has also taken an initiative by launching an ambitious project,
4 called Jawaharlal Nehru National Solar Mission (JNNSM) with a funding of USD 930
5 million in 2009 [15]. This project, complemented by solar policy framework, has set a goal to
6 account for 20,000 MW solar power by 2022. The project will promote favourable conditions
7 for solar manufacturing capability, particularly the solar thermal applications. Other countries
8 such as China [16], Israel [17], South and north Africa [18, 19], Australia [20], Algeria [21],
9 and Italy [22] are also doing remarkable progress on current commercial development of the
10 solar thermal plants.
11
12
13
14
15
16
17
18
19
20
21
22
23
24

25 The CSP technologies [23, 24] can be categorised into four types depending on the
26 way they focus the solar radiation and the technologies used to receive energy:
27
28
29

- 30 a. the parabolic trough collector
- 31
- 32 b. the solar tower
- 33
- 34
- 35 c. the parabolic dish concentrator
- 36
- 37
- 38 d. the linear- Fresnel reflector.
- 39
- 40

41 The schematic of the four types of CSP system is presented in Fig. 1. Each of these
42 different CSP technologies have some major features along with their own advantages and
43 drawbacks, which have been illustrated in detail elsewhere [25, 26].
44
45
46
47
48

49 CSP plants produce electricity in the same way as other conventional power plants,
50 but using solar radiation as energy input. In CSP systems, the solar irradiation is concentrated
51 several times by mirrors, which have very high reflectivity to reach high energy densities.
52 Recently, a new class of reflector materials based on Cu–Sn intermetallics with tailored
53 substitution of aluminium or zinc with a bulk reflectance of 89% has been developed [27]. In
54
55
56
57
58
59
60
61
62
63
64
65

1 addition, a novel δ -phase based Cu–Sn mirror through electrodeposition has been reported,
2 the material exhibits ~ 80% of specular reflectance [28]. These mirrors would enable
3
4 attaining higher temperatures in the focus of the concentrating system.
5
6

7 Materials that help in converting light energy harnessed from the Sun into heat are
8 referred as absorber materials. Usually, the absorber materials are deposited onto the receiver
9 tube, where heat transfer fluids are heated by the absorbed heat and the temperature of the
10 fluid reaches around 400 °C. The heated fluid is driven through a series of heat exchangers to
11 produce superheated steam. The steam is then used to operate a conventional power cycle,
12 such as a steam or gas turbine or a stirling engine, which drives a generator (see Fig. 2).
13
14
15
16
17
18
19
20
21

22 Hence, a typical CSP system has four essential components such as concentrator,
23 receiver or absorber, transport/storage media system (molten salt, gas, air etc.) and power
24 conversion device. Of all components, receiver plays a vital role in determining the efficiency
25 of the CSP systems. The nature of the absorber coating, deposited on to the receiver tube,
26 often controls conversion of solar energy to heat. An ideal absorber should absorb as much of
27 the incident sunlight as possible ($\alpha \geq 0.95$). This implies that the reflectance should be
28 minimised in the entire solar spectrum. Simultaneously, the loss of the heat to the
29 surroundings via convection or conduction, i.e. emittance ($\epsilon \leq 0.05$), should be very low, with
30 a thermal stability up to the operating temperature of the receiver, usually of the order of 400
31 °C. Thus, there are conflicting requirements of strong absorption in the solar spectrum, with
32 minimum emission in the far infrared range (Fig. 3).
33
34
35
36
37
38
39
40
41
42
43
44
45
46
47

48 The design of the absorber surfaces initially attracted attention while Kemp patented
49 lamp black as an absorber material in a solar water heating device in 1891 [29]. This is
50 followed by a number of invention disclosures dealing with solar water heating systems that
51 were filed in USA during the first half of the 20th century [30-32]. The black painted tubes
52 were used as collectors in these systems. However, the development of the modern solar
53
54
55
56
57
58
59
60
61
62
63
64
65

1 absorber coating can be traced to the invention of Tabor in 1955 when black nickel, NiS–
2 ZnS composite, black chrome and chemically converted black copper oxide were
3 electrodeposited on an infrared reflective aluminium substrate [33]. Since then, several
4 deposition procedures like physical vapour deposition [34], chemical vapour deposition [35],
5 electro deposition [36], sol-gel [37], paint-coating [38] etc., have been pursued to meet the
6 criteria of solar selective coating. A variety of coating structures such as intrinsic absorbers,
7 semiconductor absorbers, multilayer absorbers, metal-dielectric composite absorbers, texture
8 surfaces and dielectric-metal-dielectric (DMD) absorbers have been extensively studied to
9 increase the efficiency of photo-thermal conversion systems.
10
11
12
13
14
15
16
17
18
19
20

21
22 In a review published in 1983, Bogaerts and Lampert [39] reported commercially or
23 potentially available selective and non-selective absorber surfaces for solar heat collectors. In
24 the same year, Niklasson and Granqvist [40] summarized the development in the solar
25 selective coatings that were reported during 1955-1981. In 2002, an exhaustive review
26 emphasising the application of solar selective coating in different temperature was published
27 by Kenedy [41], while Granqvist [42] in 2003 reported potential materials that could be
28 utilised in photo-thermal as well as photo-electric applications. Several other reviews are
29 available on the subject including the work of Agnihotri and Gupta [43], Granqvist and
30 Wittwer [44], Goswami et al. [45], Amri et al. [46], Atkinson et al. [47] and Jeeva et al.[48].
31 In 2012, Selvakumar and Barshilia [49] extensively reviewed a wide variety of physical
32 vapour deposited (PVD) solar selective absorber coatings, their functionality, reliability and
33 performance at elevated temperatures. They also summarized commercially available PVD
34 coatings for flat-plate/evacuated tube collectors and solar thermal power generation
35 applications. However, there is a need for a review focused on the dielectric-metal-dielectric
36 (DMD) –based absorber coatings with the underlying physics of surface plasmon polaritons
37 (SPPs) because of their increasing importance in future solar conversion technologies. In the
38
39
40
41
42
43
44
45
46
47
48
49
50
51
52
53
54
55
56
57
58
59
60
61
62
63
64
65

1 current review, we present theoretical background of SPPs in designing metal-dielectric
2 interface and present an overview of the understanding of imparting solar selectivity. We
3 demonstrate the contextual analyses of DMD –based solar absorber coating, their
4 performance and the future directions of research that can be undertaken in harnessing the
5 solar energy in the collector of the photo-thermal conversion systems.
6
7
8
9
10

11 This article is set out as follows: The solar absorptance and the thermal emittance are
12 the most important properties that can significantly influence the solar selectivity of absorber
13 coating. Hence, to provide a contextual backdrop for this review, we have discussed the
14 correlation of solar absorptance and thermal emittance with the solar selective properties of
15 the absorber coating in Section 2. Different types of solar selective absorber coatings, their
16 examples and possible theoretical description on individual coatings have been presented in
17 Section 3. In the same section, we have also discussed different models, which can explain
18 the metallic and dielectric properties of the materials in a DMD stack. Section 4 is devoted in
19 describing SPP, the dependence of relative permittivity, refractive index, thickness etc., on
20 the dispersion relation of SPP, the effect of metal-dielectric (MD) and dielectric-metal-
21 dielectric structure (DMD) on SPP behaviour, the impact of DMD structure in the absorption
22 of solar energy. We then give a detail overview on varieties of DMD –based solar selective
23 absorber coatings, explored by several groups and their selective properties, thermal stability
24 and applicability to enhance the efficiency of CSP systems in Section 5. Section 6
25 demonstrates an idea to develop textured DMD –based absorber coating which may possess
26 significantly improved selectivity than a flat DMD coating. Finally, we have highlighted the
27 critical parameters which govern the environmental stability, cost-performance factor,
28 practical implantation of the DMD coatings in CSP systems to boost the demand of safe and
29 affordable energy.
30
31
32
33
34
35
36
37
38
39
40
41
42
43
44
45
46
47
48
49
50
51
52
53
54
55
56

57 **2. Fundamentals of solar selectivity**

58
59
60
61
62
63
64
65

1 In 1865, Maxwell first proposed the classical theory of electromagnetism and
2 predicted light as electromagnetic radiation [50]. The electromagnetic spectrum can be
3
4 further classified into different types depending on the range of wavelength varying from
5
6 cosmic and gamma rays (wavelength $\sim 10^{-8}$ μm) to long radio waves (wavelength $\sim 10^{10}$ μm).
7
8 The electromagnetic radiation, emitted by sun is known as solar spectrum, and it falls in the
9
10 wavelength range of $\lambda = 0.3 \sim 2.5$ μm . The radiation emitted from bodies at temperature of
11
12 200 °C and above spreads in the infrared region of the spectrum, which extends from $\lambda = 2.5$
13
14 ~ 50 μm . Specifically, two parts of electromagnetic spectrum, such as solar radiation and
15
16 thermal radiation, are important for solar selective absorber coating.
17
18
19
20
21

22 **2.1. Solar absorptance**

23
24

25 When light, an electromagnetic (EM) wave, incidents on a material, it interacts with
26
27 the atoms, ions and/or electrons in the material, and the corresponding effects depend on the
28
29 frequency of the light and the atomic structure of the material. Light - matter interaction
30
31 causes three common physical phenomena such as absorption, reflection and transmission, as
32
33 shown in Fig. 4. The disappearance of EM wave inside the medium is known as absorption.
34
35 Absorption occurs when the energy of an incident photon is equal to the band gap of the
36
37 material.
38
39
40
41
42

43 The term absorptance, is defined as the ratio of the radiation absorbed by the body or
44
45 surface to the incident solar radiation and can be expressed,
46
47

$$48 \alpha_{\lambda}(\lambda) = \frac{G_{\lambda,abs}(\lambda)}{G_{\lambda}(\lambda)}, \quad (1)$$

49
50
51
52

53 where $G_{\lambda,abs}(\lambda)$ and $G_{\lambda}(\lambda)$ are the absorbed and incident radiations, respectively.
54
55
56
57
58
59
60
61
62
63
64
65

Conservation of energy demands that the sum of the transmission, reflection, and absorption of the incident flux is equal to unity. Therefore, the total radiation can be characterized by the following equation

$$\alpha_{\lambda} + \rho_{\lambda} + \tau_{\lambda} = 1, \quad (2)$$

where α_{λ} , ρ_{λ} and τ_{λ} are the absorptance, reflectance and transmittance at a given wavelength. For materials that does not allow the penetration of the incident radiation through it, i.e. while the transmittance is equal to zero ($\tau_{\lambda} = 0$), the equation (2) get reduced to

$$\alpha_{\lambda} + \rho_{\lambda} = 1 \quad (3)$$

$$\alpha_{\lambda} = 1 - \rho_{\lambda} \quad (4)$$

Using equation (1) and (4), the absorptance can be expressed in terms of reflectance by the following equation

$$\alpha(\theta) = \frac{\int_{\lambda_1}^{\lambda_2} [1 - \rho_{\lambda}] G(\lambda) d\lambda}{\int_{\lambda_1}^{\lambda_2} G(\lambda) d\lambda}, \quad (5)$$

where λ is the wavelength, θ is the incident angle of light, λ_1 and λ_2 are minimum and maximum solar wavelengths, respectively. The absorptance of a solar selective coating is usually determined by the reflectance spectra of the coating, obtained using standard UV-Vis-NIR spectrophotometer. The reflectance spectra is generally measured in the solar wavelength range of 0.3 - 2.5 μm and at near normal angle of incidence ($\theta = 0^\circ$).

2.2. Thermal emittance

All objects emit electromagnetic radiation. However, before defining the term “thermal emittance”, it will be useful to introduce the definition and physical properties of a perfect black body [51]. An ideal blackbody is a hypothetical object that absorbs all radiation

1 incident on it. The expression of the radiant energy distribution from a perfect blackbody was
2 proposed by Max Planck in 1901. Planck's law can be represented as
3
4

$$5 \quad E_{b\lambda}(\lambda, T) = \frac{8\pi hc}{\lambda^5 \exp\left(\frac{hc}{\lambda k_B T} - 1\right)}, \quad (6)$$

6
7
8
9
10 where c , h and k_B are the speed of light (m/s), Planck's constant (J-s) and Boltzman's
11 constant (J-K⁻¹), respectively.
12
13
14

15 The variation of radiant power density of the blackbody at 100, 200 and 300 °C is
16 shown in Fig. 5. Some of the observations can be pointed out as,
17
18
19
20

- 21 a. the emitted radiation is a continuous function of wavelength. At a given
22 temperature, it increases with wavelength, reaches a peak and then decreases with
23 increasing wavelength.
24
25
26
- 27 b. at any wavelength, the emittance radiation increases with an increase in
28 temperature.
29
30
31
- 32 c. when temperature increases from 100 to 300 °C, a shift in the maxima of the
33 curve is observed towards shorter wavelength.
34
35
36
- 37 d. the solar spectrum, presented in the same curve is considered to be a black body at
38 approximately 5800 K.
39
40
41
42

43 The important fact is that the total radiation from the black body can be calculated by
44 integrating the blackbody spectrum over the entire wavelength range. This is known as
45 Stefan-Boltzmann law [52], given as
46
47
48
49

$$50 \quad E_b(T) = \int_0^{\infty} E_{b\lambda}(\lambda, T) d\lambda = \sigma T^4, \quad (7)$$

51 where σ is the Stefan-Boltzmann constant.
52
53
54
55
56
57
58
59
60
61
62
63
64
65

1 The above expression suggests that the total emissive power of a blackbody is
 2 proportional to the fourth power of its temperature. Therefore, emittance or thermal radiation
 3
 4 from a black body increases drastically with a small increase in the temperature.
 5
 6

7 The emittance (ϵ) of a surface is represented by the ratio of radiation emitted by the
 8 object at a given temperature (E_λ) to the radiation emitted by a perfect blackbody ($E_{b\lambda}$) at the
 9 same temperature. It is a dimensionless number that ranges from 0 to 1 i.e. $0 \leq \epsilon \leq 1$. It is a
 10 measure of how strongly a material radiates at a given wavelength and how closely a material
 11 approximates an ideal blackbody for which $\epsilon = 1$. The emittance of a physical body depends
 12 on its temperature, chemical composition, surface roughness, intrinsic geometrical structure,
 13 the wavelength to which the emitted radiation corresponds and the angle at which the
 14 radiation is emitted. The total hemispherical emittance can be expressed as,
 15
 16
 17
 18
 19
 20
 21
 22
 23
 24
 25
 26

$$27 \quad \epsilon_\lambda(\lambda, T) = \frac{E_\lambda(\lambda, T)}{E_{b\lambda}(\lambda, T)} \quad (8)$$

28
 29
 30
 31 Kirchhoff's law, on the other hand, states that the total hemispherical emittance (λ) of
 32 a surface at temperature T is equal to it's total hemispherical absorptance $\alpha(\lambda)$ from a
 33 blackbody at the same temperature. Therefore, the emissivity of a coating can be determined
 34 by the absorptance of a coating in the infrared wavelength range. Using equation (4), the
 35 emittance (ϵ) can be obtained by the following equation
 36
 37
 38
 39
 40
 41
 42
 43

$$44 \quad \epsilon_\lambda(\lambda) = \alpha_\lambda(\lambda) = 1 - \rho_\lambda(\lambda) \quad (9)$$

45
 46
 47 Combining equations (8) and (9), the emittance of a coating at a temperature, T can be
 48 calculated in terms of the reflectance,
 49
 50
 51
 52

$$53 \quad \epsilon(T) = \frac{\int_{\lambda_1}^{\lambda_2} [1 - \rho_\lambda(\lambda)] E_{b\lambda}(\lambda) d\lambda}{\int_{\lambda_1}^{\lambda_2} E_{b\lambda}(\lambda) d\lambda}, \quad (10)$$

1 where $E_b(\lambda)$ is the black body radiation spectrum. The spectral range of thermal
2 radiation emitted from a surface having a temperature of about 300 °C is found from 2.5 to
3
4 25 μm are used as λ_1 and λ_2 , respectively. The emittance of the absorber coating can be
5
6 obtained using the diffuse reflectance spectra in the wavenumber range of 400 – 4000 cm^{-1}
7
8 (2.5 - 25 μm) using FTIR spectrophotometer.
9
10

11 **2.3. Solar selectivity**

12
13 For CSP applications, the absorber materials should have high absorptance (α) > 0.95
14
15 in the solar spectrum (0.3-2.5 μm) and low thermal emittance (ϵ) < 0.05 in the thermal
16
17 radiation region i.e. infrared region (2.5-25 μm). The ratio of solar absorptance to thermal
18
19 emittance is also known as spectral solar selectivity (α/ϵ). The spectral performance of an
20
21 ideal selective solar absorber should be a step function, illustrated in Fig. 5. Fig. 5 clearly
22
23 indicates a step at 2.5 μm below which (solar spectrum) reflectance $\rho = 0$ and above (infrared
24
25 region) $\rho = 1$. The particular wavelength, where the step starts is known as plasma
26
27 wavelength, λ_{plasma} . For real selective absorber, a slight difference in the pattern of the step,
28
29 plotted by red colour can be observed.
30
31
32
33
34
35
36
37

38 **3. Performance evaluation**

39
40 While independent measurements of absorptance, emittance and selectivity are routinely
41
42 conducted for any new bulk material/coating, a few attempts are made to define some of the
43
44 performance qualifying parameters to integrate the basic properties of relevance. This
45
46 section highlights a few such functions or parameters.
47
48
49
50

51 **3.1. Merit function and absorber efficiency**

52
53 Sergeant et al. [53] proposed the merit function, $\{F(T)\}$ of an absorber coating in
54
55 terms of absorptance (α), emittance (ϵ) and the operating temperature (T) by the following
56
57 relation
58
59
60
61

$$F(T) = [1 - \varepsilon T] \quad (11)$$

Therefore, higher the α and lower the ε , better is the $F(T)$ value. Also, the spectral selectivity of an absorber coating increases with an increase in merit function. The cut off wavelength, λ_{plasma} can also be determined by the merit function. Solar to thermal conversion efficiency for an ideal selective absorber, $\eta_{\text{sol-the}}$ at a particular temperature (T) has been defined by Cindrella [54] and Ho et al. [55],

$$\eta_{\text{sol-the}} = \alpha - \frac{\varepsilon(T)\sigma T^4}{CI_s} \quad (12)$$

Where, C is the concentration ratio which is usually on the order of 10 – 1000, I is the solar flux density (W/m^2) and σ is Stefan-Boltzmann constant [56]. The cut off wavelength can also be calculated as a function of operating temperature. It has been observed that a combination of higher concentrations and lower operating temperatures lead to longer wavelength cut offs, while the opposite conditions provide a shorter wavelength cutoffs. Therefore, for a specific solar selective absorber, it is necessary to maximize the overall solar-thermal efficiency by considering a specific structure, material, working temperature and the concentration factor [57].

3.2. Levelized cost of coating (LCOC)

Ho et al. have found out an innovative way to evaluate annual performance, cost, and reliability/durability of selective coating by introducing a new parameter called Levelized Cost of Coating (LCOC) [58]. This can be defined as the ratio of total annualized coating cost to the annual thermal energy absorbed (MWh_{th}) by the receiver,

$$LCOC = \frac{C_{\text{annual}}}{E_{\text{thermal}}} \quad (13)$$

where,

C_{annual} = total annualized coating cost

= initial coating cost/life of plant + recoating cost/recoating interval + cost of additional (or fewer) heliostats to yield a baseline thermal energy production

$E_{thermal}$ = average annual energy absorbed

= annual thermal energy absorbed (new) – annualized lost energy absorbed due to degradation – annualized lost energy absorbed due to down time for re-coating

Along with the solar-thermal conversion efficiency, $\eta_{sol-the}$ and other parameters like the degradation rate, material cost, reapplication cost etc. have a huge impact on LCOC.

4. Preparation of solar selective absorbers

Over the last few decades, preparation of absorber coating has become a popular topic of research. A number of materials have been investigated as absorber coatings till date. The selection of the material, structures and fabrication procedures etc., determine the selective performance of the absorber coatings. However, the main challenge of the absorber lies on the performance of the coating at high temperature. Therefore, along with the solar selectivity few more desired properties of the absorber coatings include,

- a) high temperature stability (~ 400 °C)
- b) corrosion and humidity resistance
- c) ability to prevent oxidation
- d) high structural and chemical stability
- e) hardness and scratch resistance etc.

Among all these properties, the high temperature stability is a prime criteria for a potential solar selective absorber coating.

A number of different design principles and physical mechanisms can be used to develop spectrally selective solar absorbing surfaces. Depending on the design principle, the solar selective surfaces can be categorized in a number of different types including intrinsic

1 absorber, semiconductor coatings, multilayer coatings, metal-dielectric composite coatings,
2 textured surfaces and most importantly DMD -based coatings. The schematic diagrams of
3 these absorber coatings have been presented in Fig. 6. In the following, some of the coating
4 types and their operating principles are briefly described.
5
6
7
8
9

10 **4.1. Intrinsic absorbers**

11
12
13 As the name suggests, intrinsic absorbers inherit selectivity as a property. The
14 examples include V_2O_5 [59], LaB_6 [60], Fe_3O_4 [61], Al_2O_3 [62], few ultra-high temperature
15 ceramics (UHTCs), for example, ZrB_2 [63], ZrC , TaC , HfC [64], SiC , ZrB_2 , HfB_2 [65] etc.
16
17 These materials have attracted attention as potentially suitable candidates for solar selective
18 application. The primary component of most of these materials are from transition metal or
19 lanthanide group. They usually have many available orbitals at energy levels compatible with
20 the energy of visible light. Recently, Ankit et al. [66] explored the intrinsic selectivity of W
21 by laser sintering of micro and nano particles of W on stainless steel. The coating showed
22 excellent performance even after heat treatment at 650 °C in air for 36 hrs. Few researchers
23 have reported the intrinsic selective property of single-walled and multi-walled carbon
24 nanotubes [67, 68]. Some of the paint coatings or electrodeposited coatings made of spinel
25 pigments, such as $CuAl_2O_4$ [69], $CoCuMnO_x$ [70], $Cu_{1.5}Mn_{1.5}O_4$ [71], Mn-Fe spinel PK 3060
26 [72], $CuCr_xMn_{2-x}O_4$ [73], $CuCr_2O_4$ [74], $NiCo_2O_4$, $FeCo_2O_4$, $CoFe_2O_4$, $CuCo_2O_4$,
27
28
29
30
31
32
33
34
35
36
37
38
39
40
41
42
43
44
45
46
47
48
49
50
51
52
53
54
55
56
57
58
59
60
61
62
63
64
65
($NiFe$) Co_2O_5 , $Co_{1.5}Fe_{1.5}O_4$ [75] also show selective property. They exhibit an absorptance of
0.80 and emittance of 0.20 up to 100 °C [76]. A drawback of using most of the intrinsic
absorbers is that the crossover from low to high wavelengths, i.e. the step in the reflectance
spectra occurs at too short wavelengths or the slope at the transition wavelength is not so
steep. In addition, the low thermal conductivity of these materials (except UHTCs) is not
suitable for high temperature applications. Moreover, a thick layer of the intrinsic material is
needed to absorb maximum solar energy, while the increase of the thickness causes an

1
2
3
4
5
6
7
8
9
10
11
12
13
14
15
16
17
18
19
20
21
22
23
24
25
26
27
28
29
30
31
increase in emittance. These problems can be overcome by introducing a structural or
compositional change in the lattice of these materials. Therefore, the properties of the
intrinsic materials should be tailored to satisfy the specific needs by doping a suitable element
inside the material or preparing composites with some other materials. Doping enhances the
selectivity by two ways, firstly the donor atoms give rise to electron plasma, and secondly,
these donors act as a scattering centre, which enhances the optical path of solar radiation and
leads to maximum absorptance. For example, the doping of W in VO₂ matrix (V_{1-x}W_xO₂)
makes it suitable as solar thermal absorber [77]. A femtosecond laser treated composite
coating of 70 vol% HfC - 30 vol% MoSi₂ exceeded itself as a promising selective absorber
[78]. Fang et al. [79] demonstrated that Ti₃SiC₂ and Zr₃[Al(Si)₄]C₆ have lower emissivity and
better thermal stability than TiC and ZrC ceramics. Xu et al. [80] presented cordierite
(2MgO.2Al₂O₃.5SiO₂)/SiC composite as potential solar selective absorber material due to
excellent solar selectivity and thermal shock resistance.

32 **4.2. Semiconductor absorbers**

33
34
35
36
37
38
39
40
41
42
43
44
45
46
47
48
49
50
51
52
53
54
55
56
57
58
59
60
61
62
63
64
65
The particular interest on semiconductor absorber has been focused on the
semiconductor with the band gap (E_g) in the range of 0.5 eV (2.5 μm) to 1.26 eV (1.0 μm)
such that the plasma wavelength λ_{plasma} lies in the desired position. Thus, some of the
semiconductors Si (1.1 eV), Ge (0.7 eV), PbS (0.4 eV) have good potential as absorber
materials in solar thermal applications [81]. A novel absorber Si_{0.8}Ge_{0.2} with a band gap of
1.04 eV has been reported by Moon et al. [82] and such absorber exhibited a solar
absorptance of 0.90-0.95, while maintaining a relatively low emittance of less than 0.3. Yang
et al. [83] proposed a Ge check board structure on Ta substrate using finite-difference time
domain (FDTD) method, which shows very high absorptance below 1.2 μm and less
absorptance beyond that. Xiao et al. [84] have taken advantages of the semiconductor nature
of copper oxide (CuO, Cu₂O). The band gap of the p-type semiconductor, CuO and Cu₂O are

1.4 and 2 eV, respectively. They have developed the copper oxide coating by one-step chemical conversion method and the highest photo-thermal efficiency was achieved with an absorptance of 0.94 and an emittance of 0.08. The underlying metallic layer helps to reflect the infrared wavelength and reduces the emissivity.

The disadvantage of the semiconductor coatings is their high refractive index, which causes large reflectance loss, and as a result, the coating can absorb less amount of solar energy. The performance of such coatings can be improved by depositing an antireflection coating on top of the semiconductor. A single layer AR coating of MgF_2 , SiO_2 , Al_2O_3 [85], TiO_2 , [86] Si_3N_4 etc., can be deposited on the semiconductor to reduce the loss of absorbed energy from the coating surface. Seraphin et al. [87] fabricated a semiconductor-based multilayer coating of $\text{SS}/\text{Cr}_2\text{O}_3/\text{Ag}/\text{Cr}_2\text{O}_3/\text{Si}/\text{Si}_3\text{N}_4/\text{SiO}_2$ by chemical vapour deposition, where Si served the role of main absorber layer and Si_3N_4 and SiO_2 layer acted as anti-reflection layer. The coating exhibited an absorptance of 0.85 and emittance of 0.07 with a high thermal stability up to 500 °C.

4.3. Multilayer absorbers

The most elementary systems, like intrinsic or semiconductor absorber coatings are not suitable for high temperature applications. Therefore, in recent years, the coatings with the multilayers structures have been considered as reliable in the high temperature applications. A multilayer coating consists of several alternative layers of dielectric and semi-transparent metallic layers. The dielectrics usually absorb well in the visible wavelength range and the metals reflect the infra-red. Anti-reflection coatings are usually put on top to improve transmission to the absorbing layers. High absorptance up to 0.95 and low emittance of 0.05 can be achieved by the multilayer stack even under elevated temperature conditions.

In a multilayer coating, superposition of multiple light waves introduce interference, which depends on the relative phase of each light wave. Destructive interference prevents the

1 reflectance of the light and enhances absorptance in thin films. Destructive interference
2 occurs when two interfering waves with 180° phase difference superpose each other.
3
4 However, this phase difference for destructive interference correlates to a $\lambda/2$ shift of the
5 sinusoid wave that is best achieved by adjusting the optical thickness of the layer, a function
6 of layer thickness. The above discussion emphasises that the thickness of individual layer in a
7 multilayer coatings needs to be approximately tailored to obtain desire combination of solar
8 selective properties.
9

10
11
12 In recent years, the transition metal of group IVA, VA, and VIA and their
13 nitride/oxynitride/oxide based coatings have attracted significant attention as stable high
14 temperature absorber coating. The metal volume fraction and the refractive index of each
15 layer of these coatings usually increase from surface to substrate to enhance absorptance. The
16 metal volume fraction can be varied by the deposition time, target power and gas flow rate.
17 A large number of multilayer coatings such as TiAlN/CrAlON/Si₃N₄ [88],
18 AlCrSiN/AlCrSiON/AlCrO [89], TiAlSiN/TiAlSiON/SiO₂ [90],
19 HfMoN(H)/HfMoN(L)/HfON/Al₂O₃ [91], Mo/AlCrON(HMVF)/AlCrNO(LMVF)/AlCrO_x
20 [92], Al₂O₃/Cu/Al₂O₃/AlCuFe [93], Ti_xAl_{1-x}/(TiN-AlN)_H/(TiN-AlN)_L/AlN [94],
21 Ti_{0.5}Al_{0.5}N/Ti_{0.25}Al_{0.75}N/AlN [95], TiAlCrN/TiAlN/AlSiN [96] have been developed by
22 several groups. We have recently developed a W/WAlN/WAlON/Al₂O₃ multilayer absorber
23 coating that had a very high absorptance of 0.958 and low emittance of 0.08. The coating
24 showed very high stability at 350 °C in air for 550 hrs [97-99]. TINOX [100] (sputtered
25 titanium nitride film) developed by ALMECO group [101] is commercially available and
26 notable among these multilayer absorber coatings that exhibit an absorptance of 0.95 and
27 emittance of 0.04.
28

29
30 The main disadvantage of multilayer structure are the high fabrication cost. These
31 coatings can be manufactured by the simple, advantageous and up-scalable wet chemistry
32
33
34
35
36
37
38
39
40
41
42
43
44
45
46
47
48
49
50
51
52
53
54
55
56
57
58
59
60
61
62
63
64
65

1 method to reduce the production cost. In order to prove feasibility of fabricating multi-layer
2 coating by wet chemistry method, Bayon et al. [102] deposited $\text{CuMnSiO}_x/\text{CuMnO}_x/\text{SiO}_2$
3
4 coating on Al substrate by dip-coating and achieved the absorptance of 0.95 that can
5
6 compete with the commercially available sputter coated absorber. The coating also qualified
7
8 the long-term thermal stability test. Recently Joly et al. [103] reported a Cu-Co-Mn-Si-O -
9
10 based graded index coating by sol-gel method that showed high selectivity of 0.95/0.12 with
11
12 a high thermal stability and corrosion resistance. Therefore, it can be commented that
13
14 fabrication of multilayer coating by wet chemistry route can provide a direction towards the
15
16 future commercialization of the selective coating.
17
18
19
20

21 **4.4. Cermets or metal-dielectric composite absorbers**

22
23 Cermets, i.e. metal-dielectric composites, consist of nanoscale metal particles in a
24
25 dielectric or ceramic matrix. The multilayer coatings and cermets have similarity as dielectric
26
27 material is used in both the structure for the solar absorption, while metal serves as infrared
28
29 reflector. The metal particles in absorber coatings play an important role by acting as a
30
31 modifier for the optical response of the ceramic phase. The solar radiation is scattered by the
32
33 boundaries between the metallic and dielectric phase. As a result, the optical path length of
34
35 the radiation increases, which leads to an increase in the absorption by a factor of $4n_d^2$, where
36
37 n_d is the refractive index of the dielectric medium [104]. The light trapping in the cermet also
38
39 occurs due to quantum confinement effect and is known as surface plasmon resonance
40
41 phenomenon (SPR) [105]. SPR is the collective oscillations of the conduction electrons of
42
43 metal nanoparticles in the dielectric matrix that influences the optical absorption in the solar
44
45 spectrum.
46
47
48
49
50
51
52

53 Critical parameters for an efficient cermet coating are the dielectric constant of the
54
55 metal nanoparticles and the dielectric matrix [106]. Dielectric function of the composite can
56
57 be calculated theoretically by the following equation obtained from Maxwell-Garnett (MG)
58
59
60
61
62
63
64
65

[107] and Bruggeman theory (BR) [108], considering the identical spherical grain with the size much less than the wavelength of light:

$$\varepsilon^{MG} = \varepsilon_B \frac{\varepsilon_A + 2\varepsilon_B + 2f_A(\varepsilon_A - \varepsilon_B)}{\varepsilon_A + 2\varepsilon_B - f_A(\varepsilon_A - \varepsilon_B)} \quad \text{and} \quad (14)$$

$$f_A \frac{\varepsilon_A - \varepsilon^{BR}}{\varepsilon_A + 2\varepsilon^{BR}} + (1 - f_A) \frac{\varepsilon_B - \varepsilon^{BR}}{\varepsilon_B + 2\varepsilon^{BR}} = 0, \quad (15)$$

where ε^{MG} and ε^{BR} represent the average dielectric functions of the composite in MG and BR approximations, ε_A and ε_B indicate the dielectric function of metal (A) and ceramic (B). The metal filling factor f_A is the volume fraction occupied by metal. If f_A is less than zero, MG theory can be used to calculate the dielectric constant of composite cermet. BR theory is used otherwise. In order to get accurate value of the dielectric constant, ellipsometry measurement can be performed. Generally Mo, Pt, W, Cr, etc., are used as metallic components in SiO_2 , Al_2O_3 , Cr_2O_3 , TiO_2 , AlN matrix [109-112].

In order to improve the optical performance and thermal stability, researchers have developed cermets that are composed of four layers consisting of (i) an infrared reflective metallic layer (IR-mirror), (ii) a high metal volume fraction (HMFV) cermet, (iii) a low metal volume fraction (LMVF) cermet layer, and (iv) an anti-reflective (AR) layer [113]. Such kind of cermets, like W- Al_2O_3 [114], AlNi- Al_2O_3 [115], Ag- Al_2O_3 [116], Pt- Al_2O_3 [117] Mo- Al_2O_3 [118], Mo- SiO_2 [119, 120], Ni-NiO [121], and W-Ni-YSZ [122] have been reported for solar selective absorber coatings. Among the successful selective coatings, a few are commercially available for high temperature applications. For example, Mo- Al_2O_3 and W- Al_2O_3 have been commercialized by Siemens (Germany) due to their thermal stability in the range of 350 - 500 °C [123, 124]. Mo- SiO_2 and W- Al_2O_3 have been commercially used by Angelantoni ENEA (Italy) and Turbosun (China) commercializes AlN-based ceramics [125, 126].

However, most of the reported cermet coatings have been fabricated by sputtering, evaporation or chemical vapour deposition. The essential requirement of an optically efficient

1 solar selective coating is cost-effectiveness. Therefore, the cermet coating deposited by
2 electrodeposition or sol gel method have been extensively investigated. Wang et al. [127]
3
4 have proposed preparing Ni-nanochain- Al_2O_3 coating using solution chemical process. The
5
6 coating had a solar absorptance > 0.90 and a low thermal emittance < 0.10 . In a separate
7
8 study, Katumba et al. [128, 129] have utilised the embedded amorphous and shapeless carbon
9
10 in three different metal oxides (C/SiO_2 , C/ZnO , and C/NiO) by sol-gel method. They found
11
12 that C/NiO cermet exhibits superior selective properties with the solar absorptance of 0.93.
13
14 Roro et al. [130] believed that the selective property can also be achieved by replacing
15
16 amorphous carbon by multi-walled carbon nanotubes. The best solar absorptance and the
17
18 thermal emittance of MWCNTS/ NiO obtained were 0.84 and 0.2. The electrodeposited Co -
19
20 Al_2O_3 , prepared by Cuevas et al. [131] demonstrated a high absorptance of 0.92 and
21
22 emittance of 0.16. $\text{Co-Al}_2\text{O}_3$ structure has been engineered in such a way so that Al_2O_3 pores
23
24 have been filled by Co nano particles. The review article of Cao et al. [132] provides ample
25
26 evidence of the cermet based absorber coating in detail.
27
28
29
30
31
32

33 **4.5. Textured surfaces**

34
35 Most of the solar selective coatings reported in literature are multilayer coatings or
36
37 cermet structures. Though the optical performance of these coating is superior, these designs
38
39 fail at high temperatures (>1000 K) due to oxidation, substrate diffusion, intra and interlayer
40
41 reactions of the constituent element and thermo mechanical stresses between the layers and
42
43 interfaces. To overcome the aforementioned shortcomings while keeping the selective
44
45 property unaffected, surface texturing appears to be a technologically emerging approach
46
47 [133]. Textured surface with porous, granular, dendrite or needle-like microstructures is
48
49 capable of producing very high absorptance, capturing solar energy by multiple reflections,
50
51 while low emittance can be achieved as the surface seems to be smooth for longer
52
53 wavelengths [134].
54
55
56
57
58
59
60
61
62
63
64
65

1
2
3
4
5
6
7
8
9
10
11
12
13
14
15
16
17
18
19
20
21
22
23
24
25
26
27
28
29
30
31
32
33
34
35
36
37
38
39
40
41
42
43
44
45
46
47
48
49
50
51
52
53
54
55
56
57
58
59
60
61
62
63
64
65

Chen et al. [135] developed tapered aluminium doped zinc oxide nanorod arrays using electrodeposition which exhibited absorptance of 0.95 in the solar spectrum. The 1D CuO nanostructures like nanofibers and nanoneedles, fabricated using chemical oxidation of Cu exhibited a selectivity of 0.95/0.07 [136]. Sergeant et al. [137] proposed a design of sub-wavelength V-groove gratings coated with aperiodic metal-dielectric stacks, which could have absorptance >0.94 and emittance <0.06 at 720K. Photonic crystals [138] and metamaterials [134] have also been designed considering the challenge of stability in the high temperature and long span of operation. Wang et al. [139] simulated optical properties of a two-dimensional (2D) Mo photonic crystal (PhC) surface that exhibited a high absorptance of 0.919 and low emittance of 0.149 at 1000 °C. Rigorous Coupled-Wave Analysis (RCWA) method was used to optimize the spectral property of the system by varying the diameter, height and periodicity of the Mo column cells. In another study, a selective metamaterial absorber made of a 2D titanium grating deposited on an MgF₂ spacer and an opaque tungsten film showed an absorptance and emittance of 0.9 and 0.2, respectively, with a thermal stability up to 350 °C [140].

4.6. Dielectric/metal/Dielectric (DMD) absorbers

The ray-optics theory of light trapping using multiple reflections (in case of multilayer film or the texturing of the surfaces) is becoming traditional. Moreover, the long wavelength leaves these coatings due to specular reflection from the rear surface. In order to reduce the large loss of escaping long wavelength light, the optical path length of weakly absorbed light has to be enhanced. The DMD structure, which is another type of selective coating, can be employed to improve the absorption by the use of Surface Plasmon Polaritons (SPPs) [141, 142]. SPPs provide a tuneable high scattering cross section at larger angles and increase the optical path length. It is also worth developing light-trapping layers like DMD absorber, which is based on wave-optics in a scalable fashion. The challenge of developing such layers

1 is to identify tuneable compositions that can bridge the gap between the optical properties of
2 metals and dielectrics and increase the solar absorption without increasing any thermal heat
3 loss.
4
5

6
7 A key advantage of such a coating is the small amount of material required to fabricate
8 the structure, which reduces consumable costs. As the high temperature stability is
9 concerned, stable nanocrystalline or amorphous dielectric materials (Cr_2O_3 , MgO , Al_2O_3) are
10 highly desirable. Based on the melting point and resistance against oxidation in high
11 temperature, metals like Cr, Mo, Al, Pt, etc., are the ideal candidates for DMD absorber
12 layers.
13
14
15
16
17
18
19
20

21
22 Most of the studies on DMD -based absorber structures have shed light on some
23 parameters like refractive index (n), extinction co-efficient (k), and thickness of individual
24 layer. The amplitude ratio of parallel and perpendicular components of the reflected wave (Ψ)
25 from the coating and their relative phase change (Δ) can be obtained from the spectroscopic
26 phase modulated ellipsometry over a particular wavelength range (300 – 1200 nm). Some
27 predictive models (Tauc-Lorentz interband transition model [143], Adachi's model [144],
28 user-defined expressions for optical constants, imported dielectric functions, classical Drude
29 model [145] etc.) can be fitted with the experimental ellipsometry data to quantify the optical
30 constants (n and k) of metal and dielectric which influence the overall performance of the
31 selective coatings. Using these models, researchers predict and investigate the optimum
32 combination of the metal and dielectrics to develop highly efficient DMD -based absorbers.
33
34
35
36
37
38
39
40
41
42
43
44
45
46
47

48 In order to derive the dispersion relation for complex dielectric function of
49 semiconductor material, Ninomiya and Adachi [146, 147] correlated the energy band
50 structure and imaginary part of the complex dielectric function. The dispersion relation can
51 be expressed as
52
53
54
55
56

$$\varepsilon(E) = \frac{4e^2\hbar^2}{\pi\mu^2E^2} \int dk |P_{cv}^2| \delta[E_c(k) - E_v(k) - E], \quad (16)$$

where μ is the combined density of state mass, Dirac δ function represents the joint spectral density of state between the valence, the valance band $E_v(\mathbf{k})$ and the conduction band $E_c(\mathbf{k})$ states differing by the incident energy $E = \hbar\omega$, $P_{cv}(\mathbf{k})$ is the momentum matrix element between valance and conduction band states, which has been evaluated by the integration over the first Brillouin zone.

The analytical expression for the dielectric constant can also be obtained from TL dispersion model [148], which has been extensively used to describe the dispersion of optical constants in case of amorphous and nanocrystalline dielectric materials. The imaginary part of the dielectric function ($\varepsilon_2 = 2nk$) of the material can be expressed as,

$$\varepsilon_{2TL}(E) = \frac{A_{TL}E_0C_L(E-E_g)^2}{(E^2-E_0^2)+C_L^2E^2}, \quad (17)$$

where E_0 is the peak transition energy, while A_L and C_L determine the strength and broadening of the transition, respectively.

The expression for real part of dielectric constant ($\varepsilon_1 = n^2 - k^2$) can be obtained by Kramers–Kronig analysis as:

$$\begin{aligned} \varepsilon_{1TL}(E) = & \varepsilon_{1TL}(\infty) + \frac{1}{2} \frac{A_{TL}C_L}{\pi} \frac{\alpha_{ln}}{\xi^4 \alpha E_0} \ln \left[\frac{E_0^2 + E_g^2 + \alpha E_g}{E_0^2 + E_g^2 - \alpha E_g} \right] - \frac{A_{TL}}{\pi \xi^4} \frac{a \tan}{E_0} \left[\pi - a \tan \left(\frac{2E_g + \alpha}{C_L} \right) + \right. \\ & \left. a \tan \left(\frac{-2E_g + \alpha}{C_L} \right) \right] + \frac{2A_{TL}E_0}{\pi \xi^4 a} \left\{ E_g (E^2 - \gamma_{TL}^2) \left[\pi + 2 \operatorname{atan} \left(\frac{2\gamma_{TL}^2 - E_g^2}{\alpha C_L} \right) \right] \right\} - \\ & \frac{A_{TL}E_0C_L}{\pi \xi^4} \frac{E^2 + E_g^2}{E} \ln \left(\frac{|E - E_g|}{E - E_g} \right) + \frac{2A_{TL}E_0C_L}{\pi \xi^4} E_g \ln \left[\frac{|E - E_g|(E + E_g)}{\sqrt{(E_0^2 - E_g^2)^2 + E_g^2 C_L^2}} \right] \end{aligned} \quad (18)$$

The details of this expression can be found elsewhere [149]. The n and k of metallic layer can be modelled by Cauchy's dispersion formula [150], represented by the following equations:

$$n(\lambda) = A + \frac{B}{\lambda^2} + \frac{C}{\lambda^4} \quad \text{and} \quad (19)$$

$$k(\lambda) = D + \frac{E}{\lambda^2} + \frac{F}{\lambda^4}, \quad (20)$$

1 where A-F are the parameters of dispersion relation and λ is the wavelength of incident
2 light. The dispersion relation of metal can also be fitted by Drude –type dispersion relation
3
4 [151], represented by
5
6

$$7 \quad \varepsilon_M = \varepsilon_\infty + \frac{\omega_p^2}{-\omega^2 + i\Gamma_D\omega} , \quad (21)$$

8
9 where ε_M is the complex dielectric constant of metal, ε_∞ is the high-frequency
10 component of the dielectric constant, ω_p is the plasma frequency and Γ_D is the damping
11 factor.
12
13

14 In order to investigate optical properties of metal and dielectric thin films, the
15 measured ellipsometric spectra needs to be fitted with theoretically generated ellipsometric
16 spectra by varying thickness and parameters of dispersion relation of aforementioned
17 practically useful predictive models. Full analysis of the optical constants using the
18 comprehensive models have been performed for a number of DMD systems, such as
19 $\text{Cr}_x\text{O}_y/\text{Cr}/\text{Cr}_2\text{O}_3$ [152], $\text{Al}_x\text{O}_y/\text{Al}/\text{Al}_x\text{O}_y$ [149], $\text{HfO}_x/\text{Mo}/\text{HfO}_2$ [153] etc. The variation of the
20 optical properties (n and k) of the individual layer with respect to wavelength satisfy the
21 general characteristics of metals and dielectrics.
22
23
24
25
26
27
28
29
30
31
32
33
34
35
36
37
38

39 **5. Characteristics of surface plasmon polaritons in dielectric–metal–dielectric** 40 **structure** 41

42 In a pioneering work, Ritchie [154] first introduced the self-sustained coherent
43 electron oscillations at the metal surface in 1957. After two years, Powell and Swan [155]
44 proved the existence of these collective excitations by some electron energy-loss
45 experiments.
46
47
48
49
50
51

52 The movement of the conduction electrons of metals upon excitation with the incident
53 light builds up polarisation charges on the metal particles. The polarisation charges create an
54 electric field, which acts as restoring force in the system, allowing resonance to occur at a
55
56
57
58
59
60
61
62
63
64
65

1 particular frequency of incident radiation. The resonant interaction between the surface
2 charge oscillation and the electromagnetic field of light constitutes “surface plasmons”,
3
4 named by Stern and Ferrell [156].
5
6

7 Scientists have classified the “Surface Plasmons” in two categories: “Localised
8 surface plasmons (LSP)” [157] and “Surface Plasmon Polaritons (SPP)” [141]. In the case of
9 LSP, electromagnetic wave interacts with the metallic nanoparticles (such as Au, Ag, Pt, Pd)
10 of diameter (d) much smaller than the incident wavelength (λ), i.e. $d \ll \lambda$. LSPs are confined
11 in the closed surface of the nanoparticles and can be resonantly excited with the
12 electromagnetic wave of particular frequency irrespective of the wave vector of the incident
13 wave, which also leads to a strong amplification of the local electromagnetic field. The
14 frequency of LSPs are highly sensitive to the shape, size, size distribution, density, dielectric
15 function of metal particles and surrounding environments.
16
17
18
19
20
21
22
23
24
25
26
27

28 In contrast, SPPs are the coherent collective oscillations of conductive electrons,
29 confined at the interface of two media such as a metal and a dielectric. The SPPs propagate in
30 a wavelike manner at the interface of the metal and dielectric perpendicular to the surface.
31 The electromagnetic field of SPPs is evanescently confined in the boundary of metal-
32 dielectric, which causes an enhancement of the electromagnetic field at the interface, leading
33 to an extraordinary sensitivity of SPPs to surface conditions. The amplitude of the wave
34 decays exponentially with an increase in distance from the interface due to the surface wave
35 character of SPPs.
36
37
38
39
40
41
42
43
44
45
46
47

48 Fig. 7 demonstrates the fundamental difference between localized surface plasmons
49 and surface plasmon polaritons. For LSPs, the electron cloud oscillates locally around the
50 metallic nanoparticles, while the SPPs move in the x and y directions through the interface of
51 metal and dielectric with an evanescent decay in the z direction. Therefore, both LSPs and
52 SPPs manifest themselves in the enhancement of local field.
53
54
55
56
57
58
59
60
61
62

1
2
3
4
5
6
7
8
9
10
11
12
13
14
15
16
17
18
19
20
21
22
23
24
25
26
27
28
29
30
31
32
33
34
35
36
37
38
39
40
41
42
43
44
45
46
47
48
49
50
51
52
53
54
55
56
57
58
59
60
61
62
63
64
65

Several theoretical and experimental investigations of SPPs have been performed to explore the fundamental properties of it and to continue a great variety of experiments in the field of condensed matter and surface physics [158]. SPPs are linked with a variety of distinctive phenomenon such as the energy transfer in gas-surface interactions, the energy loss of charged particle moving outside a metal surface and the damping of surface vibrational modes etc. The properties of SPPs have also been extensively utilised in a wide spectrum of studies ranging from electrochemistry [159], photonics [160], biosensing [161], optoelectronics [162], surface plasmon microscopy [163], surface plasmon resonance sensors [164], plasmonic lasers [165], light-emitting diodes [166] etc. However, here we limit ourselves in discussing the fundamentals of SPPs and its application in solar selective absorber coatings.

The discovery of SPPs has revealed a new regime in the development of solar selective absorber coatings. There are increasing number of excellent efforts on the development of solar selective absorber coating by using plasmonic enhancement with an aim to increase the efficiency of CSP systems. A thin film composed of DMD design is one of the most promising structures that can generate SPPs to achieve high solar selectivity as the film is transparent in the thermal infra-red region, while they are strongly absorbing in the solar region. This structure is based on a thin metal film with low refractive index sandwiched by high refractive index dielectric films from both sides. The large refractive-index discontinuity at the boundary regions helps in subwavelength localisation and field enhancement effect. The combination of rapidly attenuating dielectrics and the noble metals results in a strong resonant behaviour in the thin film which leads to a considerable modifications of the optical properties in the selective coating.

Once incident sunlight is converted into SPP mode in DMD -based coatings, it will start to propagate. But the wave will gradually attenuate exponentially with increasing

1 distance into each medium from the interface. The damping is caused primarily by dispersion
2 near the resonant frequency [167], free-electron scattering in metal, and at short operating
3 wavelengths by interband transitions. The large optical attenuation of SPPs also occurs due to
4 the Joule losses ($Q = \int \mathbf{j} \cdot \mathbf{E} dV$) in metal [167]. The roughness of the surface also causes
5 additional attenuation. Moreover, the SPPs are scattered, while interacted with the surface
6 defects. The destructive interference takes place between the scattered and the incoming light.
7 All these phenomena reduce the overall reflections of the coating and increase absorption.
8
9

10
11
12
13
14
15
16
17 A complete theoretical treatment of SPPs is quite lengthy and beyond the scope of this
18 review. However, we have attempted to provide the reader a limited overview on some
19 equations related to SPPs in MD and DMD -based structures, their physical interpretations,
20 and how these properties can be implemented in a solar selective absorber stack.
21
22
23
24
25
26

27 We have discussed earlier that the SPPs, a collective oscillation of conduction
28 electrons in metal, can be generated at the interface of a metal and a dielectric material (see
29 Fig. 8(a)). The SPP is transverse-magnetic (TM) wave that can be distinguished by the
30 propagation constant and electromagnetic field distribution. The dispersion of the SPPs at the
31 interface of metal with dielectric material can be calculated by solving Maxwell's equation in
32 each medium.
33
34
35
36
37
38
39
40

41 While solving the Maxwell's equation, one need to ignore the following [168]:
42

- 43 (i) The metal and dielectric layers in real devices have a finite thickness,
44
45 (ii) There will be some initial absorption of light when it is propagating through the dielectric
46 towards the interface,
47
48 (iii) Imperfect coupling of the incoming plane wave to SPPs takes place at the interface [169].
49
50
51
52

53 Bohn et al. [168] demonstrated that the analytical solution of the electric field E_m
54 (metal) and E_d (dielectric) which represents the SPP, can be obtained by the following
55 equations:
56
57
58
59
60
61
62
63
64
65

$$E_m = \left[E_0, 0, E_0 \left(-\frac{k_x}{k_{z,m}} \right) \right] e^{i(k_x x + k_{z,m} z - \omega t)} \quad \text{and} \quad (22)$$

$$E_d = \left[E_0, 0, E_0 \left(-\frac{k_x}{k_{z,m}} \right) \right] e^{i(k_x x - k_{z,m} z - \omega t)}, \quad (23)$$

where k_x is the wave vector parallel to the interface, and $k_{z,m}$ and $k_{z,d}$ are the wave vectors perpendicular to the interface in the metal and dielectric, respectively.

The solutions of the Maxwell's equations using appropriate boundary conditions represent the SPPs in MD structure. We can obtain the following dispersion relation of the SPP propagating in the interfaces between metal and dielectric [170]:

$$k_{SP} = k_0 \sqrt{\frac{\epsilon_d \epsilon_m}{\epsilon_d + \epsilon_m}}, \quad (24)$$

where k_{SP} and k_0 are the wave vector (momentum) of the SPPs and photon respectively, and ϵ_d and ϵ_m ($\epsilon_m = \epsilon_{mr} + i\epsilon_{mi}$) are the frequency-dependent relative permittivities of the dielectric and metal, respectively.

The dissipative power of SPPs has been calculated using the Poynting Vector and power flow in the dielectric medium in a MD system. The power absorbed by the dielectric is presented by [168]:

$$P_{abs,d} = \frac{1}{2} \int_0^\infty \int_0^\infty \text{Re}\{\sigma E_d E_d^*\} dx dz = \frac{\omega \epsilon_0 \text{Im}\{\epsilon_d\} |E_0|^2}{8 \text{Im}\{k_x\} \text{Im}\{k_{z,d}\}} \left(1 + \frac{|\epsilon_m|}{|\epsilon_d|} \right). \quad (25)$$

The power is not only be absorbed inside the dielectric but also in the metal. The ratio of the dissipative power in metal and dielectric can be expressed as

$$F_{abs} = \frac{P_{abs,d}}{P_{abs,m}} = \frac{\text{Im}\{\epsilon_d\} |\epsilon_m| \text{Im}\{k_{z,m}\}}{\text{Im}\{\epsilon_m\} |\epsilon_d| \text{Im}\{k_{z,d}\}}. \quad (26)$$

The ratio of the power absorbed in the dielectric to the total power absorbed by both metal and dielectric can be expressed in terms of F_{abs} :

$$\frac{P_{abs,d}}{P_{abs,d} + P_{abs,m}} = \frac{F_{abs}}{F_{abs} + 1}. \quad (27)$$

1 In order to achieve maximum solar absorption in the meta-dielectric slab, the F_{abs} ratio
2 should be maximized. Five independent variables are responsible to absorb maximum
3 sunlight. These variables are the frequency of incoming photons, the real and imaginary
4 permittivity for the metal, and the real and imaginary permittivity for the dielectric absorber.
5 The highest absorption can be achieved in materials with small positive real permittivity and
6 large positive imaginary permittivity. This is in view of the fact that the small real
7 permittivity provides a large frequency range over which SPPs can be supported and, in
8 practical devices, will reduce reflections at the interface between the external medium, such
9 as air due to the smaller refractive index. On the other hand, the loss factor in a material can
10 be defined by the following equation,
11
12
13
14
15
16
17
18
19
20
21
22
23
24

$$25 \quad \tan\delta = \frac{\varepsilon''}{\varepsilon'} \quad (28)$$

26 where $\tan\delta$ is the loss factor; ε' and ε'' are the real and imaginary part of the relative
27 permittivity, respectively [171]. Hence the second requirement for large imaginary
28 permittivity or large extinction coefficient is necessary for the loss of the incident radiation in
29 the system, which enhances the absorption. In order to fabricate an efficient metal-dielectric
30 stack, we can also correlate the above mentioned criteria to the following equations;
31
32
33
34
35
36
37
38
39
40

$$41 \quad n = \sqrt{\frac{\varepsilon'^2 + \varepsilon''^2}{2}} + \frac{\varepsilon'}{2} \quad (29)$$

$$42 \quad k = \sqrt{\frac{\varepsilon'^2 + \varepsilon''^2}{2}} - \frac{\varepsilon'}{2} \quad (30)$$

43 where η and k are the real and imaginary part of the refractive index, respectively.
44
45 The real and imaginary parts of two appropriate parameters such as refractive index and
46 relative permittivity to evaluate the performance of any optical systems have been put
47 together in the above equations. It is evident from equations (29) and (30) that a lower value
48
49
50
51
52
53
54
55
56
57
58
59
60
61
62
63
64
65

of real part of relative permittivity (ϵ') increases the imaginary refractive index which is responsible to boost the absorption of solar energy.

Now, let us consider a multilayer system of DMD, sketched in Fig. 8(b), consists of a thin metal films of thickness $2a$ and relative permittivity ϵ_m sandwiched between two optically semi-infinite dielectrics of relative permittivity ϵ_{d1} and ϵ_{d2} [172].

In this context, it is worthy to point out that the optical properties of a DMD -based system can be obtained by computational analysis of characteristic matrix theory [173]. Considering the incidence and the emission medium of the system is half-infinite and non-absorptive, one can represent the characteristic matrix of dielectric-metal-dielectric as follows [174]:

$$\left\{ \prod_{r=1}^k \begin{bmatrix} \cos \bar{\delta}_r & j \sin \bar{\delta}_r / \bar{\eta}_r \\ j \bar{\eta}_r \sin \bar{\delta}_r & \cos \bar{\delta}_r \end{bmatrix} \right\} \begin{bmatrix} 1 \\ \eta_{k+1} \end{bmatrix}$$

Therefore, the reflectance and the transmittance of the system can be expressed by

$$R = \left(\frac{\eta_{OB-C}}{\eta_{OB+C}} \right) \left(\frac{\eta_{OB-C}}{\eta_{OB+C}} \right)^* \quad \text{and} \quad (31)$$

$$T = \frac{4\eta_O \eta_{k+1}}{(\eta_{OB+C})(\eta_{OB-C})}, \quad (32)$$

where $\bar{\delta}_r$ is the phase thickness and $\bar{\eta}_r$ is the complex admittance in the horizontal and vertical directions. B , C , $\bar{\delta}_r$ and $\bar{\eta}_r$ can be calculated using complex refractive index and variable thickness of the materials along with wavelength of the incident light. The value of the refractive index can also be found from data in Palik's handbook [175], or from earlier data derived by Johnson and Christy [176]. Different commercial software such as The Essential Macleod, Thin film Centre, Inc etc., are used to find the reflectance, absorptance and transmittance from the characteristics matrix.

The optical properties of the DMD system can also be evaluated using dispersion relation of the SPPs in each optically homogeneous, isotropic, linear media without any

influence of external charge or and current densities. The continuity of electric and magnetic field leads to the following dispersion relation of DMD system [172]:

$$e^{-4k_m a} = \frac{\frac{k_m + k_{d1}}{\epsilon_m + \epsilon_{d1}} \frac{k_m + k_{d2}}{\epsilon_m + \epsilon_{d2}}}{\frac{k_m - k_{d1}}{\epsilon_m - \epsilon_{d1}} \frac{k_m - k_{d2}}{\epsilon_m - \epsilon_{d2}}} \quad (33)$$

It is noteworthy that the SPPs can be excited in visible wavelength range while the magnitude of the real component of the metal's dielectric constant becomes larger than the corresponding (positive) value for the dielectric. In DMD structure, the incident sunlight is turned by 90° and the solar radiation is confined in the horizontal direction of the selective coating. In this case, the length of the solar selective absorber coating should be greater than optical absorption length. Depending on the properties of the metal and dielectric, SPP possesses high loss in different wavelength regime. The decay of evanescent waves occur in both metal and dielectric. However, to enhance the solar selectivity of the absorber coating, the decay of evanescent wave in dielectric is more important than in metal. Maximization of absorption can be ensured by increasing the decay length of the evanescent wave [177].

An alternative method for depicting the solar absorption in DMD structure is through the local density of optical states $\rho(r, \omega)$, which is a function of position r and radial frequency ω . ω can be determined from the local density of electromagnetic energy, which can be expressed as

$$U(r, \omega) = \frac{\rho(r, \omega) h \omega}{e^{\frac{h \omega}{k_B T}} - 1}, \quad (34)$$

where $h\omega$ and $k_B T$ are photon energy and thermal energy, respectively. The local density of optical states increases in the interface of metal and dielectric due to the presence of additional evanescent modes. As a result, trapping of solar energy can be enhanced

1 significantly in the DMD structure. The trapping in the structure raises the macroscopic limit
 2 of $4\eta_d^2$ by a factor of $\left(\frac{2\eta_d}{\eta_m} + \frac{\eta_d^5}{\eta_m^5}\right)/3$, which equals 12 when η_d/η_m is equal to 2 [106].
 3
 4

5 In case of DMD structure, the fractional absorption in the dielectric layer can be
 6 represented as:
 7

$$f_d = \frac{k_d k_m^3}{\eta_d^3 \eta_m + k_d k_m^3} \quad (35)$$

8 where η_d (η_m) and k_d (k_m) are the real and imaginary parts of the refractive index of
 9 dielectric (metal). The half of the energy will be absorbed in the dielectric if $k_s > \frac{\eta_m \eta_d^3}{k_m^3}$. A
 10 small value of η_m/k_m^3 will enhance the absorption in dielectric layer drastically.
 11
 12

13 It is worthwhile to mention that refractive index of two dielectric layer in the DMD
 14 structure should be equal or close enough to allow the effective coupling of the SP waves.
 15 Hence, in order to improve the solar selectivity in DMD -based coatings, the main approach
 16 is to use highly absorbing dielectrics where sunlight will be effectively attenuated along with
 17 a metal that have finite optical conductivity. The large optical attenuation in the highly
 18 absorbing dielectric and the infrared reflectivity of the metal give access to high solar
 19 absorptance in solar spectrum and low thermal emittance in the infrared regime.
 20
 21

22 **6. Case studies on dielectric-metal-dielectric-based solar selective absorber** 23 **materials**

24 **6.1. Cr_xO_y/Cr/Cr₂O₃**

25 Chromium (III) oxide is an important refractory material which has been widely studied
 26 in various field over last several decades. Its high melting point (~ 2435 °C) [178], superior
 27 hardness [179], low friction, oxidation and corrosion resistance [180] make it one of the
 28 choice for using as a superior protective coating. It also has been utilised as an intermediate
 29 layer in corrosion-resistant applications on semi-conductors [181] and metals, an active
 30 tunnelling barrier or pinning system for spintronic applications [182]. The attractive optical
 31
 32
 33
 34
 35
 36
 37
 38
 39
 40
 41
 42
 43
 44
 45
 46
 47
 48
 49
 50
 51
 52
 53
 54
 55
 56
 57
 58
 59
 60
 61
 62
 63
 64
 65

1 properties of chromium oxide enable it to use as a pigment powder with high NIR reflectance
2 [183], attenuated phase-shifting masks for deep ultraviolet (UV) lithography. Being thermally
3 stable [184], Cr₂O₃ has a fundamental and practical importance in the UV, visible, and IR
4 regions of the electromagnetic spectrum, Cr - Cr₂O₃-based cermet coatings have been well
5 exploited for photothermal applications [185]. Excellent solar selectivity with a high solar
6 absorptance and low emittance have been obtained from these coatings over a large
7 temperature range. Recently, most of the Cr - Cr₂O₃ solar selective coatings are deposited by
8 reactive direct current (dc) and radio frequency (rf) sputtering technique [110, 186, 187]. The
9 difficulty in the formation of the oxide and the low growth rates limit the use of dc and rf
10 sputtering in depositing Cr-Cr₂O₃ coating [188].

11
12 In response to the growing demand for the industrial use of Cr₂O₃ or black chrome [189,
13 190] in the field of solar selective coating, Barshilia et al. [152] first investigated the
14 feasibility of depositing Cr_xO_y/Cr/Cr₂O₃ -based coating using asymmetric bipolar-pulsed dc
15 generators. They found that Cr_xO_y/Cr/Cr₂O₃ (thickness - 28 nm/13 nm/64 nm) has a very high
16 selectivity with an absorptance of 0.899 – 0.912 and a low emittance of 0.05 – 0.06. The
17 agreement with experimental ellipsometric data with the theoretical models confirms that
18 Cr_xO_y and Cr layers act as main absorber layers, while top Cr₂O₃ serves the role of
19 antireflection coating. The refractive index and extinction coefficient of the layers were
20 explored using Adachi's model for Cr_xO_y and Cr₂O₃ layers while Cauchy's model was used
21 for Cr layer. X-ray diffraction study indicated the amorphous nature of the coating. XPS
22 investigations showed that the state of chromium was in the form of Cr³⁺. They have also
23 studied the thermal stability of the coating in the range of 200 – 400 °C for 2 h. They showed
24 that there was no significant change in absorptance, emittance and surface roughness after
25 heat treatment up to 300°C. At higher temperatures, selective performance degraded
26 drastically due to oxidation of Cr. The XPS and micro-Raman spectroscopy also reveal that

1 Cr metal content was responsible for absorption of solar energy in Cr₂O₃ matrix. As Cr atoms
2 turn into Cr₂O₃ at high temperature, the absorptance decreases. The emittance also increases
3 because of the sudden rise in surface roughness (> 142 nm) of the coating. Not only that, the
4 diffusion of Cu atoms towards the coating leads to form CuO and CuCr₂O₄. Moreover, the
5 differences in thermal expansion coefficient of Cu, Cr and Cr₂O₃ also results the degradation
6 of optical properties and delamination of coating. The coating was shown to be stable for 250
7 hrs at 250 °C in air with an absorptance and emittance of 0.898/0.11. However, the coating
8 was thermally stable up to 500°C while heat treated in vacuum. When the annealing
9 temperature reaches more than 500°C, the absorptance decreases. They also calculated the
10 activation energy required for the degradation using Arrhenius equation which can be
11 presented by the following equation.
12
13
14
15
16
17
18
19
20
21
22
23
24
25

$$26 \ln(\Delta\alpha) = \frac{E_a}{RT} + constant \quad (36)$$

27 where $\Delta\alpha$ is change in absorptance while heat treated at temperature T and R is the
28 universal constant. The activation energy of this coating came out to be 100 kJ/mol using the
29 slope of the $\ln(\Delta\alpha)$ vs $1000/T$ plot (Fig. 9.) i.e. Arrhenius plot for five temperatures (200,
30 250, 300, 325, 350 °C) for longer and 2 hrs durations. However, this study not only
31 demonstrates the fabrication of a novel coating but also addresses the improvements in
32 thermal performance comparison with Cr - Cr₂O₃ –based coating.
33
34
35
36
37
38
39
40
41
42
43

44 **6.2. MgO/Zr/MgO**

45 Magnesium oxide with the rock salt structure [191] has become one of the most
46 representative materials among the oxides due to its wide band gap (7.8 eV), good thermal
47 conductivity [192], an excellent chemical and thermal stability (melting point 2800 °C) [193].
48 These properties enable it to be used in ceramic construction of thermocouples and energy
49 converters [194], thermal shock transducers for electrical insulation [195] and in AC plasma
50 display panel for protecting layer [196]. Not only that, considerable interest has been shown
51
52
53
54
55
56
57
58
59
60
61
62
63
64
65

1 in the use of MgO as a buffer layer for high-temperature superconductor applications [197].

2 Based on the outstanding properties of MgO, it has been chosen as a suitable material for
3 high temperature solar selective absorber coating.
4

5
6
7 Maziere-Bezes et al. [198] first developed Au - MgO solar selective cermet by DC
8 reactive sputtering, and they concluded that a high metallic volume fraction ($f \geq 0.35$) is
9 required to absorb solar radiation. Motivated with this, Nuru et al. [199] fabricated
10 MgO/Zr/MgO –based solar selective coating on Zr-coated SS substrate. The absorptance of
11 the film was found to be 0.92 and the emittance was 0.09. They found that the selective
12 coating formed a banana like columnar structure with an average column length of $17.02 \pm$
13 0.15 nm, as revealed from AFM image (shown in Fig. 10(a)). They also measured the
14 reflectance spectra using SCOUT software by fitting the dielectric constant and the thickness
15 of the coating, Fig. 10(b) indicates that calculated and the measured reflectance spectra
16 matches exactly. The coating exhibited less than 25% reflectance up to a wavelength of 1200
17 nm and after that the reflectance of the coating increases. The thickness of individual layer of
18 the MgO/Zr/MgO/Zr coating was found to be 92.6, 10, 78.3 and 74.8 nm from surface to
19 substrate.
20
21
22
23
24
25
26
27
28
29
30
31
32
33
34
35
36
37
38

39 The coating also exhibited high thermal stability up to 400 °C for 2 hrs in vacuum with a
40 high absorptance of 0.918 and low emittance of 0.10. The absorptance of the coating reduced
41 to 0.893 and thermal emittance increased to 0.12 when heat treated at 500 °C in vacuum. In a
42 separate study, they investigated the thermal stability of the coating in air [200], and was
43 observed that the coating shows efficient performance up to 300 °C in air ($\alpha = 0.91$; $\varepsilon =$
44 0.12). The efficiency of the coating decreased, while heat treated at 400°C for 2 hrs ($\alpha =$
45 0.85 ; $\varepsilon = 0.14$). They performed the heavy Ion ERDA measurement to investigate the reason
46 behind the degradation of the coating and concluded that the loss of oxygen at the surface and
47 an increase in the oxygen content at the Zr base layer/substrate interface caused the failure of
48
49
50
51
52
53
54
55
56
57
58
59
60
61
62
63
64
65

1 the coating. The oxygen content in MgO on top surface decreases due to thermal stress. As a
2 result the metal component of MgO layer, i.e. Mg, a highly reflecting metal, affected the
3 absorptance of the coating. Moreover, the formation of ZrO₂ due to oxidation of Zr metal
4 changed the configuration of the coating from MgO/Zr/MgO to MgO-ZrO₂ matrix. The two
5 transparent dielectric in the coating did not help to absorb the solar energy, and most of the
6 portion of the solar spectrum transmitted through the layer. On the other hand, the metallic
7 interlayer of Zr, no more worked as infrared reflector due to the formation of ZrO₂ and
8 consequently the emittance increased. However, as far as the long-term stability of the
9 coating is concerned, the coating exhibited thermal stability up to 250 °C for 24 hrs. The
10 thermal stability of MgO/Zr/MgO coating have been presented in Fig. 10(c).
11
12
13
14
15
16
17
18
19
20
21
22

23 **6.3. Al₂O₃/Mo/Al₂O₃**

24 A large number of Al₂O₃ -based cermet coatings such as Ni-Al₂O₃ [201], Mo-Al₂O₃
25 [118], Au-Al₂O₃ [202] , Ag-Al₂O₃ [116], W-Al₂O₃ [114], Co-Al₂O₃ [203], Fe-Al₂O₃ [204] and
26 Pt-Al₂O₃ [205] have shown promising selective properties. However, the structure with a
27 metallic layer (Ni, Mo, Al) in between two Al₂O₃ layers have become a versatile and
28 potential structure for successful use as selective coatings in solar thermal system.
29
30
31
32
33
34
35
36
37

38 Schmidt and Park [206] engineered an attractive design of absorber coating consisting
39 of multiple alternate layer of Mo and Al₂O₃, and fabricated it using electron beam
40 evaporation technique. Al₂O₃/Mo/Al₂O₃/Mo/Al₂O₃/Mo/Al₂O₃/Mo –based absorber coating on
41 Mo substrate exhibits high absorptance and emittance of 0.91 and 0.085 at 260 °C in vacuum.
42 The emittance value recorded was 0.16 at 538 °C. Another Al₂O₃/Mo/Al₂O₃ coating on Mo
43 substrate was prepared by Peterson and Ramsey [207], which showed exotic thermal
44 resistance by withstanding 10,000 cycles between 820 and 860 °C. This absorber satisfied a
45 reasonable goal of selectivity with absorptance of 85% and thermal emittance of 11% and
46 22% in 500 °C and 1000 °C respectively. As shown in Fig. 11, there is no change in the
47
48
49
50
51
52
53
54
55
56
57
58
59
60
61
62
63
64
65

1 reflectance spectra even if after heating the sample beyond 500 hrs at 920 °C, which signified
2 extremely good thermal stability of coating. In order to reduce the cost of the entire stack,
3 they replaced the expensive Mo substrate by a Mo coated (thickness 3000 – 6000 Å) stainless
4 steel substrate and studied the thermal stability in vacuum for 1 hr. They found that coating
5 on Mo substrate was stable up to ~ 1050 °C while the coating deposited on stainless steel
6 substrate started degrading at ~ 900 °C due to diffusion of Fe and Cr atoms from substrates to
7 the Al₂O₃/Mo/Al₂O₃ coating. Lifetime of both the coating was estimated using high
8 temperature results. The estimation indicated that the coating on Mo substrate can survive
9 more than 20 years at 800 °C, whereas a longer life time at 400 °C is expected for the coating
10 on Mo coated stainless steel substrate. However, the high temperature stability of the coating
11 in air is lacking in their study.

12
13
14
15
16
17
18
19
20
21
22
23
24
25
26
27 John et al. [208] prepared Al₂O₃/Mo/Al₂O₃ coating by cylindrical magnetron
28 sputtering onto a Mo coated glass and stainless steel substrates. The thickness of the infrared
29 reflector and the diffusion barrier of Mo layer on both the substrates was 80 nm. They
30 prepared different types of coating by varying the deposition condition (Ar environment, i.e.,
31 without presence of O₂ and in Ar + O₂ environment, i.e., with presence of O₂) of the
32 intermediate metallic Mo layer, sandwiched between two Al₂O₃ layers. The Mo layer,
33 deposited in the Ar environment is indicated by Al₂O₃/Mo/Al₂O₃, while the latter is denoted
34 by Al₂O₃/Mo(O)/Al₂O₃. Al₂O₃/Mo/Al₂O₃ coating exhibited hemispherical absorptance and
35 emittance of 0.90 ~ 0.92 and 0.08, respectively whereas Al₂O₃/Mo(O)/Al₂O₃ exhibited 0.94
36 ~ 0.95 and 0.06 – 0.07. It can also be noted that the optimized thickness for Al₂O₃/Mo/Al₂O₃
37 and Al₂O₃/Mo(O)/Al₂O₃ with the highest achievable optical properties are 70 nm/8 nm/70 nm
38 and 90 nm/20 nm/50 nm, respectively. The presence of oxygen in the middle layer i.e. in
39 Mo(O) layer changes the selectivity of multi-layer in such a way so that the coating could not
40 possess selectivity with the optimized thickness of Al₂O₃/Mo/Al₂O₃ stack and there was a
41
42
43
44
45
46
47
48
49
50
51
52
53
54
55
56
57
58
59
60
61
62
63
64
65

1 need of repetitive optimization of thickness for $\text{Al}_2\text{O}_3/\text{Mo(O)}/\text{Al}_2\text{O}_3$ coating . Hence it is clear
2 from the study that a small change in the composition of the individual layer can drastically
3 change the entire property as well as other optimized parameter of the stack. One of the major
4 focus of the study was on to the optical properties of the coating, represented in Fig. 12(a),
5 which clearly showed that the refractive index and extinction coefficient of Mo(O) layer is
6 significantly lesser in the long wavelength in comparison to those of Mo layer, and this was
7 considered the reason for the low emittance of $\text{Al}_2\text{O}_3/\text{Mo(O)}/\text{Al}_2\text{O}_3$ coating.
8
9

10
11
12
13
14
15
16
17 The Al_2O_3 layers were fabricated using two different types of targets, such as reactive
18 sputtering from Al and r.f. sputtering from Al_2O_3 targets. The coatings with reactively
19 sputtered Al_2O_3 layers were thermally stable at 300 °C in air and 400 °C in vacuum. After
20 heat treatment of the coating at 500 °C in vacuum, the distinct Mo layer was completely
21 intermixed with Al_2O_3 layer, which was obtained from Auger depth profile study, presented
22 in Fig. 12(b). On the other hand, the coatings with direct r.f sputtered Al_2O_3 appeared to be
23 stable up to 700 °C in vacuum (see Fig. 12(c). In this case, it was observed that though
24 chromium and iron have diffused from stainless steel surface, they were strongly restrained
25 by Al_2O_3 and there was no intermixing between Mo and Al_2O_3 layers. Hence, the solar
26 selectivity was not affected in high temperature. They concluded that direct r.f sputtered
27 Al_2O_3 provides a superior diffusion barrier. Therefore, it can be stated from these
28 observations that the high temperatures stability of the DMD stack not only depends on the
29 materials but also the method used for deposition. One of the interesting achievement of the
30 study was to use a dielectric layer (r.f. sputtered Al_2O_3 of thickness 50 nm) as a diffusion
31 barrier instead of a metal. The metallic layers as the infrared reflector and diffusion barrier in
32 such coatings are highly appreciated by the scientific community [209, 210]. However,
33 surprisingly Al_2O_3 coating as a diffusion barrier on the stainless steel surface thermally
34
35
36
37
38
39
40
41
42
43
44
45
46
47
48
49
50
51
52
53
54
55
56
57
58
59
60
61
62
63
64
65

1 protected Al₂O₃/Mo/Al₂O₃/Mo coating on Al₂O₃ coated stainless steel substrate in air at 550
2 °C after 14 hrs without any change in the optical properties.
3

4 In a separate study, they fabricated Al₂O₃/M/Al₂O₃/R coatings where M is a semi-
5 transparent absorbing layer and R is a low emittance reflecting layer [211]. The M layers
6 could be different metals, such as Cr, Ni, Mo, Ta. The R layer was of same metal as the M
7 layer. Alike the previous work, they used direct r.f sputtering and reactive sputtering to
8 prepare Al₂O₃ layers. The multilayer absorber coatings were heat-treated in air and vacuum
9 over the temperature range of 300 – 700 °C for periods from 8 to about 1000 hrs. The results
10 of the thermal stability, presented in Table 1, are in good agreement with the previous
11 findings [208] on cylindrical-magnetron-sputtered Al₂O₃/Mo/Al₂O₃ coatings. The coating
12 with r.f sputtered Al₂O₃ layer showed better performance than reactively sputtered Al₂O₃.
13 Hence, it can be confirmed that the deposition procedure is a crucial parameter to improve the
14 thermal stability of CSP systems.
15
16
17
18
19
20
21
22
23
24
25
26
27
28
29
30

31 **6.4. Al_xO_y/Al/Al_xO_y**

32 A well-known example of a DMD absorber is Al_xO_y/Al/Al_xO_y, which has been
33 developed by Barshilia et al. [149] on Cu and Mo substrates using asymmetric bipolar-
34 pulsed DC generators for high-temperature applications. The optimized absorber, with a total
35 thickness of 150 - 170 nm (97 nm of Al_xO_y anti-reflection layer, 15 nm of metallic Al layer
36 and 40 nm of absorber Al_xO_y layer) had a solar absorptance of 0.950-0.970 and thermal
37 emittance of 0.05-0.08. The spectroscopic ellipsometry was used to find out the refractive
38 index and the extinction co-efficient of the individual layer. The ellipsometric data was fitted
39 by Drude's and Tauc Lorentz model, and the fitting confirms the metallic and the dielectric
40 nature of Al and Al_xO_y layers, respectively. Fig. 13 indicates the variation of refractive index
41 (n) and extinction co-efficient (k) with respect to wavelength of Al and Al_xO_y layers. The
42 ellipsometry results reveal the same value of n and k for top and bottom Al_xO_y layers. The n
43
44
45
46
47
48
49
50
51
52
53
54
55
56
57
58
59
60
61
62
63
64
65

1 value of Al_xO_y layer decreases with an increase in wavelength while k value was zero in the
2 whole wavelength range, representing dielectric nature of Al_xO_y [174]. In contrast, there was
3 an increase of n and k value throughout the whole wavelength range for Al, indicating the
4 metallic behaviour of Al. The heat treatment of the coating, deposited on Cu substrate, was
5 carried out in different temperatures for 2 hrs to evaluate the thermal stability. The annealing
6 upto 400 °C in air did not affect the selective property ($\alpha/\varepsilon \sim 0.901/0.06$) of the coating. The
7 spectral and structural degradation was found at $T > 450$ °C ($\alpha/\varepsilon \sim 0.790/0.07$). The structural
8 delamination was confirmed by the Raman spectroscopy in Fig. 14. Two Raman peaks of
9 CuO at 211 and 291 cm^{-1} are an indication of outward diffusion of Cu substrate. However,
10 they found different reasons behind the degradation of optical properties at high temperature,
11 such as oxidation of Cu substrate, formation of $CuAl_2O_4$ compound due to intermixing of Cu
12 and Al in high temperature, the transformation of nanocrystalline Al to metastable aluminium
13 oxide, and differences in thermal expansion coefficient of Al ($24 \times 10^{-6}/^{\circ}C$), Al_2O_3 ($8.1 \times 10^{-6}/^{\circ}C$)
14 and Cu ($16.5 \times 10^{-6}/^{\circ}C$) substrates.

15 Thermal stability of the coating deposited on Mo substrate in vacuum was also
16 investigated. After annealing at 800 °C for 2 hrs in vacuum, though the solar absorptance
17 decrease, thermal emittance of the coating also decreased ($\Delta\alpha = -0.004$; $\Delta\varepsilon = -0.04$). The
18 solar absorptance decreased and thermal emittance increased a lot when heat treated at 900
19 °C ($\Delta\alpha = -0.246$, $\Delta\varepsilon = 0.004$). Accelerated aging test of the coating on Cu substrate suggested
20 that the coating was efficient even after heat treatment up to 200 and 75 hrs at 250 ($\Delta\alpha = -$
21 0.022 ; $\Delta\varepsilon = 0$) and 300 °C ($\Delta\alpha = -0.031$; $\Delta\varepsilon = 0$), respectively. A performance criterion
22 function (PC) for domestic hot water system has been defined by the International Energy
23 Agency Solar Heating and Cooling Program (IEASHC) Task X,

$$24 \quad PC = -\Delta\alpha + 0.25\Delta\varepsilon < 0.05 \quad (37)$$

1 The change in the absorptance and emittance after performing the accelerated aging tests
2 confirmed service life time of at least 25 years for $\text{Al}_x\text{O}_y/\text{Al}/\text{Al}_x\text{O}_y$ coating. They have also
3
4 calculated the activation energy for the degradation of the multilayer stack using Arrhenius
5 equation (equation 36), and determined it to be 64 KJ/mole.
6
7

9 **6.5. $\text{Al}_x\text{O}_y/\text{Pt}/\text{Al}_x\text{O}_y$**

10
11
12 Despite the fact that Pt is expensive, the good electrical conductivity, unreactive
13 chemical behaviour and corrosion resistance of Pt made it one of the choices for the metallic
14 layer of $\text{Al}_x\text{O}_y/\text{Pt}/\text{Al}_x\text{O}_y$ stack. Nuru et al. reported a series of observations [209, 212-216] on
15
16
17
18
19
20
21
22
23
24
25
26
27
28
29
30
31
32
33
34
35
36
37
38
39
40
41
42
43
44
45
46
47
48
49
50
51
52
53
54
55
56
57
58
59
60
61
62
63
64
65

Al_xO_y/Pt/Al_xO_y stack. In one of their studies [212], they used electron beam evaporation technique to successfully deposit the coating onto 1737 corning glass, silicon (111) and copper substrates. They also demonstrated that the thickness is a very important criterion to be a selective absorber coating. They have noticed a decrease in the refractive index of top and bottom Al_xO_y layer with a decrease in the thickness and increase in wavelength (Fig. 15(a) & (b)). However, the extinction coefficient remains unchanged with a constant value of zero in overall wavelength range, suggesting the dielectric behaviour of Al_xO_y layer. In contrary, the refractive index of Pt layer increases with increasing wavelength and thickness, while extinction co-efficient decreases with an increase in thickness which confirms the semi-transparent nature of Pt metal {see Fig. 15(c) and 15(d)}. Moreover, the refractive index of the top Al_xO_y layer is lesser than that of Pt layer revealing the anti-reflection property of the top Al_xO_y layer. They have also investigated the change in the reflectance spectra by varying the thickness of individual layer. They found that an increase of top Al_xO_y layer thickness leads to high reflectance in visible region along with a shift to higher wavelengths. In addition, more number of interference peaks appeared in the visible region. The thicker Al_xO_y layer (900 Å) helped to absorb more sunlight by shifting the reflectance spectra towards higher wavelength side, which can be seen in Fig. 16(a). For base Al_xO_y layer, the reflectance

1 decreases monotonically with an increase in thickness from 100 to 400 Å, and an interference
2 peak is observed in the lower wavelength regime at the thickness of 500 and 600 Å in Fig.
3
4
5 16(b). The optimised thickness was found to be 900 Å for the Al_xO_y top layer, 70 Å for the
6
7 middle Pt layer and 400 Å for the base Al_xO_y layer to achieve highest selectivity. They
8
9 determined the thickness using the Rutherford backscattering spectrometer (RBS). The
10
11 coating exhibited a high solar absorptance of $\alpha = 0.94 \pm 0.01$ and thermal emittance of $\varepsilon =$
12
13 0.06 ± 0.01 . XRD study suggested the amorphous nature of Al_xO_y while the SEM study
14
15 showed that flake like morphology of the multilayer stack consists of the Pt nano particles
16
17 with an average diameter and interparticles distance of 146 and 6-10 nm, in and between the
18
19 rims of Al_xO_y [213]. The surface roughness (6.5 ± 0.13 nm) of the stack was found to be
20
21 comparable to the interparticle distance. The optical constants (refractive index and extinction
22
23 coefficient) were measured to confirm the metallic and dielectric property of Pt and Al₂O₃,
24
25 respectively, in different thickness by ellipsometry measurements. Using the optical constants
26
27 for different thicknesses as input, the reflectance spectra of the multilayer was computed in
28
29 an optical spectrum simulation program SCOUT. The simulated and the experimental
30
31 reflectance spectra of the coating shown in Fig. 16(c) are in good agreement with each other.
32
33
34
35
36
37
38
39
40
41
42
43
44
45
46
47
48
49
50
51
52
53
54
55
56
57
58
59
60
61
62
63
64
65

The absorptance and emittance value along with the reflectance spectra confirms the potential
of Al_xO_y/Pt/Al_xO_y as good absorber.

The heat treatment of the coating shows that the coating is thermally stable up to 500
°C in air with solar selectivity 0.951/0.09 [214]. The SEM images of the coating, shown in
Fig. 17 suggests that the size of the Pt nanopartilces increases with temperature and the
particles agglomerate at the temperature more than 500 °C. As a result, the surface roughness
of the coating also increases. The agglomeration of Pt particle and formation of CuO and
Cu₂O due to surface diffusion leads to degradation of the selective property of the coating
(0.846/0.11). The high temperature heat treatment also caused a decrease in the constituents

1 of the absorber coating, which was confirmed by heavy ion elastic recoil detection analysis
2 [215]. The reflectance spectra of the coating, heat treated at 600 and 700 °C in Fig. 18(a)
3 shows a huge deviation from that of as-deposited coating. However, long temperature
4 stability study showed that the coating is stable up to 450 °C in air for 24 hrs (see Fig 18 (b)).
5
6

7
8
9 To improve the thermal stability further in a separate study, Nuru et al. [209] used
10 Tantalum layer as a diffusion barrier on top of copper substrate. The incorporation of Ta layer
11 increased the stability of the coating up to 700 °C for 2 hrs and the coating showed superior
12 selectivity with absorptance of 0.932 and emittance of 0.10. When the long term thermal
13 stability experiment was performed they found that the Ta/Al_xO_y/Pt/Al_xO_y is stable upto 550
14 °C for 24 hrs.
15
16

17
18
19 In a separate study, Nuru et al. [216] studied the effect of substrate temperature on
20 selective property of e-beam evaporated Al_xO_y/Pt/Al_xO_y coating . They have observed that the
21 particle size and the roughness of the coating increase when the substrate temperature has
22 been changed from room temperature to 50, 100, 150 and 250 °C. The reason behind this can
23 be attributed to the distant migration of the atoms which causes formation of denser grains
24 and larger particles. As a result the solar absorptance of the coating decreases and the
25 reflectance spectra shift towards shorter wavelength. Hence, it is evident from the study that
26 substrate temperature during deposition is also a prime factor to reach the spectral selectivity.
27
28
29

30 **6.6. Al_xO_y/Ni/Al_xO_y**

31
32
33 Tsai et al. [217] proposed that the configuration of three layer coatings consists of a metal
34 Ni layer in between two Al_xO_y layer. The Al_xO_y/Ni/Al_xO_y coating was deposited on a
35 stainless-steel substrate using reactive DC magnetron sputtering. They investigated a group of
36 samples to study the influence of target power and oxygen flow in the structure, surface
37 morphology and chemical composition of the film. The Al_xO_y coatings deposited using
38 various DC powers and oxygen flow rates are represented as A (DC power/oxygen flow rate).
39
40
41
42
43
44
45
46
47
48
49
50
51
52
53
54
55
56
57
58
59
60
61
62
63
64
65

1 The transmission electron microscopy images in Figs. 19(a), (b) & (c) suggest that the
2 coating deposited with lower oxygen flow rate (2 sccm) are loose and the surface of the
3 coatings were rough, whereas the coating prepared in higher oxygen flow rate (8 sccm)
4 appears to be very dense and the film surface is also very smooth. In addition, they observed
5 that the film surface had become looser and rougher with an increase in target power from
6 150 W to 250 W. An increase in sputtering power and decrease in oxygen flow rates result
7 an increase in Al_xO_y deposition rate. Therefore, the reason behind the difference surface
8 morphology and density of the film may be caused due to difference in the deposition rates.
9

10 In addition, XRD study showed that the structure of all the coatings were amorphous as
11 the crystallization temperature of Al_2O_3 is more than 900 °C. The diffraction pattern in Fig.
12 19(d), obtained from transmission electron microscopy is also in good agreement with the
13 XRD study. The transmission spectra of the coating in Fig. 20 suggested that the loose
14 coating with voids showed less transmission than the dense coatings, which indicates the
15 voids and loose pattern helps in increasing the light absorption.
16

17 They also investigated the effect of different thickness in the optical properties of the
18 coatings. To satisfy the criterion of destructive interference for light absorption, the optical
19 thickness, i.e. (refractive index \times film thickness) of the coating, should be quarter of incident
20 wavelength. The thickness of the top layers were kept at 90 nm, 70 nm and 40 nm. The
21 coating SS/ Al_xO_y (70 nm)/Ni (20 nm)/ Al_xO_y (70 nm) exhibited highest selectivity among all
22 other coatings with an absorptance of 0.932 and emittance of 0.038. The coating, deposited
23 in the operating condition of 150W power and 8 sccm O_2 flow, exhibited thermal stability at
24 least up to 12 hrs at 400 °C.
25

26 **6.7. $HfO_x/Mo/HfO_2$**

27 Different properties of hafnium oxide (HfO_2) are being currently investigated with
28 great interest in various applications such as semiconductor devices [218], electronics [219],
29
30
31

1 thermal barrier for turbine blades [220], high power lasers [221], waveguides [222] etc, due
2 to its high dielectric constant ($k \sim 25$) [223], wide band gap ($E_g \sim 5.8$ eV) [224], high
3 refractive index (1.85 - 2.15) [225, 226], transparency over a wide range of wavelength,
4 extending from UV (200 nm) to near-IR range (1.2 μm) [227], low chemical reactivity and
5 high structural stability [228], excellent thermal stability [229], good abrasion/scratch
6 resistance and hardness [230]. The HfO_2 coating have also been explored in various optical
7 applications like anti-reflection coating [231], UV mirrors with a high damage threshold
8 [232], optical filters [233], heat-mirrors in energy-efficient windows [234], astronomically
9 charged couple devices [235] etc., because of anti-reflection property, high reflectance in IR
10 region, high melting point (2800 $^\circ\text{C}$) [229] and the hydrophobic property of HfO_2 [236].

24 Barshilia et al. [153] explored $\text{HfO}_x/\text{Mo}/\text{HfO}_2$ as a promising solar selective absorber
25 coatings. Unlike other DMD film, the top stoichiometric HfO_2 layer allows the sunlight to
26 reach to MO surface, whereas non stoichiometric HfO_x layer helps to absorb solar radiation.
27 The coating was deposited on Cu and SS substrate using a DC unbalanced magnetron
28 sputtering. Optimized film on Cu substrate exhibited high absorptance (0.905 - 0.923) and a
29 low thermal emittance (0.07 - 0.09), while films on SS substrate had absorptance of ~ 0.902 -
30 0.917 and emittance of ~ 0.15 - 0.17. The coating was thermally stable up to 400 $^\circ\text{C}$ for 2 hrs
31 in air. The selective property of the coating entirely lost ($\Delta\alpha = -0.111$ and $\Delta\varepsilon = +0.05$) after
32 heat treatment at 425 $^\circ\text{C}$ in air due to diffusion of copper into the coating and formation of
33 CuO . In order to enhance thermal stability, an additional Mo layer of thickness 40 nm was
34 introduced on Cu substrate. The improvement in the thermal stability was reasonable after
35 deposition of Mo layer as it acted as a diffusion barrier. The $\text{Mo}/\text{HfO}_x/\text{Mo}/\text{HfO}_2$ coatings on
36 both Cu and SS substrate were thermally stable up to 500 $^\circ\text{C}$ in air and 800 $^\circ\text{C}$ in vacuum.
37 However, the coating degraded at 525 $^\circ\text{C}$ in air due to oxidation and phase transformation of
38 Mo and formation of unwanted impurities such as MoO_2 , MoO_3 , and HfMo_2O_8 .

6.8. MgF₂/Mo/MgF₂

1
2
3 In 1965, Schmidt and Park [206] prepared some interesting coating in different
4 combinations of MgF₂, CeO₂ and Mo by electron beam evaporation techniques. The
5 absorptance and emittance measurements were performed at 260 and 538 °C in vacuum.
6
7 MgF₂/Mo/MgF₂/Mo/MgF₂ -based absorber coating on Mo substrate possesses high
8
9 absorptance of 0.89 and low emittance of 0.075 while MgF₂/Mo/CeO₂ coating had
10
11 absorptance and emittance of 0.85 and 0.053, respectively. A high absorptance of 0.85 and
12
13 low emittance of 0.073 have been achieved by MgF₂/CeO₂/Mo/MgF₂/CeO₂ -based absorber
14
15 coating. All the aforementioned absorptance and emittance value was collected at 260 °C in
16
17 vacuum. At 538 °C, the emittance value for all these coatings increased while absorptance
18
19 was constant. The emissivity of the coating increased slightly to 0.090 at 538 °C while the
20
21 absorptance was constant.
22
23
24
25
26
27
28

29 Sergeant [53] modelled a DMD multilayer stack in very interesting way using the
30 standard transfer matrix method where MgF₂ and TiO₂ with refractive index 1.37 and 2.75 at
31
32 1 μm respectively, served the function of dielectrics in the same coating, while Mo and W
33
34 was used as the metal substrate as well as metallic layer, sandwiched between dielectrics. The
35
36 combination of MgF₂ and TiO₂ was preferred as dielectric due to contrast in their refractive
37
38 index ($\Delta n = 1.38$; $\lambda = 1 \mu\text{m}$) and high thermal resistance. Two sets of four DMD coatings
39
40 made of Mo, MgF₂, TiO₂ and W, MgF₂, TiO₂ with no of layers = 5,7,9,11 have been
41
42 optimised at 720K. The coating structures are presented in Fig. 21 and Fig. 22. The metal
43
44 substrate W or Mo is counted as L = 1. The optimized coating exhibited high solar
45
46 absorptance (> 94%) in the wavelengths shorter than 2.24 μm, and low absorption (< 7%) in
47
48 the wavelength beyond 2.24 μm which is shown by Fig. 23(a) & Fig. 23(b). They have also
49
50 demonstrated that the merit function of the absorber coating (see Eq. 11) increases with
51
52 increasing the number of layers up to L=11, which is presented in Fig. 23(c). However, the
53
54
55
56
57
58
59
60
61
62
63
64
65

1 performance saturates while the number of layers exceed than 11. If the number of layers is
2 increased more than 11, an increase in emittance has been observed due to thicker coating.
3
4 The angular spectral selectivity of both the DMD absorbers have been studied and the
5 coatings have a wide angular absorption. The wide angle absorption along with high
6 selectivity and thermal stability indicates the coatings as a potential candidate for CSP
7 applications.
8
9

10
11
12 We have attempted to give the reader an overview of the research findings on the DMD -
13 based solar selective absorber coatings till date in detail. DMD-based absorber coatings show
14 their significant potential as a different class of solar selective absorber coatings; their
15 exceptional attraction lies on the thin film design with a combination of metal and dielectric
16 layers. Table (2-4) summarize the absorptance, emittance, short and long term thermal
17 stability in air and vacuum of the DMD –based absorber coatings studied using different
18 deposition techniques or modelling method. It can be commented that further advancements
19 in DMD –based absorber coating can be made to obtain selectivity like an ideal solar
20 selective absorber.
21
22
23
24
25
26
27
28
29
30
31
32
33
34
35

36 **7. A way forward towards subwavelength texturing of DMD stack**

37
38
39 So far we have discussed about different solar selective absorber coatings based on DMD
40 configuration. Even though the coatings are extremely effective, a common feature of the top
41 dielectric layers is their higher refractive index than air. Therefore, these materials in a planar
42 form inevitably produce a strong, undesired loss of sunlight in air/dielectric interface, because
43 of Fresnel reflection [237]. Based on the strong light concentration and scattering properties,
44 light-trapping layers employing metallic nanostructures have gained significant attention over
45 the past decade [238, 239]. It can be an interesting idea to combine the DMD stack with a
46 proper light-trapping texture at a subwavelength scale on the dielectric surface to manipulate
47 light absorption by suppressing Fresnel reflection over a wide range of wavelengths. The
48
49
50
51
52
53
54
55
56
57
58
59
60
61
62
63
64
65

1 texturing of the surface may include V-shaped groove, nanowires, particles, voids, dual-
2 diameter nanopillars, nanocones and domes, etc., which support strong optical resonances
3 that can enhance and effectively control broad-band light absorption as well as scattering
4 processes. In Fig. 24, we have shown a comparison between the flat surface with an ideal
5 textured surface of 45°. The later configuration gives the incident light an opportunity to
6 interact with the surface for a second time [237]. A careful engineering of the texture designs
7 with proper size and shape will allow very strong optical resonances that can further boost
8 light–matter interaction compared to flat surfaces [240]. This light trapping concept offers a
9 great flexibility and tunability and can be extended for use in many other applications. The
10 texturing of the surface have already enabled performance improvement in crystalline silicon
11 (c-Si) solar cells and nanoscale optoelectronic devices [241, 242]. With the advances in
12 nanofabrication techniques over the past decade, such structures now can be synthesized by
13 inexpensive, scalable deposition or wet-chemical etching techniques and can provide high
14 efficiency at extremely low cost. It can be anticipated that the implementation of textured
15 surface in DMD stack can spark a wave of new research aiming to reach the highest selective
16 performance by utilizing the incident solar radiation more efficiently.
17
18
19
20
21
22
23
24
25
26
27
28
29
30
31
32
33
34
35
36
37
38

39 **8. Outlook and future directions**

40
41 It is evident from the review that the research on solar selective absorber coating is a
42 dynamic field, whose significance and industrial viability will undoubtedly progress in the
43 future. The DMD -based absorber coatings have accomplished the desired selective property
44 close to an ideal solar selective absorber coating as serious research has been conducted on it
45 in recent decades.
46
47
48
49
50
51

52
53 The confinement of electromagnetic wave using a plasmonic geometry DMD stack
54 introduces many advantages for the conversion of solar energy to thermal energy as well as
55 the thermal stability of the coating. Researchers have exploited the ellipsometry
56
57
58
59
60
61
62
63
64
65

1 measurements to identify the metallic or dielectric nature of individual layer of DMD –based
2 solar selective absorber coatings. However, more attention should be paid theoretically and
3
4 experimentally to explore the underlying physical mechanisms that govern the excellent
5
6 selectivity of the coatings rather than demonstrating the metallic and dielectric properties. In
7
8 fact, the in depth study will help to carefully design an absorber consisting of multiple
9
10 numbers of periodic metal and dielectric layers. It has been reported that a dielectric layer
11
12 with very high refractive index ($n_d > 2$) and a relatively thick metal layer can satisfy a “zero
13
14 reflection condition”, i.e. highest absorptance [170]. Therefore, it is proposed to investigate
15
16 the selection of proper combination of the metals and dielectrics to boost the absorptance
17
18 properties.
19
20
21
22
23

24 Despite the fact that there are number of DMD -based absorber coatings, their
25
26 practical applications in the actual field still remain a challenge and are liable to numerous
27
28 other important properties. In this regard, it should be prime aim to concentrate on their
29
30 corrosion resistance, scratch resistance, hardness, abrasion, hydrophobic nature and
31
32 performance in humid environment. A year round performance assessment in different
33
34 climatic conditions is required to prove reliability and weather proofing capability of the
35
36 absorbers. While evaluating the annual performance and designing the operational strategy,
37
38 one needs to take into account the variation of solar radiation in different time throughout the
39
40 year.
41
42
43
44
45

46 The optical absorptance in DMD coating is enhanced due to the surface plasmon
47
48 polaritons in the metal-dielectric interface. In order to boost the absorptance further, an
49
50 intriguing approach could be to stack multiple metal dielectric layers in alternative way. It is
51
52 essential to take into account optical constants of the metals and dielectric components of the
53
54 multilayer DMD coating over a wide wavelength range. Furthermore, theoretical absorptance
55
56 and emittance is needed to explore before starting experimental procedures.
57
58
59
60
61
62
63
64
65

1
2
3
4
5
6
7
8
9
10
11
12
13
14
15
16
17
18
19
20
21
22
23
24
25
26
27
28
29
30
31
32
33
34
35
36
37
38
39
40
41
42
43
44
45
46
47
48
49
50
51
52
53
54
55
56
57
58
59
60
61
62
63
64
65

To develop a highly efficient CSP system, it is also required to investigate how the incident angle of solar radiation can change the optical properties of the absorber coating [97]. The slight change in incident angle can introduce a large variation in optical thickness as well as phase difference between incident and reflected rays, which cause a noticeable difference in the reflectance spectra of absorber coating [170]. Hence, the sensitive angular dependence of the absorber coating should be unveiled before practical application of it in CSP plants.

In current research trend of developing solar selective materials, another issue is the high temperature stability, which is of extreme significance. The prolonged exposure under concentrated solar radiation is likely to provoke substrate-absorber layer inter diffusion, and consequently, modify layer interfaces, compositions and optical properties. Therefore, attractiveness lies in choosing the reliable materials which should yield high melting point and high activation energy for oxidation.

Another strategy is to introduce a metallic diffusion barrier in between the absorber coating and the substrate [243]. This layer hinders metal atoms from entering the absorber layer at high temperatures and prevents the change in optical properties of the coating. The substrate diffusion can also be restricted by pre-heat treatment of stainless steel in air before depositing any layer. In terms of long term durability under high temperature conditions, the single dielectric layer on top of the coating is vulnerable. Inclusion of another dense anti-reflection layer on top of the dielectric will protect the film by preventing oxidation from the surroundings [201]. Along with the anti-reflection properties, the top layer should have extremely high hardness and scratch resistance property [244, 245], so that the entire stack can be handled easily.

Most published studies on DMD based coating were focused on new design concepts of the metal dielectric stack, investigation on optical properties and the thermal stability of

1 the coating. However, none of the papers have mentioned the economic analysis or LCOE
2 (levelized cost of electricity) [246] using these coatings. The lack of such important
3 information would lead to uncertainty and confusion in the scientific community. It may also
4 be an interesting approach to calculate the LCOC (levelized cost of coating) to compare the
5 selectivity of different alternative coating as a function of durability. Therefore, it is of utmost
6 importance to provide a possible description on cost analysis which may be helpful for initial
7 commercialization of the film.
8
9

10
11
12
13
14
15
16
17 It is also worth noting that although the magnetron sputtering technique is
18 exceptionally attractive for fabricating DMD coating, the essential problem of this method is
19 the high cost due to the advanced system and energy consumption. There should be an
20 optimum balance between efficiency, durability, high temperature stability, costs and the
21 manufacture procedure for large scale applications [247]. To address this issue, it is
22 necessary to fabricate the DMD coatings by cost-effective wet chemistry route. However, it
23 has been noted that wet chemistry route can produce high surface roughness, non-uniformity
24 and defect on the coating, which result a low solar selective property [248]. Hence, many
25 technical limitations need to overcome before developing potential DMD coating by cheap
26 and moderately efficient wet-chemistry method as most of the coatings prepared by this
27 techniques exhibit less selectivity and low thermal stability. Appropriate understanding on
28 thin-film deposition procedures can help in accomplishing highly efficient selective coating,
29 which can be demonstrated commercially in different CSP systems. To further promote and
30 engineer new, exotic and more efficient coating structures, a number of approaches can be
31 pursued by utilizing the basic principles of physics and chemistry.
32
33
34
35
36
37
38
39
40
41
42
43
44
45
46
47
48
49
50
51
52

53 It is also exceptionally fascinating to study which deposition technique or which
54 absorber structure will at last succeed commercially. However, it would unquestionably be
55 dictated by the straightforwardness of manufacturability and expense of the power per watt.
56
57
58
59
60
61
62
63
64
65

1 The DMD –based solar selective coatings can also be utilized in a proficient thermo-
2 photovoltaic system, an integrated system combining a solar photovoltaic and solar thermal
3 panel. In such systems, the DMD-based absorber will confine the sun rays, heat up, and emit
4 towards a solar cell a narrow-banded spectrum directly above the band-gap of the solar cell.
5
6
7

8
9 In summary, it will be interesting to perceive how the performance and applications of
10 DMD-based absorber coatings evolve in terms of cost, reliability of the materials, testing
11 requirements, market strength, and most importantly the constant demand on renewable
12 energy along with enormous research effort to make the CSP system competitive with the
13 conventional power generation. It can be anticipated that the combined efforts into the
14 further progress on fabrication procedures, structure and material optimization, energy
15 conversion and effectiveness, performance testing will have significant impact in developing
16 superior DMD -based absorber coatings.
17
18
19
20
21
22
23
24
25
26
27

28 **9. Conclusions**

29 In this paper, we have made an attempt to discuss various types of solar selective absorber
30 coatings including intrinsic absorbers, semiconductor absorbers, multilayer absorbers,
31 cermet or metal-dielectric absorbers, textured surface, with emphasis on dielectric – metal –
32 dielectric absorbers (DMD). Undoubtedly DMD -based coatings are a promising approach in
33 energy conversion from abundant solar energy to thermal energy. From our perspective, the
34 beneficial effects associated with SPP have proven DMD stack as universal and versatile
35 plasmonic structure to concentrate the entire solar spectrum and to meet the growing demand
36 of low-cost, environment friendly solar energy. The DMD absorbers cover a vast number of
37 materials from different metals (Cr, Zr, Mo, Al, Pt, Ni) to dielectrics (Cr₂O₃, MgO, Al₂O₃,
38 HfO₂, MgF₂). These coatings offer a wide variety of choices in terms of the optical properties
39 of different metals and dielectrics. Such adaptability permits customizing and designing the
40 coating as well as aims at enhancing the spectral performance. As high temperature stability
41
42
43
44
45
46
47
48
49
50
51
52
53
54
55
56
57
58
59
60
61
62
63
64
65

1 is concerned, some crucial changes are needed to acquire the desired performances of the
2 coatings. Therefore, we anticipate that increasing number of studies on DMD-based coating
3 are needed as there is adequate room for good and innovative work to design industrially
4 accessible specific coatings. Furthermore, we believe, this review will bridge the literature
5 gap on DMD -based solar absorber coatings and point a way towards the future of renewable
6 energy.
7
8
9
10
11
12
13

14 **Acknowledgements**

15
16 This paper is based upon work supported in part under the US-India Partnership to
17 Advance Clean Energy-Research (PACE-R) for the Solar Energy Research Institute for India
18 and the United States (SERIUS), funded jointly by the U.S. Department of Energy (Office of
19 Science, Office of Basic Energy Sciences, and Energy Efficiency and Renewable Energy,
20 Solar Energy Technology Program, under Subcontract DE-AC36-08GO28308 to the National
21 Renewable Energy Laboratory, Golden, Colorado) and the Government of India, through the
22 Department of Science and Technology under Subcontract IUSSTF/JCERDC-SERIUS/2012
23 dated 22nd Nov. 2012. Atasi Dan thanks DST for providing INSPIRE scholarship.
24
25
26
27
28
29
30
31
32
33
34
35
36
37
38
39
40
41
42
43
44
45
46
47
48
49
50
51
52
53
54
55
56
57
58
59
60
61
62
63
64
65

Table 1: Thermal stability of Al₂O₃/M/Al₂O₃/R coating in air and vacuum [211]

Coatings	Thermal stability			
	In air		In vacuum	
	Stable (°C)	Failure (°C)	Stable (°C)	Failure (°C)
M ≡ Cr ; R ≡ Cr Reactively sputtered Al ₂ O ₃ , Cold	—	300	—	350 - 400
R.f sputtered Al ₂ O ₃ , Cold	450	500		
R.f sputtered Al ₂ O ₃ , hot	500	550	650 – 700	—
M ≡ Mo; R ≡ Mo Reactively sputtered Al ₂ O ₃ , Cold	400	400 - 450	400	450-500
Reactively sputtered Al ₂ O ₃ , hot	500	—		
R.f sputtered Al ₂ O ₃ , Cold	500 - 550	—		
R.f sputtered Al ₂ O ₃ , hot	500 - 550	—	650-700	—
M ≡ Ni; R ≡ Ni Reactively sputtered Al ₂ O ₃ , Cold	350	400	400	450
Reactively sputtered Al ₂ O ₃ , hot	400	400-500		
R.f sputtered Al ₂ O ₃ , Cold	400	450		
R.f sputtered Al ₂ O ₃ , hot	500	550	650 – 700	—
M = Ta; R = Ta				
Reactively sputtered Al ₂ O ₃ , Cold	—	350		

Table 2: Optical properties and thermal stability of dielectric-metal-dielectric (DMD) -based absorber coatings deposited by sputtering

Coatings	Substrate	Thickness (nm) (bottom to top)	Deposition method	Absorptance (α)	Emittance (ϵ)	Thermal stability				References
						Short-term		Long term		
						air	vac	air	vac	
Cr _x O _y /Cr/Cr ₂ O ₃	Cu	28 /13/ 64	Reactive DC sputtering	0.899 – 0.912	0.05 – 0.06	300 °C, 2 hrs	500 °C, 2 hrs	250 °C, 250 hrs	-	[152]
Al _x O _y /Al/Al _x O _y	Cu, Mo	40/15/97	Reactive DC magnetron sputtering	0.950 - 0.970	0.05 - 0.08	400 °C, 2hrs	800 °C, 2hrs	250 °C, 200 hrs 300 °C, 25 hrs	-	[149]
Al _x O _y /Ni/Al _x O _y	SS	70/20/70	Reactive DC sputtering	0.932	0.038	-	-	400 °C, 12 hrs	-	[217]
HfO _x /Mo/HfO ₂	Cu	26/31/67	Reactive DC sputtering	0.905-0.923	0.07-0.09	400 °C, 2hrs	-	-	-	[153]
Mo/HfO _x /Mo/HfO ₂	Cu	Mo interlayer ~ 40 nm	Reactive DC sputtering	''	''	500 °C, 2hrs	-	800 °C, 2hrs	-	[153]
HfO _x /Mo/HfO ₂	SS	-	Reactive DC sputtering	0.902-0.917	0.15-0.17	-	-	-	-	[153]
Mo/HfO _x /Mo/HfO ₂	SS	Mo interlayer ~ 40 nm	Reactive DC sputtering	''	''	500 °C, 2hrs	-	800 °C, 2hrs	-	[153]

Table 3: Dielectric-metal-dielectric (DMD) -based solar selective absorber coatings fabricated by e-beam and vacuum evaporation techniques

Coatings	Substrate	Thickness (nm) (bottom to top)	Deposition method	Absorptance (α)	Emittance (ϵ)	Thermal stability				References
						Short term		Long term		
						air	vac	air	vac	
MgO/Zr/MgO	Zr coated SS	78.3/10/92.6	e-beam evaporation	0.92	0.09	300 °C, 2 hrs	400 °C, 2 hrs	250 °C, 24 hrs	-	[199, 200]
Al ₂ O ₃ /Pt/Al ₂ O ₃	Cu	40/7/90	e-beam evaporation	0.94 ± 0.01	0.06 ± 0.01	500 °C, 2hrs	-	450 °C, 24 hrs	-	[212, 214]
Ta/ Al ₂ O ₃ /Pt/Al ₂ O ₃	Cu	40/7/90	e-beam evaporation	0.940	0.09	700 °C, 2hrs	-	550 °C, 24 hrs	-	[209]
MgF ₂ /Mo/CeO ₂	Mo	-	e-beam evaporation	0.85	0.053 (260 °C), 0.062 (538 °C)	-	538 °C	-	-	[206]
MgF ₂ /Mo/MgF ₂ /Mo/MgF ₂	Mo	-	e-beam evaporation	0.89	0.075 (260 °C), 0.090 (538 °C)	-	538 °C	-	-	[206]
MgF ₂ /CeO ₂ /Mo/MgF ₂ / CeO ₂	Mo	-	e-beam evaporation	0.85	0.073 (260 °C), 0.084 (538 °C)	-	538 °C	-	-	[206]
Al ₂ O ₃ /Mo/Al ₂ O ₃ /Mo/Al ₂ O ₃ /Mo /Al ₂ O ₃ /Mo	Mo	-	e-beam evaporation	0.91	0.085 (260 °C) 0.016 (538 °C)	-	538 °C	-	-	[206]
Al ₂ O ₃ /Mo/Al ₂ O ₃ /Mo/Al ₂ O ₃ /Mo /Al ₂ O ₃	Mo	-	e-beam evaporation	0.91	0.085 (260 °C), 0.16 (538 °C)	-	-	-	-	[206]
Al ₂ O ₃ /Mo/Al ₂ O ₃	Mo	Mo ~ 200 Å	Vacuum evaporation	0.85	0.11 (500 °C), 0.22 (1000 °C)	-	1050 °C, 1 hr	-	920 °C, 500 hrs	[207]
Al ₂ O ₃ /Mo/Al ₂ O ₃	Mo (3000 - 6000 Å) coated SS	Mo ~ 200 Å	Vacuum evaporation	-	-	-	900 °C, 1 hr	-	-	[207]

Table 4: Optically modelled Dielectric-metal-dielectric (DMD) -based solar selective absorber coatings

Coatings	Substrate	Thickness (nm) (bottom to top)	Modelling method	Absorptance (α)	Emittance (ϵ)	Thermal stability				References
						Short term		Long term		
						air	vac	air	vac	
Mo/TiO ₂ /MgF ₂ (No of layers: 11)	Mo	-	Transfer matrix approach	0.94	0.06 (447 °C)	Short term	Long term	-	-	[53]
W/TiO ₂ /MgF ₂ (No of layers: 11)	W	-	Transfer matrix approach	0.95	0.06 (447 °C)	air	vac	air	vac	[53]

Appendix I

List of symbols

Symbol	Definition
α	solar absorptance
ε	thermal emittance
λ	wavelength
$G_{\lambda,abs}$	absorbed radiation
G_{λ}	incident radiation
$E_{b\lambda}$	radiant energy from a black body
c	speed of light
h	Planck's constant
k_B	Boltzmann's constant
T	temperature
σ	Stefan-Boltzmann constant
E_g	band gap
$\eta_{sol-ther}$	solar to thermal conversion efficiency
C_{annual}	total annualized coating costs
$E_{thermal}$	average annual energy absorbed
C	solar concentration ratio
I	solar flux density
ε^{MG}	average dielectric functions of the composite in MG approximations
ε^{BR}	average dielectric functions of the composite in BR approximations

ϵ_A	dielectric function of metal
ϵ_B	dielectric function of ceramic
f_A	volume fraction occupied by metal
μ	combined density of state mass
$E_v(\mathbf{k})$	energy of valance band
$E_c(\mathbf{k})$	energy of conductance band
$P_{cv}(\mathbf{k})$	momentum matrix element between valance and conduction band states
E_O	peak transition energy
A_L	strength of the transition
C_L	broadening of the transition
n	refractive index
k	extinction co-efficient
ϵ_M	complex dielectric constant of metal
ϵ_∞	high-frequency component of the dielectric constant
ω_p	plasma frequency
Γ_D	damping factor
d	diameter of nano particle
Q	Joule losses in metal
\mathbf{E}	electric field
E_m	electric field in metal
E_d	electric field in dielectric
k_x	wavevector parallel to the interface
$k_{z,m}$	perpendicular to the interface in the metal

$k_{z,d}$	perpendicular to the interface in dielectric
k_{SP}	wave vector (momentum) of the SPPs
k_o	wave vector (momentum) of the photon
$P_{abs,d}$	power absorbed by the dielectric
$P_{abs,m}$	power absorbed by the metal
F_{abs}	ratio of dissipative power in metal and dielectric
$\tan\delta$	Loss factor
ϵ'	real part of the relative permittivity
ϵ''	imaginary part of the relative permittivity
$\bar{\delta}_r$	phase thickness
$\bar{\eta}_r$	complex admittance in the horizontal and vertical directions
$\rho(r, \omega)$	local density of optical states
$\hbar\omega$	photon energy
$k_B T$	thermal energy
η_d	real part of the refractive index of dielectric
η_m	real part of the refractive index of metal
k_d	imaginary part of the refractive index of dielectric
k_m	imaginary part of the refractive index of metal
R	universal gas constant

1
2
3
4
5
6
7
8
9
10
11
12
13
14
15
16
17
18
19
20
21
22
23
24
25
26
27
28
29
30
31
32
33
34
35
36
37
38
39
40
41
42
43
44
45
46
47
48
49
50
51
52
53
54
55
56
57
58
59
60
61
62
63
64
65

<u>List of acronyms</u>	
CSP	Concentrating Solar Power
SPP	Surface Plasma Polariton
DMD	Dielectric-Metal-Dielectric
MD	Metal-Dielectric
TES	Thermal Energy Storage
BS	Backup Systems
IEA	International Energy Agency
ESTELA	European Solar Thermal Electricity Association
JNNSM	Jawaharlal Nehru National Solar Mission
LCOC	Levelized Cost of Coating
PVD	Physical Vapour Deposition
EM	Electromagnetic
UHTCs	Ultra-High Temperature Ceramics
FDTD	Finite-Difference Time Domain
AR	Anti reflection
MG	Maxwell-Garnett
BR	Bruggeman
HMVF	High Metal Volume Fraction
LMVF	Low Metal Volume Fraction
PhC	Photonic Crystal
RCWA	Rigorous Coupled-Wave Analysis

1
2
3
4
5
6
7
8
9
10
11
12
13
14
15
16
17
18
19
20
21
22
23
24
25
26
27
28
29
30
31
32
33
34
35
36
37
38
39
40
41
42
43
44
45
46
47
48
49
50
51
52
53
54
55
56
57
58
59
60
61
62
63
64
65

LSP	Localised Surface Plasmon
TM	Transverse-Magnetic
XPS	X-ray photoelectron spectroscopy
XRD	X-ray diffraction
SEM	Scanning Electron microscopy
DC	Direct Current
RF	Radio Frequency
PC	Performance criterion function
LCOE	Levelized Cost of Electricity

List of Figures:

Fig. 1. Schematic of four CSP systems a) parabolic trough collector b) solar tower c) parabolic dish concentrator and d) linear Fresnel reflector [23, 24].

Fig. 2. Schematic of the mechanism to produce electricity from solar energy in CSP systems.

Fig. 3. Schematic of an ideal solar selective absorber.

Fig. 4. Interaction of electromagnetic radiation with matter.

Fig. 5. The solar spectrum (blue); the blackbody radiation at 100, 200 and 300 °C (green, yellow, maroon, respectively); The reflectance spectrum of an ideal (black) and real (red) solar selective absorbers [46].

Fig. 6. Different types of solar selective absorber coatings; (a) Intrinsic absorber, (b) Semiconductor absorber, (c) Multilayer absorber, (d) Cermet absorber (e) Textured surface (f) Dielectric – metal – dielectric –based absorber [42].

Fig. 7: (a) Formation of localised surface plasmons (LSPs); (b) The propagation of surface plasmon polaritons (SPPs) in metal-dielectric interface in response to electro-magnetic field.

Fig. 8: Schematic of the (a) metal-dielectric and (b) dielectric-metal-dielectric structures for SPP propagation.

Fig. 9. The Arrhenius plot for $\text{Cr}_x\text{O}_y/\text{Cr}/\text{Cr}_2\text{O}_3$ coatings [152].

Fig. 10. (a) AFM images (b) Experimental and calculated reflectance spectra and (c) thermal stability of $\text{MgO}/\text{Zr}/\text{MgO}$ coating [199, 200].

Fig. 11. Spectra reflectance of $\text{Al}_2\text{O}_3/\text{Mo}/\text{Al}_2\text{O}_3$ coating after long term annealing at 920 °C [207].

Fig. 12. The wavelength dependence of refractive index and extinction coefficient of Mo films, sputtered in pure Ar and in an Ar + O₂ mixture; Auger depth profile-composition analysis of heat-treated $\text{Al}_2\text{O}_3/\text{Mo}/\text{Al}_2\text{O}_3$ coating in vacuum, deposited on Mo coated stainless

1 steel substrate a) Al_2O_3 layer deposited by reactive sputtering; (b) Al_2O_3 layer deposited by
2 r.f sputtering of alumina [208].

3 **Fig. 13.** Dependence of experimentally determined n and k values with respect to wavelength
4 for (a) Al_xO_y (layers 1 and 3) (b) Al layer in $\text{Al}_x\text{O}_y/\text{Al}/\text{Al}_x\text{O}_y$ absorber coating deposited on
5 Cu substrate [149]
6
7
8
9

10 **Fig. 14.** Raman spectra of (a) as-deposited and heat treated absorbers annealed in air at (b)
11 250 °C, (c) 350 °C, (d) 450 °C and (e) 500 °C for 2h in vacuum. The Raman spectrum of
12 CuO has been represented in the inset [149].
13
14
15
16
17

18 **Fig. 15.** The variation of optical constants as a function of wavelength in difference thickness
19 of (a) top Al_xO_y layer, (b) base Al_xO_y layer (c) & (d) [212].
20
21
22

23 **Fig. 16.** The thickness dependence of reflectance spectra (a) top Al_xO_y layer (b) base Al_xO_y
24 layer and (c) simulated and experimental spectra of $\text{Al}_x\text{O}_y\text{-Pt-}\text{Al}_x\text{O}_y$ absorber coating [212].
25
26
27

28 **Fig. 17.** SEM images of as deposited (a) and heat treated coatings in air at (b) 300 °C (c) 400
29 °C (d) 500 °C (e) 600 °C and (f) 700 °C of $\text{Al}_x\text{O}_y/\text{Pt}/\text{Al}_x\text{O}_y$ coating on Cu substrates [214].
30
31
32

33 **Fig. 18.** Thermal stability study of $\text{Al}_x\text{O}_y/\text{Pt}/\text{Al}_x\text{O}_y$ in different temperatures in air for a) 2 hrs
34 and b) 24 hrs [214].
35
36
37

38 **Fig. 19.** TEM cross-sectional images of as-deposited coating (a) A(150/2), (b) A (250/2) and
39 (c) A (150/8) (c) films; (d) diffraction pattern of as-deposited A(150/2) [217].
40
41
42

43 **Fig. 20.** Transmittance spectra of Al_xO_y in different deposition conditions [217].
44

45 **Fig. 21.** Schematic of DMD coatings with Mo, MgF_2 and TiO_2 layers. Optimized stacks with
46 no of layers $L = 5, 7, 9$ and 11 are shown [53].
47
48
49

50 **Fig. 22.** Schematic of DMD coatings with W, MgF_2 and TiO_2 layers. Optimized stacks with
51 no of layers $L = 5, 7, 9$ and 11 are shown [53].
52
53
54

55 **Fig. 23.** Absorption spectra of the metal-dielectric stack composed of a) Mo, TiO_2 and MgF_2
56 b) W, TiO_2 and MgF_2 . The spectra selectivity of ideal selective absorber at 720 K has also
57 been plotted as reference (c) The variation of merit function of the metal-dielectric stack
58
59
60
61
62
63
64
65

1 using Mo, TiO₂, MgF₂ and W, TiO₂, MgF₂. The substrate (Mo or W) has been considered as
2 L = 1 [53].
3

4 **Fig. 24.** The interaction of light with (a) flat and (b) textured DMD coatings [237].
5
6
7
8
9

10 11 12 13 14 15 16 17 18 19 20 21 22 23 24 25 26 27 28 29 30 31 32 33 34 35 36 37 38 39 40 41 42 43 44 45 46 47 48 49 50 51 52 53 54 55 56 57 58 59 60 61 62 63 64 65

- [1] Unruh GC. Escaping carbon lock-in. *Energy policy*. 2002;30:317-25.
- [2] Gupta PK. Renewable energy sources—A longway to go in India. *Renewable Energy*. 1999;16:1216-9.
- [3] Athienitis AK, Santamouris M. *Thermal analysis and design of passive solar buildings*: Routledge; 2013.
- [4] Kalkan N, Dagtekin I. *Passive Solar Techniques to Improve Thermal Comfort and Reduce Energy Consumption of Domestic Use*. World Academy of Science, Engineering and Technology, *International Journal of Electrical, Computer, Energetic, Electronic and Communication Engineering*. 2016;10:432-7.
- [5] Mazarrón FR, Porrás-Prieto CJ, García JL, Benavente RM. Feasibility of active solar water heating systems with evacuated tube collector at different operational water temperatures. *Energy Conversion and Management*. 2016;113:16-26.
- [6] Singh DB, Yadav JK, Dwivedi VK, Kumar S, Tiwari GN, Al-Helal IM. Experimental studies of active solar still integrated with two hybrid PVT collectors. *Solar Energy*. 2016;130:207-23.
- [7] Chow TT. A review on photovoltaic/thermal hybrid solar technology. *Applied energy*. 2010;87:365-79.
- [8] Price H, Kearney D. Reducing the cost of energy from parabolic trough solar power plants. *American Society of Mechanical Engineers*. p. 591-9.
- [9] Zhang HL, Baeyens J, Degreè J, Cacères G. Concentrated solar power plants: Review and design methodology. *Renewable and Sustainable Energy Reviews*. 2013;22:466-81.
- [10] OECD/IEA, *technology roadmap, concentrating solar power*, 2010.
- [11] Lotker M. *Barriers to commercialization of large-scale solar electricity: Lessons learned from the LUZ experience*. Sandia National Labs., Albuquerque, NM (United States); 1991.

- 1
2
3
4
5
6
7
8
9
10
11
12
13
14
15
16
17
18
19
20
21
22
23
24
25
26
27
28
29
30
31
32
33
34
35
36
37
38
39
40
41
42
43
44
45
46
47
48
49
50
51
52
53
54
55
56
57
58
59
60
61
62
63
64
65
- [12] Osuna R, Fernandez V, Romero M, Marcos MJ. PS10, A 10 MW Solar Tower Power Plant for Southern Spain. 2001.
- [13] Fthenakis V, Mason JE, Zweibel K. The technical, geographical, and economic feasibility for solar energy to supply the energy needs of the US. *Energy Policy*. 2009;37:387-99.
- [14] Bettzng MO, P E. Concentrationg solar power in Europe, the middle east and north Africa: A review of development issues and potential to 2050. *Journal of Solar Energy Engineering*. 2012;134:024501-6.
- [15] Purohit I, Purohit P. Techno-economic evaluation of concentrating solar power generation in India. *Energy policy*. 2010;38:3015-29.
- [16] Hang Q, Jun Z, Xiao Y, Junkui C. Prospect of concentrating solar power in China—the sustainable future. *Renewable and Sustainable Energy Reviews*. 2008;12:2505-14.
- [17] Müller-Steinhagen H, Trieb F. Concentrating solar power. A review of the technology *Ingenia Inform QR Acad Eng*. 2004;18:43-50.
- [18] Trieb F, Müller-Steinhagen H. Concentrating solar power for seawater desalination in the Middle East and North Africa. *Desalination*. 2008;220:165-83.
- [19] Fluri TP. The potential of concentrating solar power in South Africa. *Energy Policy*. 2009;37:5075-80.
- [20] Hinkley JT, Hayward JA, Curtin B, Wonhas A, Boyd R, Grima C, et al. An analysis of the costs and opportunities for concentrating solar power in Australia. *Renewable energy*. 2013;57:653-61.
- [21] Abbas M, Boumeddane B, Said N, Chikouche A. Dish Stirling technology: A 100 MW solar power plant using hydrogen for Algeria. *International journal of hydrogen energy*. 2011;36:4305-14.
- [22] Cau G, Cocco D. Comparison of medium-size concentrating solar power plants based on parabolic trough and linear Fresnel collectors. *Energy Procedia*. 2014;45:101-10.
- [23] Romero M, González- Aguilar J. Solar thermal CSP technology. *Wiley Interdisciplinary Reviews: Energy and Environment*. 2014;3:42-59.
- [24] Ummadisingu A, Soni MS. Concentrating solar power—technology, potential and policy in India. *Renewable and Sustainable Energy Reviews*. 2011;15:5169-75.
- [25] Kuravi S, Trahan J, Goswami DY, Rahman MM, Stefanakos EK. Thermal energy storage technologies and systems for concentrating solar power plants. *Progress in Energy and Combustion Science*. 2013;39:285-319.

- [26] Barlev D, Vidu R, Stroeve P. Innovation in concentrated solar power. *Solar energy materials and solar cells*. 2011;95:2703-25.
- [27] Alex S, Chattopadhyay K, Basu B. Tailored specular reflectance properties of bulk Cu based novel intermetallic alloys. *Solar Energy Materials and Solar Cells*. 2016;149:66-74.
- [28] Alex S, Basu B, Sengupta S, Pandey UK, Chattopadhyay K. Electrodeposition of δ -phase based Cu-Sn mirror alloy from sulfate-aqueous electrolyte for solar reflector application. *Applied Thermal Engineering*. 2016.
- [29] Chen CJ. *Physics of solar energy*: John Wiley & Sons; 2011.
- [30] Skiff FA. *Solar heater*. Google Patents; 1913.
- [31] Anderson WA. *Solar heating element*. Google Patents; 1926.
- [32] Miller KW. *Solar heat trap*. Google Patents; 1954.
- [33] Zvi TH. *Receiver for solar energy collectors*. Google Patents; 1959.
- [34] Barshilia HC, Selvakumar N, Rajam KS, Rao DVS, Muraleedharan K. Deposition and characterization of TiAlN/TiAlON/Si₃N₄ tandem absorbers prepared using reactive direct current magnetron sputtering. *Thin Solid Films*. 2008;516:6071-8.
- [35] Choy KL. Chemical vapour deposition of coatings. *Progress in materials science*. 2003;48:57-170.
- [36] Alami AH, Allagui A, Alawadhi H. Synthesis and optical properties of electrodeposited crystalline Cu₂O in the Vis–NIR range for solar selective absorbers. *Renewable Energy*. 2015;82:21-5.
- [37] Kaluža L, Orel B, Dražič G, Kohl M. Sol–gel derived CuCoMnO_x spinel coatings for solar absorbers: Structural and optical properties. *Solar energy materials and solar cells*. 2001;70:187-201.
- [38] Orel ZC, Gunde MK. Spectrally selective paint coatings: Preparation and characterization. *Solar energy materials and solar cells*. 2001;68:337-53.
- [39] Bogaerts WF, Lampert CM. *Materials for photothermal solar energy conversion*. *Journal of Materials Science*. 1983;18:2847-75.
- [40] Niklasson GA, Granqvist CG. Surfaces for selective absorption of solar energy: an annotated bibliography 1955–1981. *Journal of Materials science*. 1983;18:3475-534.
- [41] Kennedy CE. *Review of mid-to high-temperature solar selective absorber materials*: National Renewable Energy Laboratory Golden, Colo, USA; 2002.
- [42] Granqvist CG. *Solar energy materials*. *Advanced Materials*. 2003;15:1789-803.
- [43] Gadgil SB, Thangaraj R, Iyer JV, Sharma AK, Gupta BK, Agnihotri OP. Spectrally selective copper sulphide coatings. *Solar Energy Materials*. 1981;5:129-40.

- 1
2
3
4
5
6
7
8
9
10
11
12
13
14
15
16
17
18
19
20
21
22
23
24
25
26
27
28
29
30
31
32
33
34
35
36
37
38
39
40
41
42
43
44
45
46
47
48
49
50
51
52
53
54
55
56
57
58
59
60
61
62
63
64
65
- [44] Granqvist CG, Wittwer V. Materials for solar energy conversion: An overview. *Solar Energy Materials and solar cells*. 1998;54:39-48.
- [45] Wijewardane S, Goswami DY. A review on surface control of thermal radiation by paints and coatings for new energy applications. *Renewable and Sustainable Energy Reviews*. 2012;16:1863-73.
- [46] Amri A, Jiang ZT, Pryor T, Yin C-Y, Djordjevic S. Developments in the synthesis of flat plate solar selective absorber materials via sol-gel methods: A review. *Renewable and Sustainable Energy Reviews*. 2014;36:316-28.
- [47] Atkinson C, Sansom CL, Almond HJ, Shaw CP. Coatings for concentrating solar systems—a review. *Renewable and Sustainable Energy Reviews*. 2015;45:113-22.
- [48] P.A.Jeeva SN, S.Karthikeyan. A review on Black coatings for Solar Energy Storing Systems. *International Journal of ChemTech Research*. 2016;9(03):589-96.
- [49] Selvakumar N, Barshilia HC. Review of physical vapor deposited (PVD) spectrally selective coatings for mid-and high-temperature solar thermal applications. *Solar Energy Materials and Solar Cells*. 2012;98:1-23.
- [50] Jackson JD. *Classical electrodynamics*: Wiley; 1999.
- [51] Kuhn TS. *Black-body theory and the quantum discontinuity, 1894-1912*: University of Chicago Press; 1978.
- [52] Cardy J. The ubiquitous ‘c’: from the Stefan–Boltzmann law to quantum information Boltzmann Medal Lecture, Statphys24, Cairns, July 2010. *Journal of Statistical Mechanics: Theory and Experiment*. 2010;2010:P10004.
- [53] Sergeant NP, Pincon O, Agrawal M, Peumans P. Design of wide-angle solar-selective absorbers using aperiodic metal-dielectric stacks. *Optics express*. 2009;17:22800-12.
- [54] Cindrella L. The real utility ranges of the solar selective coatings. *Solar Energy Materials and Solar Cells*. 2007;91:1898-901.
- [55] Ho CK, Mahoney AR, Ambrosini A, Bencomo M, Hall A, Lambert TN. Characterization of Pyromark 2500 for high-temperature solar receivers. *American Society of Mechanical Engineers*. p. 509-18.
- [56] Bermel P, Lee J, Joannopoulos JD, Celanovic I, Soljacic M. Selective solar absorbers. *Annual Review of Heat Transfer*. 2012;15.
- [57] Li P, Liu B, Ni Y, Liew KK, Sze J, Chen S, et al. Large- Scale Nanophotonic Solar Selective Absorbers for High- Efficiency Solar Thermal Energy Conversion. *Advanced Materials*. 2015;27:4585-91.

- 1
2
3
4
5
6
7
8
9
10
11
12
13
14
15
16
17
18
19
20
21
22
23
24
25
26
27
28
29
30
31
32
33
34
35
36
37
38
39
40
41
42
43
44
45
46
47
48
49
50
51
52
53
54
55
56
57
58
59
60
61
62
63
64
65
- [58] Ho CK, Pacheco JE. Levelized Cost of Coating (LCOC) for selective absorber materials. *Solar Energy*. 2014;108:315-21.
- [59] Ehrenreich H, Seraphin BO. Symposium on the Fundamental Optical Properties of Solids Relevant to Solar Energy Conversion. NASA STI/Recon Technical Report N. 1975;77:12538.
- [60] Touloukian YS, Powell RW, Ho CY, Nicolaou MC. Thermophysical Properties of Matter-The TPRC Data Series. Volume 10. Thermal Diffusivity. DTIC Document; 1974.
- [61] González F, Barrera-Calva E, Huerta L, Mane RS. Coatings of Fe₃O₄ Nanoparticles as Selective Solar Absorber. *The Open Surface Science Journal*. 2011;3:131-5.
- [62] Ienei E, Isac L, Duta A. Synthesis of alumina thin films by spray pyrolysis. *Rev Roum Chim*. 2010;55:161-5.
- [63] Randich E, Allred DD. Chemically vapor-deposited ZrB₂ as a selective solar absorber. *Thin Solid Films*. 1981;83:393-8.
- [64] Sani E, Mercatelli L, Sansoni P, Silvestroni L, Sciti D. Spectrally selective ultra-high temperature ceramic absorbers for high-temperature solar plants. *Journal of Renewable and Sustainable Energy*. 2012;4:033104.
- [65] Sani E, Mercatelli L, Francini F, Sans JL, Sciti D. Ultra-refractory ceramics for high-temperature solar absorbers. *Scripta Materialia*. 2011;65:775-8.
- [66] Shah AA, Ungaro C, Gupta MC. High temperature spectral selective coatings for solar thermal systems by laser sintering. *Solar Energy Materials and Solar Cells*. 2015;134:209-14.
- [67] Chen Z, Boström T. Anti-reflection coated spectrally selective carbon nanotube solar absorbers. *Renewable Energy and Environmental Sustainability*. 2016;1:2.
- [68] Chen Z, Boström T. Electrophoretically deposited carbon nanotube spectrally selective solar absorbers. *Solar Energy Materials and Solar Cells*. 2016;144:678-83.
- [69] Ding D, Cai W, Long M, Wu H, Wu Y. Optical, structural and thermal characteristics of Cu–CuAl₂O₄ hybrids deposited in anodic aluminum oxide as selective solar absorber. *Solar Energy Materials and Solar Cells*. 2010;94:1578-81.
- [70] Geng QF, Zhao X, Gao XH, Liu G. Sol–Gel Combustion- Derived CoCuMnO_x Spinel as Pigment for Spectrally Selective Paints. *Journal of the American Ceramic Society*. 2011;94:827-32.
- [71] Pal S, Diso D, Franza S, Licciulli A, Rizzo L. Spectrally selective absorber coating from transition metal complex for efficient photothermal conversion. *Journal of Materials Science*. 2013;48:8268-76.

- [72] Jerman I, Mihelčič M, Verhovšek D, Kovač J, Orel B. Polyhedral oligomeric silsesquioxane trisilanols as pigment surface modifiers for fluoropolymer based Thickness Sensitive Spectrally Selective (TSSS) paint coatings. *Solar Energy Materials and Solar Cells*. 2011;95:423-31.
- [73] Geng Q, Zhao X, Gao X, Yu H, Yang S, Liu G. Optimization design of $\text{CuCr}_x\text{Mn}_{2-x}\text{O}_4$ -based paint coatings used for solar selective applications. *Solar Energy Materials and Solar Cells*. 2012;105:293-301.
- [74] Geng Q, Zhao X, Gao X, Yang S, Liu G. Low-temperature combustion synthesis of CuCr_2O_4 spinel powder for spectrally selective paints. *Journal of sol-gel science and technology*. 2012;61:281-8.
- [75] Ambrosini A, Lambert TN, Bencomo M, Hall A, Siegel NP, Ho CK. Improved high temperature solar absorbers for use in concentrating solar power central receiver applications. *American Society of Mechanical Engineers*. p. 587-94.
- [76] Orel ZC, Gunde MK, Hutchins MG. Spectrally selective solar absorbers in different non-black colours. *Solar energy materials and solar cells*. 2005;85:41-50.
- [77] Paone A, Geiger M, Sanjines R, Schüler A. Thermal solar collector with VO_2 absorber coating and $\text{V}_{1-x}\text{W}_x\text{O}_2$ thermochromic glazing—Temperature matching and triggering. *Solar Energy*. 2014;110:151-9.
- [78] Sciti D, Silvestroni L, Trucchi DM, Cappelli E, Orlando S, Sani E. Femtosecond laser treatments to tailor the optical properties of hafnium carbide for solar applications. *Solar Energy Materials and Solar Cells*. 2015;132:460-6.
- [79] Fang Z, Lu C, Guo C, Lu Y, Gao D, Ni Y, et al. Suitability of layered Ti_3SiC_2 and $\text{Zr}_3[\text{Al}(\text{Si})_4\text{C}_6]$ ceramics as high temperature solar absorbers for solar energy applications. *Solar Energy Materials and Solar Cells*. 2015;134:252-60.
- [80] Xiaohong XU, Zhenggang RAO, Jianfeng WU, Yonghua LI, Zhang Y, Xinbin LAO. In-situ synthesis and thermal shock resistance of cordierite/silicon carbide composites used for solar absorber coating. *Solar Energy Materials and Solar Cells*. 2014;130:257-63.
- [81] Agnihotri OP, Gupta BK. *Solar selective surfaces*. 1981.
- [82] Moon J, Lu D, VanSaders B, Kim TK, Kong SD, Jin S, et al. High performance multi-scaled nanostructured spectrally selective coating for concentrating solar power. *Nano Energy*. 2014;8:238-46.
- [83] Yang L, Mo L, Chen T, Forsberg E, He S. A checkerboard selective absorber with excellent spectral selectivity. *Journal of Applied Physics*. 2015;118:183103.

- 1 [84] Wang KK, Wu ZZ, Peng CJ, Wang KP, Cheng B, Song CL, et al. A facile process to
2 prepare crosslinked nano-graphites uniformly dispersed in titanium oxide films as solar
3 selective absorbers. *Solar Energy Materials and Solar Cells*. 2015;143:198-204.
4
- 5 [85] Kuckelkorn T, Graf W. Radiation-selective absorber coating with an adherent oxide
6 layer and method of making same. Google Patents; 2010.
7
- 8 [86] Richards BS. Comparison of TiO_2 and other dielectric coatings for buried- contact solar
9 cells: a review. *Progress in Photovoltaics: Research and Applications*. 2004;12:253-81.
10
- 11 [87] Seraphin BO. Chemical vapor deposition of thin semiconductor films for solar energy
12 conversion. *Thin Solid Films*. 1976;39:87-94.
13
- 14 [88] Selvakumar N, Barshilia HC, Rajam KS, Biswas A. Spectrally selective
15 $\text{TiAlN/CrAlON/Si}_3\text{N}_4$ tandem absorber for high temperature solar applications. 2008.
16
- 17 [89] Zou C, Xie W, Shao L. Functional multi-layer solar spectral selective absorbing coatings
18 of $\text{AlCrSiN/AlCrSiON/AlCrO}$ for high temperature applications. *Solar Energy Materials and*
19 *Solar Cells*. 2016;153:9-17.
20
- 21 [90] Rebouta L, Capela P, Andritschky M, Matilainen A, Santilli P, Pischow K, et al.
22 Characterization of $\text{TiAlSiN/TiAlSiON/SiO}_2$ optical stack designed by modelling
23 calculations for solar selective applications. *Solar energy materials and solar cells*.
24 2012;105:202-7.
25
- 26 [91] Selvakumar N, Manikandanath NT, Biswas A, Barshilia HC. Design and fabrication of
27 highly thermally stable $\text{HfMoN/HfON/Al}_2\text{O}_3$ tandem absorber for solar thermal power
28 generation applications. *Solar Energy Materials and Solar Cells*. 2012;102:86-92.
29
- 30 [92] Liu HD, Fu TR, Duan MH, Wan Q, Chen YM, Fu DJ, et al. Structure and thermal
31 stability of spectrally selective absorber based on AlCrON coating for solar-thermal
32 conversion applications. *Solar Energy Materials and Solar Cells*. 2016;157:108-16.
33
- 34 [93] Eisenhammer T, Haugeneder A, Mahr A. High-temperature optical properties and
35 stability of selective absorbers based on quasicrystalline AlCuFe . *Solar energy materials and*
36 *solar cells*. 1998;54:379-86.
37
- 38 [94] Hao L, Du M, Liu X, Wang S, Jiang L, Lü F, et al. Thermal stability of nitride solar
39 selective absorbing coatings used in high temperature parabolic trough current. *Science China*
40 *Technological Sciences*. 2010;53:1507-12.
41
- 42 [95] Du M, Hao L, Mi J, Lv F, Liu X, Jiang L, et al. Optimization design of
43 $\text{Ti}_{0.5}\text{Al}_{0.5}\text{N/Ti}_{0.25}\text{Al}_{0.75}\text{N/AlN}$ coating used for solar selective applications. *Solar Energy*
44 *Materials and Solar Cells*. 2011;95:1193-6.
45
46
47
48
49
50
51
52
53
54
55
56
57
58
59
60
61
62
63
64
65

- [96] Valleti K, Krishna DM, Joshi SV. Functional multi-layer nitride coatings for high temperature solar selective applications. *Solar Energy Materials and Solar Cells*. 2014;121:14-21.
- [97] Dan A, Chattopadhyay K, Barshilia HC, Basu B. Angular solar absorptance and thermal stability of W/WAIN/WAlON/Al₂O₃-based solar selective absorber coating. *Applied Thermal Engineering*. 2016.
- [98] Dan A, Jyothi J, Chattopadhyay K, Barshilia HC, Basu B. Spectrally selective absorber coating of WAIN/WAlON/Al₂O₃ for solar thermal applications. *Solar Energy Materials and Solar Cells*. 2016;157:716-26.
- [99] Dan A, Chattopadhyay K, Barshilia HC, Basu B. Colored selective absorber coating with excellent durability. *Thin Solid Films*. 2016;620:17-22.
- [100] Zettl M. High performance coatings for solar receivers and new dedicated manufacturing solution. *Energy Procedia*. 2014;48:701-6.
- [101] ALMECO Group SBoT, 2014. <http://www.almecogroup.com/en/pagina/16-solar>.
- [102] Bayón R, San Vicente G, Morales Á. Durability tests and up-scaling of selective absorbers based on copper–manganese oxide deposited by dip-coating. *Solar Energy Materials and Solar Cells*. 2010;94:998-1004.
- [103] Joly M, Antonetti Y, Python M, Gonzalez M, Gascou T, Scartezzini J-L, et al. Novel black selective coating for tubular solar absorbers based on a sol–gel method. *Solar energy*. 2013;94:233-9.
- [104] Khan MR, Wang X, Alam MA. Fundamentals of PV efficiency: limits for light absorption. arXiv preprint arXiv:12122897. 2012.
- [105] Berini P. Long-range surface plasmon polaritons. *Advances in Optics and Photonics*. 2009;1:484-588.
- [106] Green MA, Pillai S. Harnessing plasmonics for solar cells. *Nature Photonics*. 2012;6:130-2.
- [107] Garnett JCM. Colours in metal glasses, in metallic films, and in metallic solutions. II. *Philosophical Transactions of the Royal Society of London Series A, Containing Papers of a Mathematical or Physical Character*. 1906:237-88.
- [108] Bruggeman VDAG. Berechnung verschiedener physikalischer Konstanten von heterogenen Substanzen. I. Dielektrizitätskonstanten und Leitfähigkeiten der Mischkörper aus isotropen Substanzen. *Annalen der physik*. 1935;416:636-64.
- [109] Craighead HG, Howard RE, Sweeney JE, Buhrman RA. Graded- index Pt- Al₂O₃ composite solar absorbers. *Applied Physics Letters*. 1981;39:29-31.

- [110] Fan JCC, Spura SA. Selective black absorbers using rf- sputtered Cr₂O₃/Cr cermet films. *Applied Physics Letters*. 1977;30:511-3.
- [111] Kumar SN, Malhotra LK, Chopra KL. Nickel pigmented anodized aluminium as solar selective absorbers. *Solar energy materials*. 1983;7:439-52.
- [112] Zhang Q-C. Stainless-steel–AlN cermet selective surfaces deposited by direct current magnetron sputtering technology. *Solar energy materials and solar cells*. 1998;52:95-106.
- [113] Cespedes E, Wirz M, Sánchez-García JA, Alvarez-Fraga L, Escobar-Galindo R, Prieto C. Novel Mo–Si₃N₄ based selective coating for high temperature concentrating solar power applications. *Solar Energy Materials and Solar Cells*. 2014;122:217-25.
- [114] Antonaia A, Castaldo A, Addonizio ML, Esposito S. Stability of W–Al₂O₃ cermet based solar coating for receiver tube operating at high temperature. *Solar Energy Materials and Solar Cells*. 2010;94:1604-11.
- [115] Xue Y, Wang C, Wang W, Liu Y, Wu Y, Ning Y, et al. Spectral properties and thermal stability of solar selective absorbing AlNi–Al₂O₃ cermet coating. *Solar Energy*. 2013;96:113-8.
- [116] Barshilia HC, Kumar P, Rajam KS, Biswas A. Structure and optical properties of Ag–Al₂O₃ nanocermet solar selective coatings prepared using unbalanced magnetron sputtering. *Solar Energy Materials and Solar Cells*. 2011;95:1707-15.
- [117] Nuru ZY, Arendse CJ, Nemutudi R, Nemraoui O, Maaza M. Pt–Al₂O₃ nanocoatings for high temperature concentrated solar thermal power applications. *Physica B: Condensed Matter*. 2012;407:1634-7.
- [118] Xinkang D, Cong W, Tianmin W, Long Z, Buliang C, Ning R. Microstructure and spectral selectivity of Mo–Al₂O₃ solar selective absorbing coatings after annealing. *Thin Solid Films*. 2008;516:3971-7.
- [119] Wang J, Wei B, Wei Q, Li D. Optical property and thermal stability of Mo/Mo–SiO₂/SiO₂ solar- selective coating prepared by magnetron sputtering. *physica status solidi (a)*. 2011;208:664-7.
- [120] Zheng L, Zhou F, Zhou Z, Song X, Dong G, Wang M, et al. Angular solar absorptance and thermal stability of Mo–SiO₂ double cermet solar selective absorber coating. *Solar Energy*. 2015;115:341-6.
- [121] Adsten M, Joerger R, Järrendahl K, Wäckelgård E. Optical characterization of industrially sputtered nickel–nickel oxide solar selective surface. *Solar Energy*. 2000;68:325-8.

- 1 [122] Cao F, Kraemer D, Tang L, Li Y, Litvinchuk AP, Bao J, et al. A high-performance
2 spectrally-selective solar absorber based on a yttria-stabilized zirconia cermet with high-
3 temperature stability. *Energy & Environmental Science*. 2015;8:3040-8.
4
- 5 [123] Zhang Q-C, Yin Y, Mills DR. High efficiency Mo · Al₂O₃ cermet selective surfaces
6 for high-temperature application. *Solar Energy materials and solar cells*. 1996;40:43-53.
7
- 8 [124] Zhang Q-C, Mills D, Monger A. Thin film solar selective surface coating. Google
9 Patents; 1996.
10
- 11 [125] Esposito S, Antonaia A, Addonizio ML, Aprea S. Fabrication and optimisation of
12 highly efficient cermet-based spectrally selective coatings for high operating temperature.
13 *Thin Solid Films*. 2009;517:6000-6.
14
- 15 [126] Zhang Q-C. Metal-AlN cermet solar selective coatings deposited by direct current
16 magnetron sputtering technology. *Journal of Physics D: Applied Physics*. 1998;31:355.
17
- 18 [127] Wang X, Li H, Yu X, Shi X, Liu J. High-performance solution-processed plasmonic Ni
19 nanochain-Al₂O₃ selective solar thermal absorbers. *Applied Physics Letters*.
20 2012;101:203109.
21
- 22 [128] Katumba G, Makiwa G, Baisitse TR, Olumekor L, Forbes A, Wäckelgård E. Solar
23 selective absorber functionality of carbon nanoparticles embedded in SiO₂, ZnO and NiO
24 matrices. *physica status solidi (c)*. 2008;5:549-51.
25
- 26 [129] Katumba G, Olumekor L, Forbes A, Makiwa G, Mwakikunga B, Lu J, et al. Optical,
27 thermal and structural characteristics of carbon nanoparticles embedded in ZnO and NiO as
28 selective solar absorbers. *Solar energy materials and solar cells*. 2008;92:1285-92.
29
- 30 [130] Roro KT, Tile N, Mwakikunga B, Yalisi B, Forbes A. Solar absorption and thermal
31 emission properties of multiwall carbon nanotube/nickel oxide nanocomposite thin films
32 synthesized by sol-gel process. *Materials Science and Engineering: B*. 2012;177:581-7.
33
- 34 [131] Cuevas A, Martinez L, Romero R, Dalchiele EA, Marotti R, Leinen D, et al.
35 Electrochemically grown cobalt-alumina composite layer for solar thermal selective
36 absorbers. *Solar Energy Materials and Solar Cells*. 2014;130:380-6.
37
- 38 [132] Cao F, McEnaney K, Chen G, Ren Z. A review of cermet-based spectrally selective
39 solar absorbers. *Energy & Environmental Science*. 2014;7:1615-27.
40
- 41 [133] Konttinen P, Lund PD, Kilpi RJ. Mechanically manufactured selective solar absorber
42 surfaces. *Solar energy materials and solar cells*. 2003;79:273-83.
43
- 44 [134] Konttinen P, Kilpi R, Lund PD. Microstructural analysis of selective C/Al₂O₃/Al solar
45 absorber surfaces. *Thin Solid Films*. 2003;425:24-30.
46
47
48
49
50
51
52
53
54
55
56
57
58
59
60
61
62
63
64
65

- [135] Chen J, Ye H, Ae L, Tang Y, Kieven D, Rissom T, et al. Tapered aluminum-doped vertical zinc oxide nanorod arrays as light coupling layer for solar energy applications. *Solar Energy Materials and Solar Cells*. 2011;95:1437-40.
- [136] Kumar SK, Suresh S, Murugesan S, Raj SP. CuO thin films made of nanofibers for solar selective absorber applications. *Solar Energy*. 2013;94:299-304.
- [137] Sergeant NP, Agrawal M, Peumans P. High performance solar-selective absorbers using coated sub-wavelength gratings. *Optics express*. 2010;18:5525-40.
- [138] Joannopoulos JD, Johnson SG, Winn JN, Meade RD. *Photonic crystals: molding the flow of light*: Princeton university press; 2011.
- [139] Wang J, Chen Z, Li D. Simulation of two- dimensional Mo photonic crystal surface for high- temperature solar- selective absorber. *physica status solidi (a)*. 2010;207:1988-92.
- [140] Wang H, Sivan VP, Mitchell A, Rosengarten G, Phelan P, Wang L. Highly efficient selective metamaterial absorber for high-temperature solar thermal energy harvesting. *Solar Energy Materials and Solar Cells*. 2015;137:235-42.
- [141] Barnes WL, Dereux A, Ebbesen TW. Surface plasmon subwavelength optics. *Nature*. 2003;424:824-30.
- [142] Zayats AV, Smolyaninov II, Maradudin AA. Nano-optics of surface plasmon polaritons. *Physics reports*. 2005;408:131-314.
- [143] von Blanckenhagen B, Tonova D, Ullmann J. Application of the Tauc-Lorentz formulation to the interband absorption of optical coating materials. *Applied optics*. 2002;41:3137-41.
- [144] Adachi S. Optical dispersion relations for Si and Ge. *Journal of applied physics*. 1989;66:3224-31.
- [145] Kreibig U, Vollmer M. *Optical properties of metal clusters*: Springer Science & Business Media; 2013.
- [146] Ninomiya S, Adachi S. Optical properties of wurtzite CdS. *Journal of Applied Physics*. 1995;78:1183-90.
- [147] Adachi S, Mori H, Ozaki S. Model dielectric function for amorphous semiconductors. *Physical Review B*. 2002;66:153201.
- [148] Jellison Jr GE, Modine FA. Parameterization of the optical functions of amorphous materials in the interband region. *Applied Physics Letters*. 1996;69:371-3.
- [149] Barshilia HC, Selvakumar N, Vignesh G, Rajam KS, Biswas A. Optical properties and thermal stability of pulsed-sputter-deposited Al_xO_y/Al/Al_xO_y multilayer absorber coatings. *Solar Energy Materials and Solar Cells*. 2009;93:315-23.

- 1
2 [150] Sahoo NK, Thakur S, Senthilkumar M, Bhattacharyya D, Das NC. Reactive electron
3 beam evaporation of gadolinium oxide optical thin films for ultraviolet and deep ultraviolet
4 laser wavelengths. *Thin Solid Films*. 2003;440:155-68.
- 5 [151] Wooten F. *Optical properties of solids*: Academic press; 2013.
- 6
7 [152] Barshilia HC, Selvakumar N, Rajam KS, Biswas A. Structure and optical properties of
8 pulsed sputter deposited $\text{Cr}_x\text{O}_y/\text{Cr}/\text{Cr}_2\text{O}_3$ solar selective coatings. *Journal of Applied Physics*.
9 2008;103:023507.
- 10
11 [153] Selvakumar N, Barshilia HC, Rajam KS, Biswas A. Structure, optical properties and
12 thermal stability of pulsed sputter deposited high temperature $\text{HfO}_x/\text{Mo}/\text{HfO}_2$ solar selective
13 absorbers. *Solar Energy Materials and Solar Cells*. 2010;94:1412-20.
- 14
15 [154] Ritchie RH. Plasma losses by fast electrons in thin films. *Physical Review*.
16 1957;106:874.
- 17
18 [155] Powell CJ, Swan JB. Origin of the characteristic electron energy losses in aluminum.
19 *Physical Review*. 1959;115:869.
- 20
21 [156] Stern EA, Ferrell RA. Surface plasma oscillations of a degenerate electron gas.
22 *Physical Review*. 1960;120:130.
- 23
24 [157] Hutter E, Fendler JH. Exploitation of localized surface plasmon resonance. *Advanced*
25 *Materials*. 2004;16:1685-706.
- 26
27 [158] Stockman MI. Slow propagation, anomalous absorption, and total external reflection of
28 surface plasmon polaritons in nanolayer systems. *Nano letters*. 2006;6:2604-8.
- 29
30 [159] Baba A, Advincula RC, Knoll W. In situ investigations on the electrochemical
31 polymerization and properties of polyaniline thin films by surface plasmon optical
32 techniques. *The Journal of Physical Chemistry B*. 2002;106:1581-7.
- 33
34 [160] Brongersma ML, Kik PG. *Surface plasmon nanophotonics*: Springer; 2007.
- 35
36 [161] Kabashin AV, Evans P, Pastkovsky S, Hendren W, Wurtz GA, Atkinson R, et al.
37 Plasmonic nanorod metamaterials for biosensing. *Nature materials*. 2009;8:867-71.
- 38
39 [162] Boltasseva A, Nikolajsen T, Leosson K, Kjaer K, Larsen MS, Bozhevolnyi SI.
40 Integrated optical components utilizing long-range surface plasmon polaritons. *Journal of*
41 *Lightwave Technology*. 2005;23:413.
- 42
43 [163] Kawata S. Near-field microscope probes utilizing surface plasmon polaritons. *Near-*
44 *Field Optics and Surface Plasmon Polaritons*: Springer; 2001. p. 15-27.
- 45
46 [164] Homola J, Yee SS, Gauglitz G. *Surface plasmon resonance sensors: review*. *Sensors*
47 *and Actuators B: Chemical*. 1999;54:3-15.
- 48
49
50
51
52
53
54
55
56
57
58
59
60
61
62
63
64
65

- 1 [165] Oulton RF, Sorger VJ, Zentgraf T, Ma R-M, Gladden C, Dai L, et al. Plasmon lasers at
2 deep subwavelength scale. *Nature*. 2009;461:629-32.
- 3 [166] Hobson PA, Wedge S, Wasey JAE, Sage I, Barnes WL. Surface Plasmon Mediated
4 Emission from Organic Light- Emitting Diodes. *Advanced Materials*. 2002;14:1393-6.
- 5 [167] Krokhin AA. Long-range surface plasmons in dielectric-metal-dielectric structure with
6 highly anisotropic substrates. *Physical Review B*. 2010;81:085426.
- 7 [168] Bohn CD, Agrawal A, Lee Y, Choi CJ, Davis MS, Haney PM, et al. Design
8 considerations for enhancing absorption in semiconductors on metals through surface
9 plasmon polaritons. *Physical Chemistry Chemical Physics*. 2014;16:6084-91.
- 10 [169] Koev ST, Agrawal A, Lezec HJ, Aksyuk VA. An efficient large-area grating coupler
11 for surface plasmon polaritons. *Plasmonics*. 2012;7:269-77.
- 12 [170] Kim S, Lee J-L. Design of dielectric/metal/dielectric transparent electrodes for flexible
13 electronics. *Journal of Photonics for Energy*. 2012;2:021215-.
- 14 [171] Kasap SO. Principles of electronic materials and devices: McGraw-Hill; 2006.
- 15 [172] Maier SA. Surface plasmon polaritons at metal/insulator interfaces. *Plasmonics:
16 Fundamentals and Applications*. 2007:21-37.
- 17 [173] Liddell HM, Jerrard HG. Computer-aided techniques for the design of multilayer
18 filters: IOP Publishing Ltd.; 1981.
- 19 [174] Liu X, Cai X, Qiao J, Mao J, Jiang N. The design of ZnS/Ag/ZnS transparent
20 conductive multilayer films. *Thin Solid Films*. 2003;441:200-6.
- 21 [175] Palik ED. Handbook of optical constants of solids: Academic press; 1998.
- 22 [176] Johnson PB, Christy RW. Optical constants of the noble metals. *Physical review B*.
23 1972;6:4370.
- 24 [177] Ramakrishna SA, Armour AD. Propagating and evanescent waves in absorbing media.
25 *American Journal of Physics*. 2003;71:562-7.
- 26 [178] Gibot P, Vidal L. Original synthesis of chromium (III) oxide nanoparticles. *Journal of
27 the European Ceramic Society*. 2010;30:911-5.
- 28 [179] Kim D-W, Shin S-I, Lee J-D, Oh S-G. Preparation of chromia nanoparticles by
29 precipitation–gelation reaction. *Materials Letters*. 2004;58:1894-8.
- 30 [180] Dube DC, Agrawal D, Agrawal S, Roy R. High temperature dielectric study of Cr₂O₃
31 in microwave region. *Applied physics letters*. 2007;90:124105-9900.
- 32 [181] Sahoo S, Petravic O, Binek C, Kleemann W, Sousa JB, Cardoso S, et al. Superspin-
33 glass nature of discontinuous Co₈₀Fe₂₀/Al₂O₃ multilayers. *Physical Review B*.
34 2002;65:134406.

- 1 [182] Sahoo S, Binek C. Piezomagnetism in epitaxial Cr₂O₃ thin films and spintronic
2 applications. *Philosophical Magazine Letters*. 2007;87:259-68.
- 3 [183] Thongkanluang T, Kittiauchawal T, Limsuwan P. Preparation and characterization of
4 Cr₂O₃-TiO₂-Al₂O₃-V₂O₅ green pigment. *Ceramics International*. 2011;37:543-8.
- 5 [184] Berdahl P. Pigments to reflect the infrared radiation from fire. *Journal of Heat Transfer*.
6 1995;117:355-8.
- 7 [185] Khamlich S, McCrindle R, Nuru ZY, Cingo N, Maaza M. Annealing effect on the
8 structural and optical properties of Cr/ α -Cr₂O₃ monodispersed particles based solar
9 absorbers. *Applied Surface Science*. 2013;265:745-9.
- 10 [186] Teixeira V, Sousa E, Costa MF, Nunes C, Rosa L, Carvalho MJ, et al. Chromium-based
11 thin sputtered composite coatings for solar thermal collectors. *Vacuum*. 2002;64:299-305.
- 12 [187] Gall D, Gampp R, Lang HP, Oelhafen P. Pulsed plasma deposition of chromium
13 oxide/chromium- cermet coatings. *Journal of Vacuum Science & Technology A*.
14 1996;14:374-9.
- 15 [188] Barshilia HC, Rajam KS. Reactive sputtering of hard nitride coatings using
16 asymmetric-bipolar pulsed DC generator. *Surface and Coatings Technology*. 2006;201:1827-
17 35.
- 18 [189] Lampert CM. Thermal degradation of a black chrome solar selective absorber coating:
19 Short term. Lawrence Berkeley National Laboratory. 2011.
- 20 [190] Survilienė S, Češūnienė A, Juškėnas R, Selskienė A, Bučinskienė D, Kalinauskas P, et
21 al. The use of trivalent chromium bath to obtain a solar selective black chromium coating.
22 *Applied Surface Science*. 2014;305:492-7.
- 23 [191] Benedetti S, Benia H-M, Nilius N, Valeri S, Freund H-J. Morphology and optical
24 properties of MgO thin films on Mo (001). *Chemical Physics Letters*. 2006;430:330-5.
- 25 [192] Kingery WD, Francl J, Coble RL, Vasilos T. Thermal conductivity: X, Data for several
26 pure oxide materials corrected to zero porosity. *Journal of the American Ceramic Society*.
27 1954;37:107-10.
- 28 [193] Skvortsova V, Trinkler L. The optical properties of magnesium oxide containing
29 transition metal ions and defects produced by fast neutron irradiation. *World Scientific and
30 Engineering Academy and Society (WSEAS)*. p. 150-4.
- 31 [194] Tsang KL, Chen Y. Suppression of dielectric breakdown in MgO crystals at high
32 temperatures by impurity doping. *Journal of applied physics*. 1983;54:4531-5.
- 33 [195] Charles E, Lorival R, Boyer A, Malbrunot P. A fast-response high-temperature high-
34 pressure surface thermocouple. *Sensors and Actuators*. 1984;6:135-42.

- 1
2 [196] Joo MH, Park KH, Lee JW. In-situ Characterization of MgO Surface with Discharge
3 Aging at Elevated Temperatures of AC-Plasma Display Panels. *Journal of Surface Analysis*.
4 2008;14:412-5.
- 5 [197] Shih I, Wu SL, Li L, Qiu CX, Grant P, Denhoff MW. Effects of heat treatment on a
6 MgOSi structure: a possible buffer layer structure for high-Tc superconductors. *Materials*
7 *Letters*. 1991;11:161-3.
- 8
9 [198] Maziere-Bezes D, Valignat J. Optical properties of gold-magnesia selective cermets.
10 *Solar Energy Materials*. 1982;7:203-11.
- 11 [199] Nuru ZY, Msimanga M, Muller TFG, Arendse CJ, Mtshali C, Maaza M.
12 Microstructural, optical properties and thermal stability of MgO/Zr/MgO multilayered
13 selective solar absorber coatings. *Solar Energy*. 2015;111:357-63.
- 14 [200] Nuru ZY, Perez D, Kaviyarasu K, Vantomme A, Maaza M. Annealing effect on the
15 optical properties and interdiffusion of MgO/Zr/MgO multilayered selective solar absorber
16 coatings. *Solar Energy*. 2015;120:123-30.
- 17 [201] Boström TK, Wäckelgård E, Westin G. Anti-reflection coatings for solution-chemically
18 derived nickel—alumina solar absorbers. *Solar energy materials and solar cells*. 2004;84:183-
19 91.
- 20 [202] Woods BW, Thompson DW, Woollam JA. Gold-alumina cermet photothermal films.
21 *Thin solid films*. 2004;469:31-7.
- 22 [203] Niklasson GA, Granqvist CG. Optical properties and solar selectivity of coevaporated
23 Co- Al₂O₃ composite films. *Journal of applied physics*. 1984;55:3382-410.
- 24 [204] Sella C, Kaba A, Berthier S, Lafait J. Low cost selective absorber based on a Fe-Al₂O₃
25 cermet film. *Solar energy materials*. 1987;16:143-54.
- 26 [205] Lafait J, Berthier S, Sella C, Vien TK. Pt-Al₂O₃ selective absorber coatings for
27 photothermal conversion up to 600° C. *Vacuum*. 1986;36:125-7.
- 28 [206] Schmidt RN, Park KC. High-temperature space-stable selective solar absorber coatings.
29 *Applied Optics*. 1965;4:917-25.
- 30 [207] Peterson RE, Ramsey JW. Thin film coatings in solar – thermal power systems. *Journal*
31 *of Vacuum Science & Technology*. 1975;12:174-81.
- 32 [208] Thornton JA, Penfold AS, Lamb JL. Sputter-deposited Al₂O₃/Mo/Al₂O₃ selective
33 absorber coatings. *Thin Solid Films*. 1980;72:101-10.
- 34 [209] Nuru ZY, Arendse CJ, Khamlich S, Kotsedi L, Maaza M. A tantalum diffusion barrier
35 layer to improve the thermal stability of Al_xO_y/Pt/Al_xO_y multilayer solar absorber. *Solar*
36 *Energy*. 2014;107:89-96.
- 37
38
39
40
41
42
43
44
45
46
47
48
49
50
51
52
53
54
55
56
57
58
59
60
61
62
63
64
65

- [210] Usmani B, Vijay V, Chhibber R, Dixit A. Optimization of sputtered zirconium thin films as an infrared reflector for use in spectrally-selective solar absorbers. *Thin Solid Films*. 2017;627:17-25.
- [211] Thornton JA, Lamb JL. Thermal stability studies of sputter-deposited multilayer selective absorber coatings. *Thin Solid Films*. 1982;96:175-83.
- [212] Nuru ZY, Arendse CJ, Khamlich S, Maaza M. Optimization of $\text{Al}_x\text{O}_y/\text{Pt}/\text{Al}_x\text{O}_y$ multilayer spectrally selective coatings for solar–thermal applications. *Vacuum*. 2012;86:2129-35.
- [213] Nuru ZY, Arendse CJ, Muller TFG, Maaza M. Structural and optical properties of $\text{Al}_x\text{O}_y/\text{Pt}/\text{Al}_x\text{O}_y$ multilayer absorber. *Materials Science and Engineering: B*. 2012;177:1194-9.
- [214] Nuru ZY, Arendse CJ, Muller TF, Khamlich S, Maaza M. Thermal stability of electron beam evaporated $\text{Al}_x\text{O}_y/\text{Pt}/\text{Al}_x\text{O}_y$ multilayer solar absorber coatings. *Solar Energy Materials and Solar Cells*. 2014;120:473-80.
- [215] Nuru ZY, Msimanga M, Arendse CJ, Maaza M. Heavy ion elastic recoil detection analysis of $\text{Al}_x\text{O}_y/\text{Pt}/\text{Al}_x\text{O}_y$ multilayer selective solar absorber. *Applied Surface Science*. 2014;298:176-81.
- [216] Nuru ZY, Arendse CJ, Mongwaketsi N, Gohshal SK, Nkosi M, Maaza M. Effects of substrate temperatures on the thermal stability of $\text{Al}_x\text{O}_y/\text{Pt}/\text{Al}_x\text{O}_y$ multilayered selective solar absorber coatings. *Renewable Energy*. 2015;75:590-7.
- [217] Tsai TK, Hsueh SJ, Fang JS. Optical Properties of $\text{Al}_x\text{O}_y/\text{Ni}/\text{Al}_x\text{O}_y$ Multilayered Absorber Coatings Prepared by Reactive DC Magnetron Sputtering. *Journal of Electronic Materials*. 2014;43:229-35.
- [218] Tsai P-H, Chang-Liao K-S, Liu C-Y, Wang T-K, Tzeng PJ, Lin CH, et al. Novel SONOS-type nonvolatile memory device with optimal Al doping in HfAlO charge-trapping layer. *IEEE Electron Device Letters*. 2008;29:265-8.
- [219] Kingon AI, Maria J-P, Streiffer SK. Alternative dielectrics to silicon dioxide for memory and logic devices. *Nature*. 2000;406:1032-8.
- [220] Singh J, Wolfe DE, Miller RA, Eldridge JI, Zhu D-M. Tailored microstructure of zirconia and hafnia-based thermal barrier coatings with low thermal conductivity and high hemispherical reflectance by EB-PVD. *Journal of materials science*. 2004;39:1975-85.
- [221] Wang Y, Zhao Y, Shao J, Fan Z. Effect of native defects and laser-induced defects on multi-shot laser-induced damage in multilayer mirrors. *Chinese Optics Letters*. 2011;9:093102.

- 1 [222] Liu ZS, Tibuleac S, Shin D, Young PP, Magnusson R. High-efficiency guided-mode
2 resonance filter. *Optics letters*. 1998;23:1556-8.
- 3 [223] Vargas M, Murphy NR, Ramana CV. Structure and optical properties of
4 nanocrystalline hafnium oxide thin films. *Optical Materials*. 2014;37:621-8.
- 5 [224] Jena S, Tokas RB, Misal JS, Rao KD, Udupa DV, Thakur S, et al. Effect of O₂/Ar gas
6 flow ratio on the optical properties and mechanical stress of sputtered HfO₂ thin films. *Thin
7 Solid Films*. 2015;592:135-42.
- 8 [225] Jain RK, Gautam YK, Dave V, Chawla AK, Chandra R. A study on structural, optical
9 and hydrophobic properties of oblique angle sputter deposited HfO₂ films. *Applied Surface
10 Science*. 2013;283:332-8.
- 11 [226] Lin S-S, Li H-R. The optical properties of hydrophilic Hf-doped HfO₂ nanoceramic
12 films. *Ceramics International*. 2013;39:7677-83.
- 13 [227] Vlček J, Belosludtsev A, Rezek J, Houška J, Čapek J, Čerstvý R, et al. High-rate
14 reactive high-power impulse magnetron sputtering of hard and optically transparent HfO₂
15 films. *Surface and Coatings Technology*. 2016;290:58-64.
- 16 [228] Vargas M, Murphy NR, Ramana CV. Tailoring the index of refraction of
17 nanocrystalline hafnium oxide thin films. *Applied Physics Letters*. 2014;104:101907.
- 18 [229] Wang J, Li HP, Stevens R. Hafnia and hafnia-toughened ceramics. *Journal of materials
19 science*. 1992;27:5397-430.
- 20 [230] Liu W, Su X-p, Zhang S-y, Wang H-b, Hao P. Preparation and Properties of Hafnium
21 Oxide Protective Films on ZnS Substrates [J]. *Laser & Infrared*. 2007;8:021.
- 22 [231] Fadel M, Omer OA, Basily RR. A study of some optical properties of hafnium dioxide
23 (HfO₂) thin films and their applications. *Applied Physics A*. 1998;66:335-43.
- 24 [232] Torchio P, Gatto A, Alvisi M, Albrand G, Kaiser N, Amra C. High-reflectivity
25 HfO₂/SiO₂ ultraviolet mirrors. *Applied optics*. 2002;41:3256-61.
- 26 [233] Khoshman JM, Khan A, Kordesch ME. Amorphous hafnium oxide thin films for
27 antireflection optical coatings. *Surface and Coatings Technology*. 2008;202:2500-2.
- 28 [234] Al-Kuhaili MF. Optical properties of hafnium oxide thin films and their application in
29 energy-efficient windows. *Optical Materials*. 2004;27:383-7.
- 30 [235] Lesser M. Antireflection coatings for silicon charge-coupled devices. *Optical
31 Engineering*. 1987;26:269911-.
- 32 [236] Jain RK, Gautam YK, Dave V, Chawla AK, Chandra R. A study on structural, optical
33 and hydrophobic properties of oblique angle sputter deposited HfO₂ films. *Applied Surface
34 Science*. 2013;283:332-8.

- 1
2
3
4
5
6
7
8
9
10
11
12
13
14
15
16
17
18
19
20
21
22
23
24
25
26
27
28
29
30
31
32
33
34
35
36
37
38
39
40
41
42
43
44
45
46
47
48
49
50
51
52
53
54
55
56
57
58
59
60
61
62
63
64
65
- [237] Sai H, Matsui T, Saito K, Kondo M, Yoshida I. Photocurrent enhancement in thin- film silicon solar cells by combination of anti- reflective sub- wavelength structures and light- trapping textures. *Progress in Photovoltaics: Research and Applications*. 2015;23:1572-80.
- [238] Ferry VE, Sweatlock LA, Pacifici D, Atwater HA. Plasmonic nanostructure design for efficient light coupling into solar cells. *Nano letters*. 2008;8:4391-7.
- [239] Collin S, Pardo F, Teissier R, Pelouard J-L. Efficient light absorption in metal– semiconductor–metal nanostructures. *Applied physics letters*. 2004;85:194-6.
- [240] Brongersma ML, Cui Y, Fan S. Light management for photovoltaics using high-index nanostructures. *Nature materials*. 2014;13:451-60.
- [241] Grandidier J, Weitekamp RA, Deceglie MG, Callahan DM, Battaglia C, Bukowsky CR, et al. Solar cell efficiency enhancement via light trapping in printable resonant dielectric nanosphere arrays. *physica status solidi (a)*. 2013;210:255-60.
- [242] Lee Y-J, Ruby DS, Peters DW, McKenzie BB, Hsu JWP. ZnO nanostructures as efficient antireflection layers in solar cells. *Nano letters*. 2008;8:1501-5.
- [243] Sibin KP, John S, Barshilia HC. Control of thermal emittance of stainless steel using sputtered tungsten thin films for solar thermal power applications. *Solar energy materials and solar cells*. 2015;133:1-7.
- [244] Yin Y, Hang L, Zhang S, Bui XL. Thermal oxidation properties of titanium nitride and titanium–aluminum nitride materials—A perspective for high temperature air-stable solar selective absorber applications. *Thin Solid Films*. 2007;515:2829-32.
- [245] Roos A, Georgson M. Tin-oxide-coated anodized aluminium selective absorber surfaces II. Aging and durability. *Solar energy materials*. 1991;22:29-41.
- [246] Branker K, Pathak MJM, Pearce JM. A review of solar photovoltaic levelized cost of electricity. *Renewable and Sustainable Energy Reviews*. 2011;15:4470-82.
- [247] Wäckelgård E, Hultmark G. Industrially sputtered solar absorber surface. *Solar Energy Materials and Solar Cells*. 1998;54:165-70.
- [248] Vince J, Vuk AŠ, Krašovec UO, Orel B, Köhl M, Heck M. Solar absorber coatings based on CoCuMnO_x spinels prepared via the sol–gel process: structural and optical properties. *Solar Energy Materials and Solar Cells*. 2003;79:313-30.

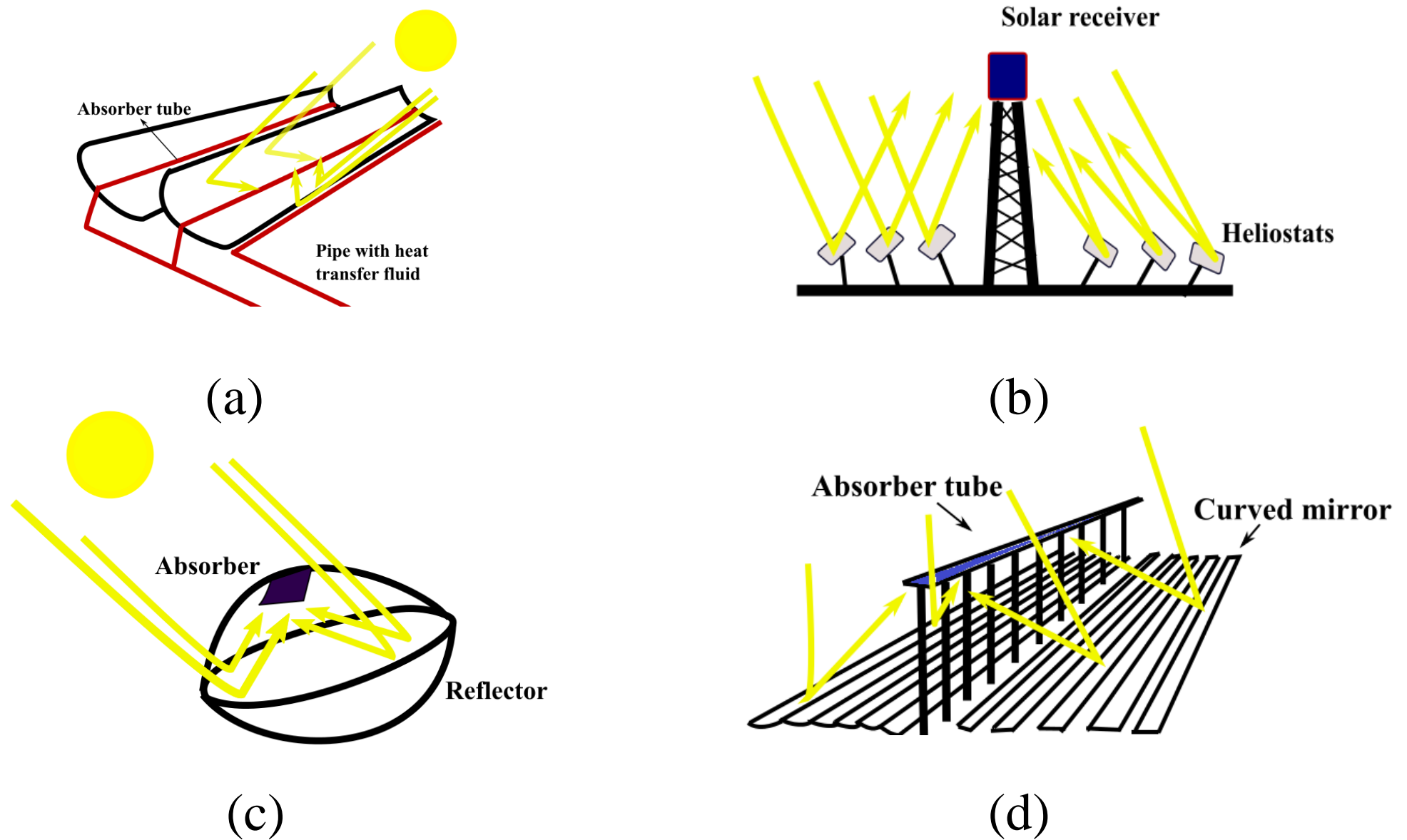


Fig. 1. Schematic of four CSP systems (a) parabolic trough collector (b) solar tower (c) parabolic dish concentrator and (d) linear Fresnel reflector [23, 24]

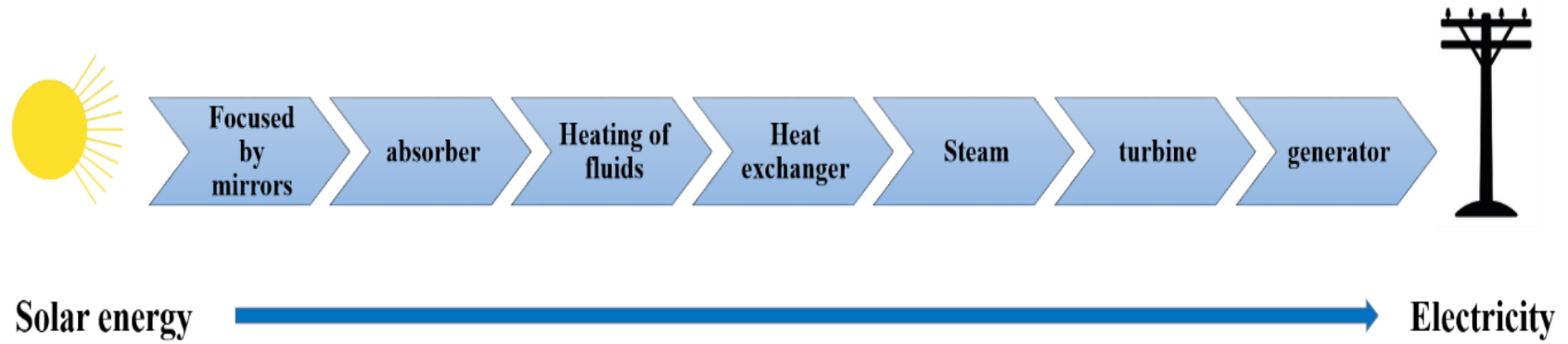


Fig 2. Schematic of the mechanism to produce electricity from solar energy in CSP systems.

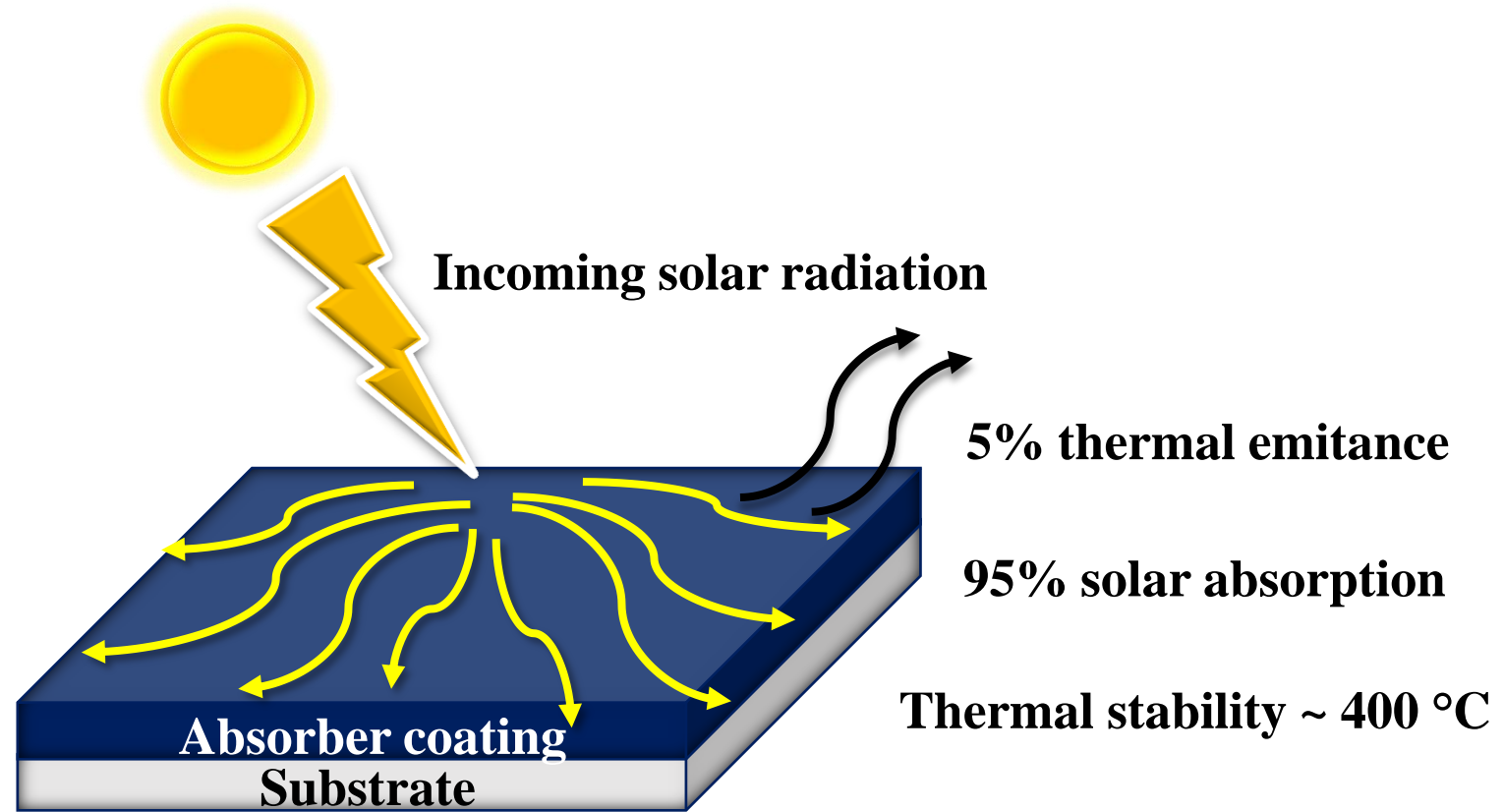


Fig 3. Schematic of an ideal solar selective absorber

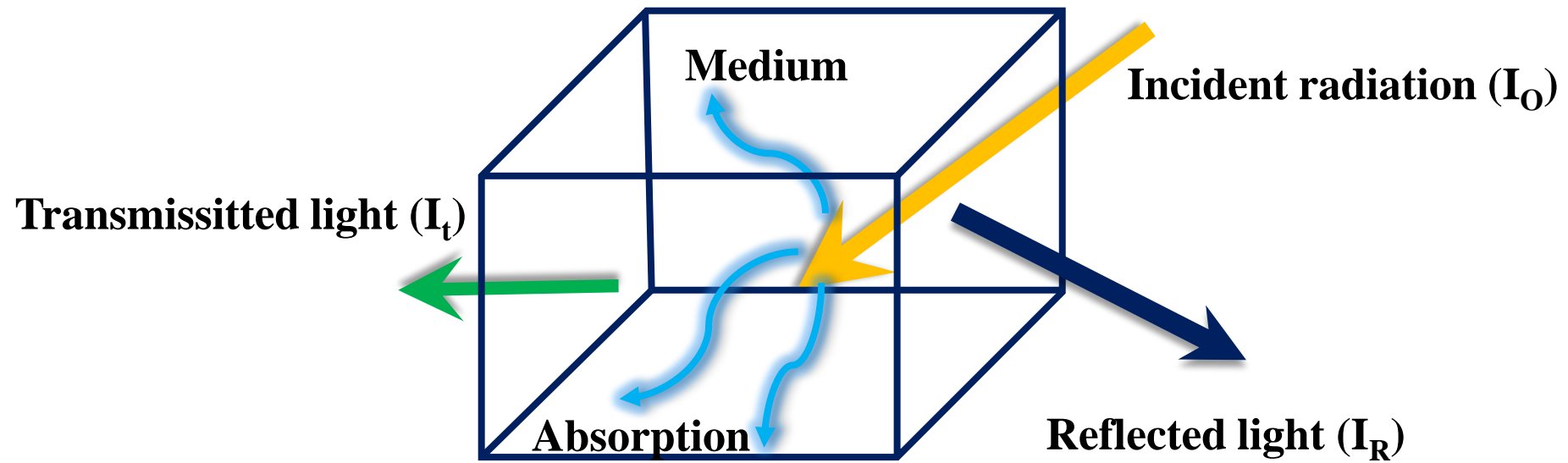


Fig 4. Interaction of electromagnetic radiation with matter

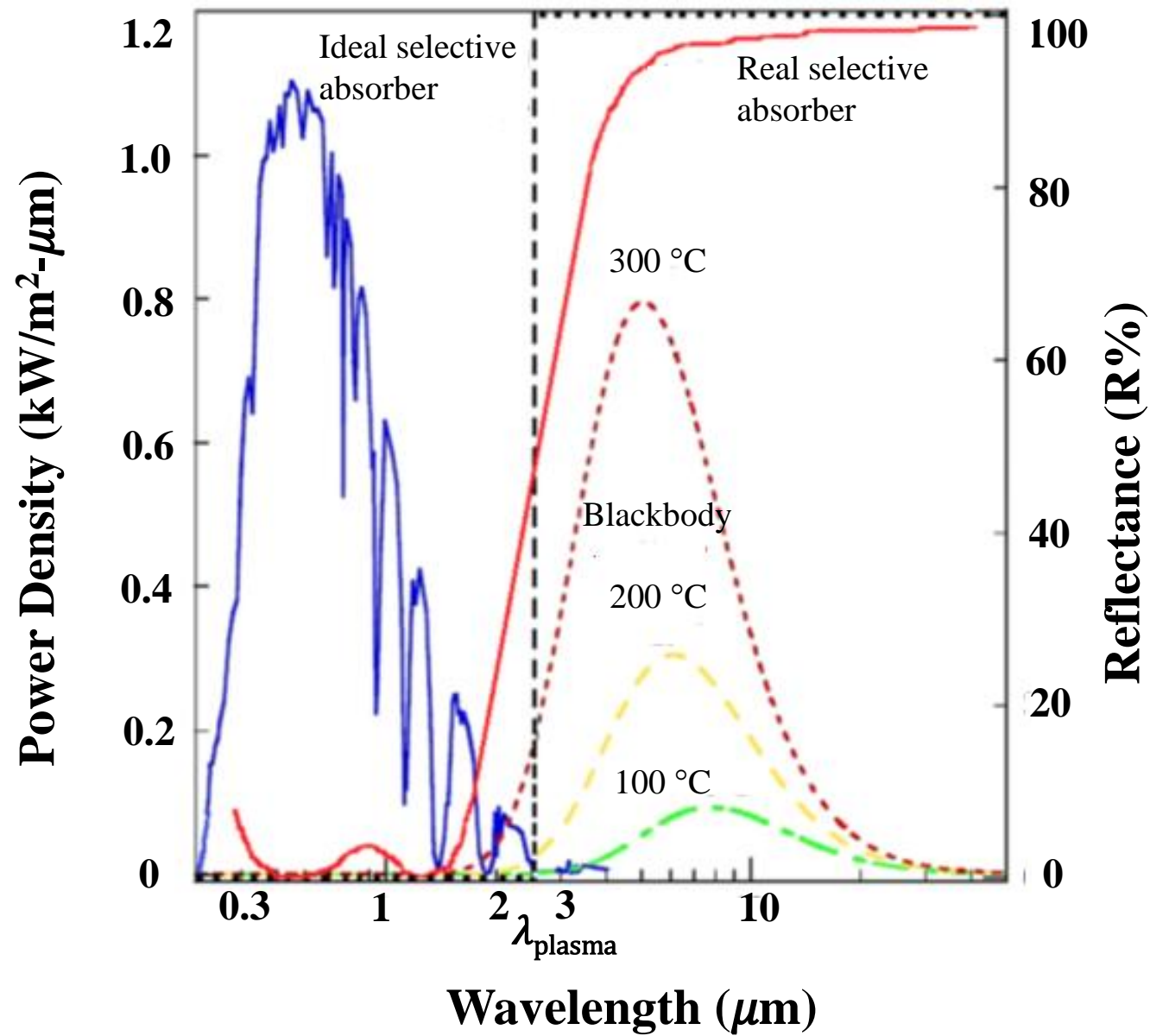


Fig. 5. The solar spectrum (blue); the blackbody radiation at 100, 200 and 300 °C (green, yellow, maroon, respectively); The reflectance spectrum of an ideal (black) and real (red) solar selective absorbers [46].

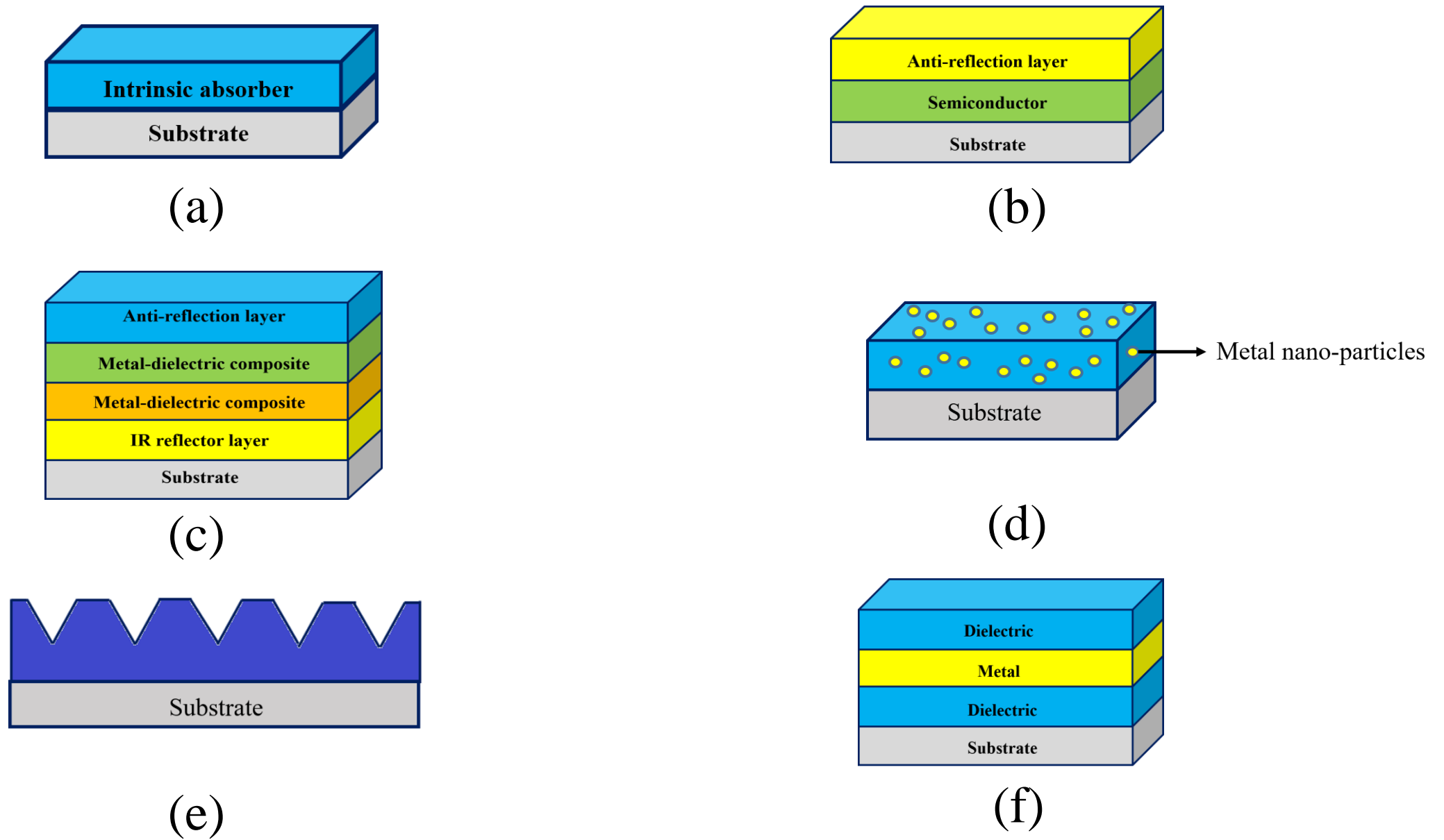


Fig. 6. Different types of solar selective absorber coatings; (a) Intrinsic absorber, (b) Semiconductor absorber, (c) Multilayer absorber, (d) Cermet absorber (e) Textured surface (f) Dielectric – metal – dielectric –based absorber [42].

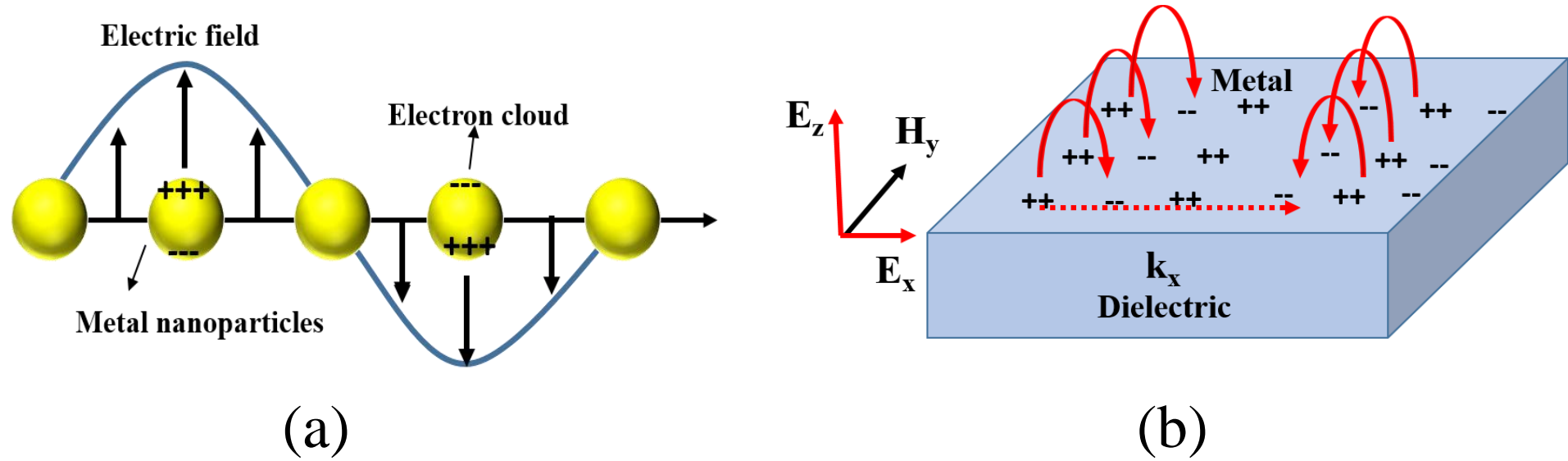


Fig. 7: (a) Formation of localised surface plasmons (LSPs); (b) The propagation of surface plasmon polaritons (SPPs) in metal-dielectric interface in response to electro-magnetic field.

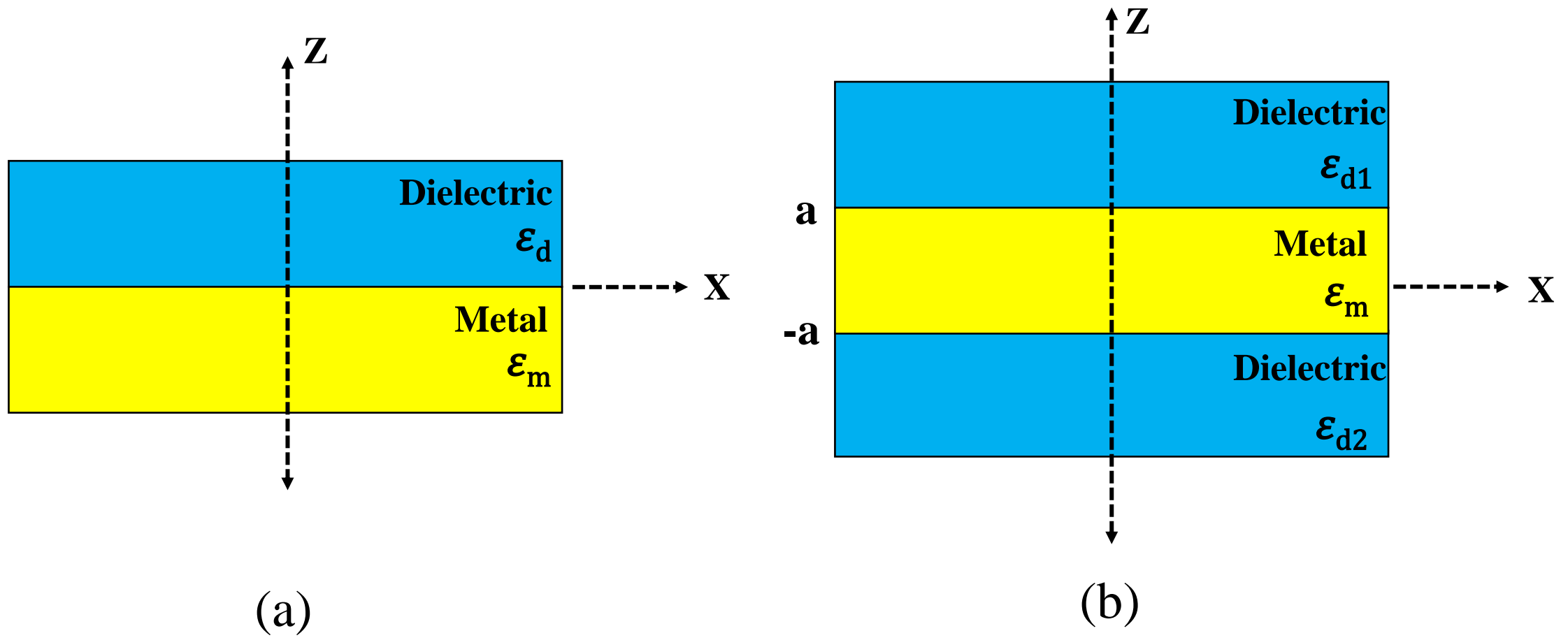
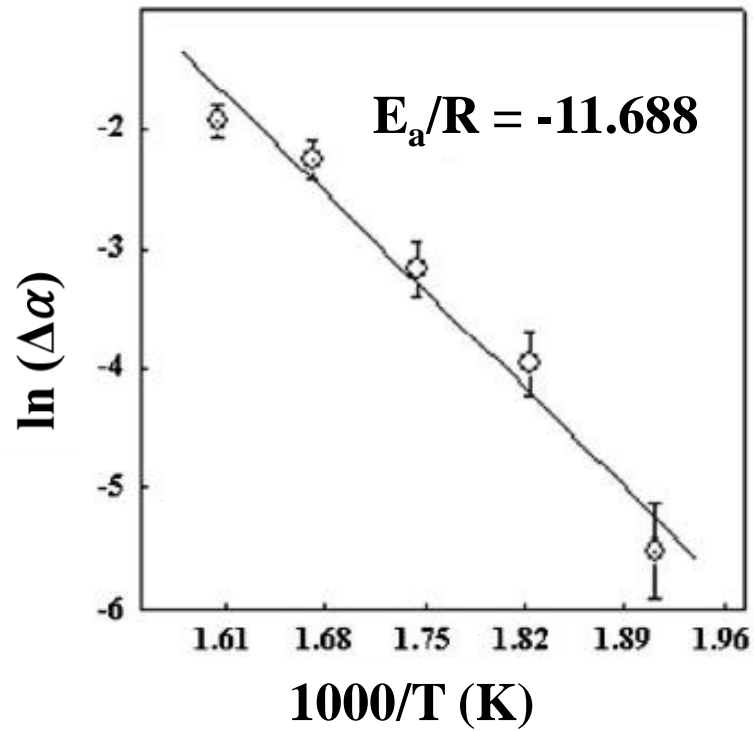
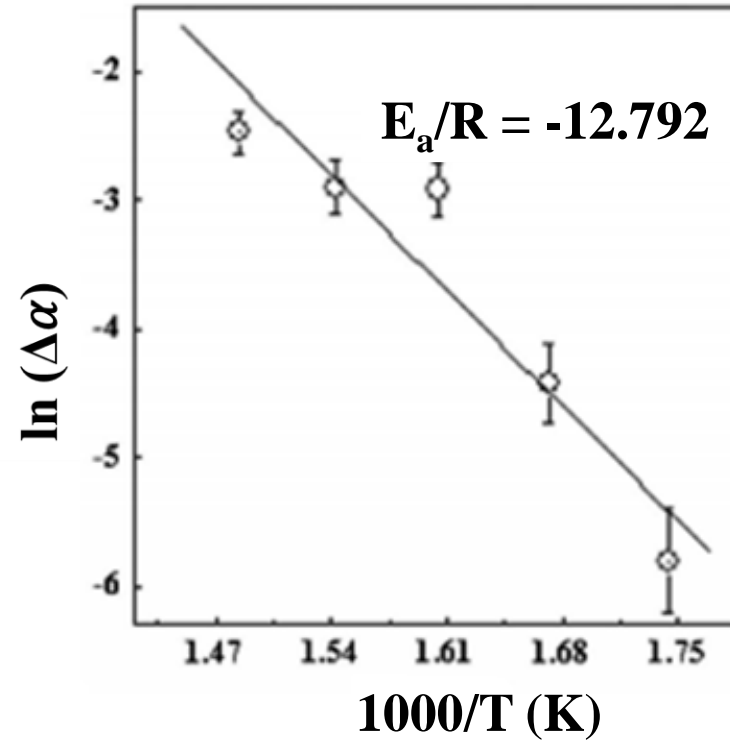


Fig. 8: Schematic of the (a) metal-dielectric and (b) dielectric-metal-dielectric structures for SPP propagation.

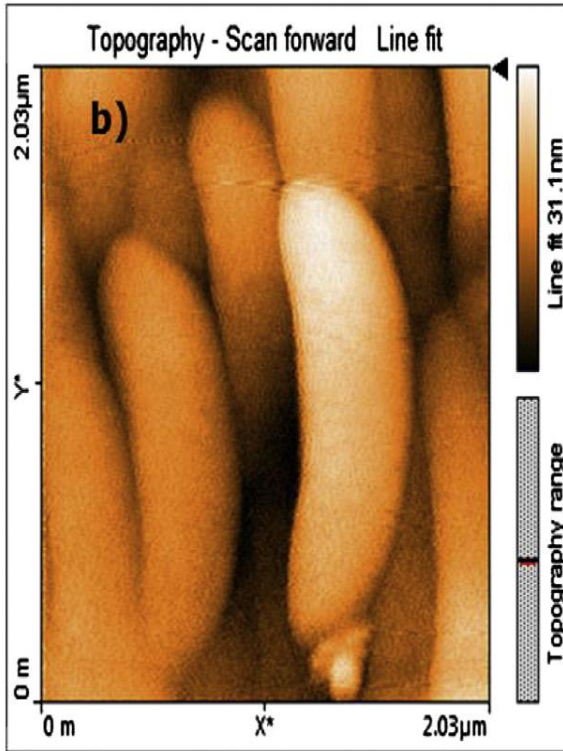


(a)

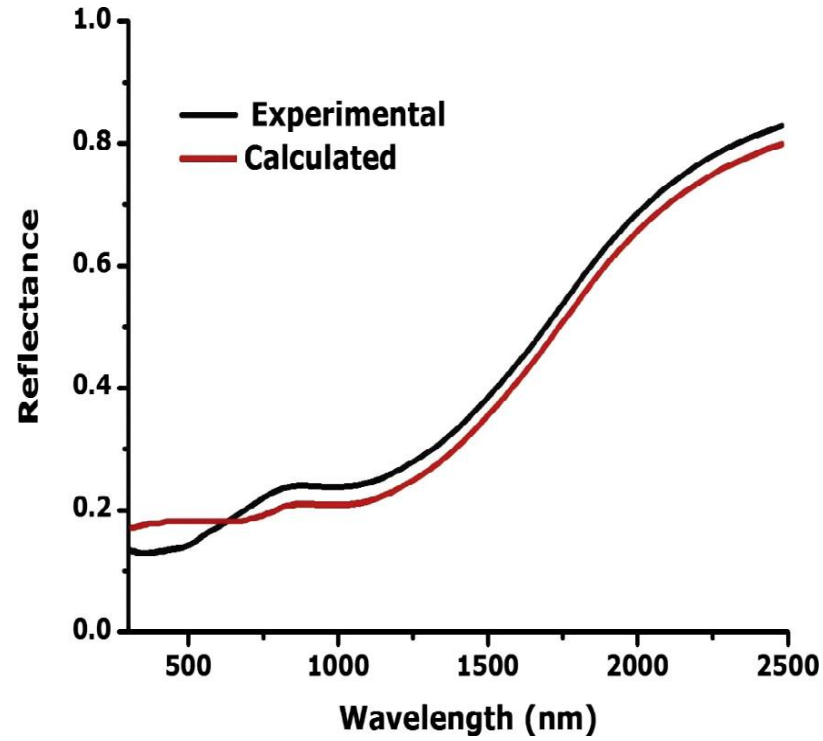


(b)

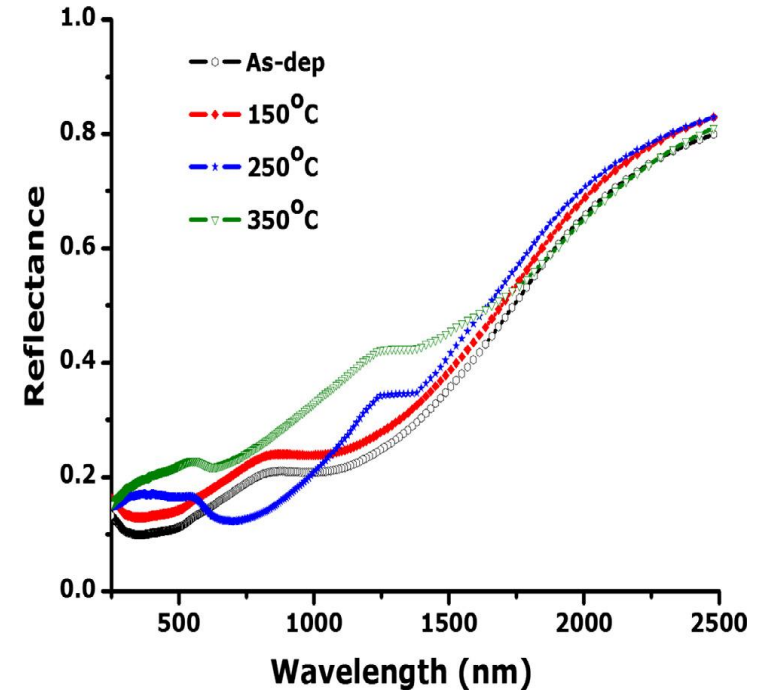
Fig. 9. The Arrhenius plot for $\text{Cr}_x\text{O}_y/\text{Cr}/\text{Cr}_2\text{O}_3$ coatings (a) longer duration (b) 2 hrs [152].



(a)



(b)



(c)

Fig. 10. (a) AFM images (b) Experimental and calculated reflectance spectra and (c) thermal stability of MgO/Zr/MgO coating [199, 200].

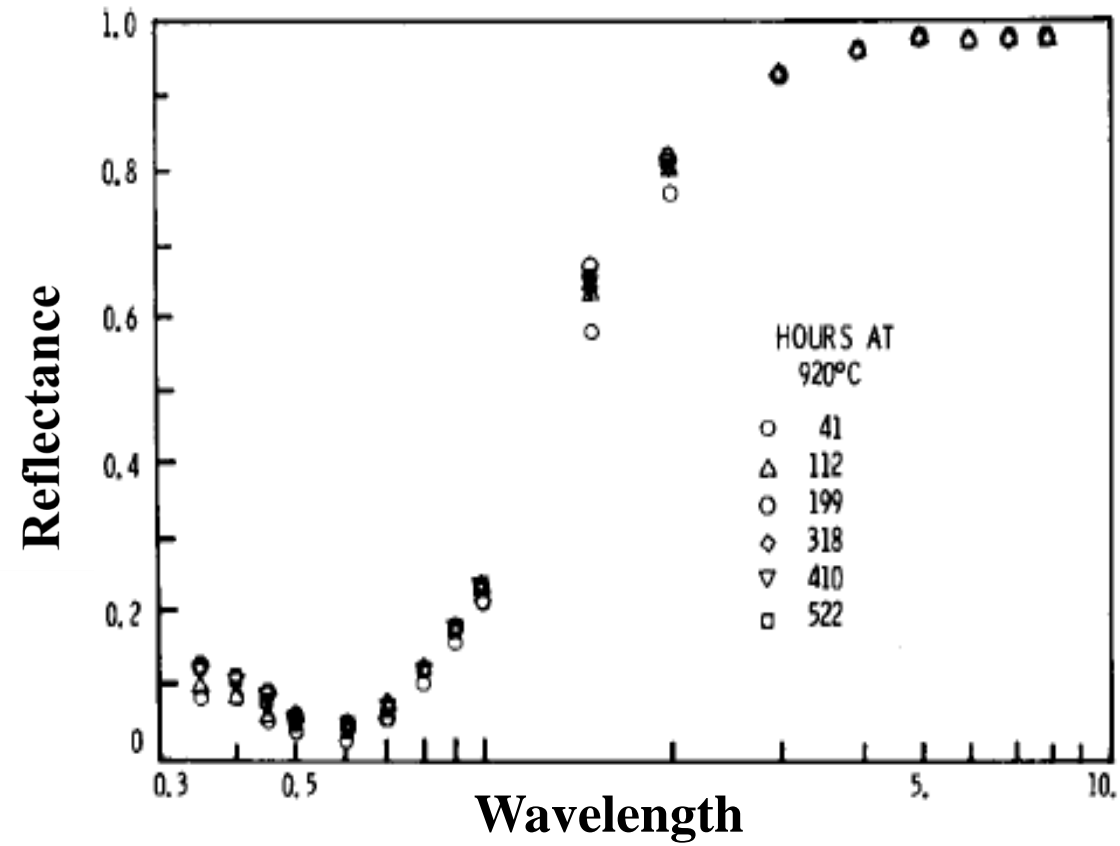
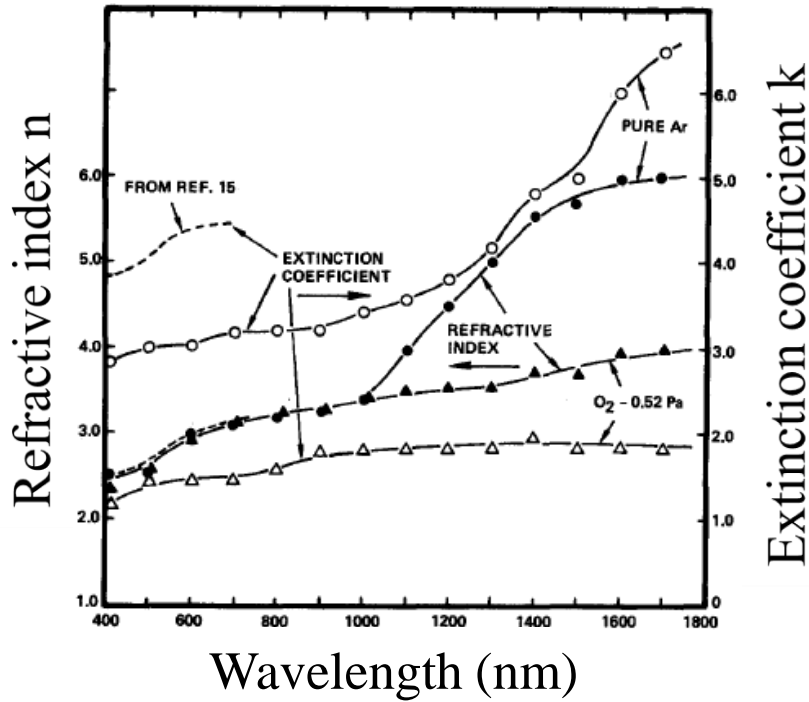
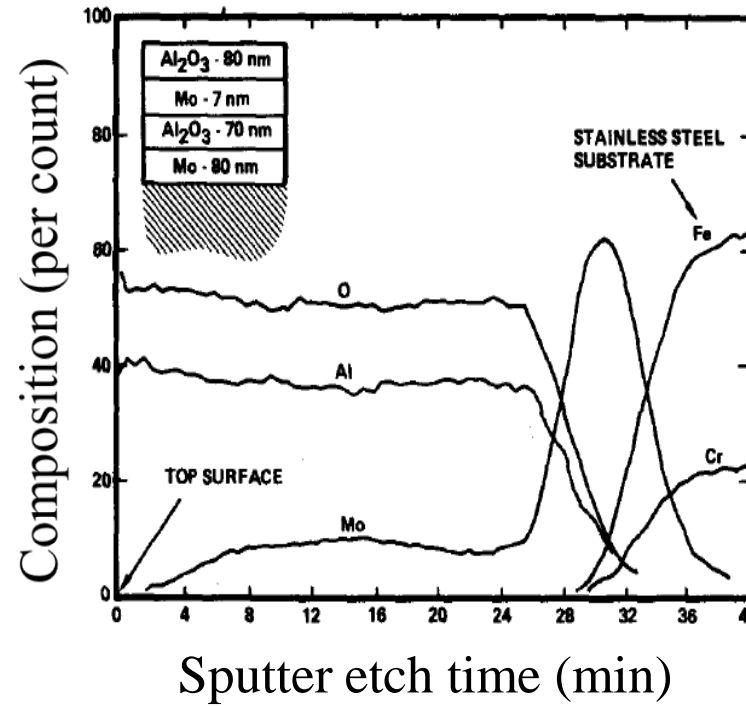


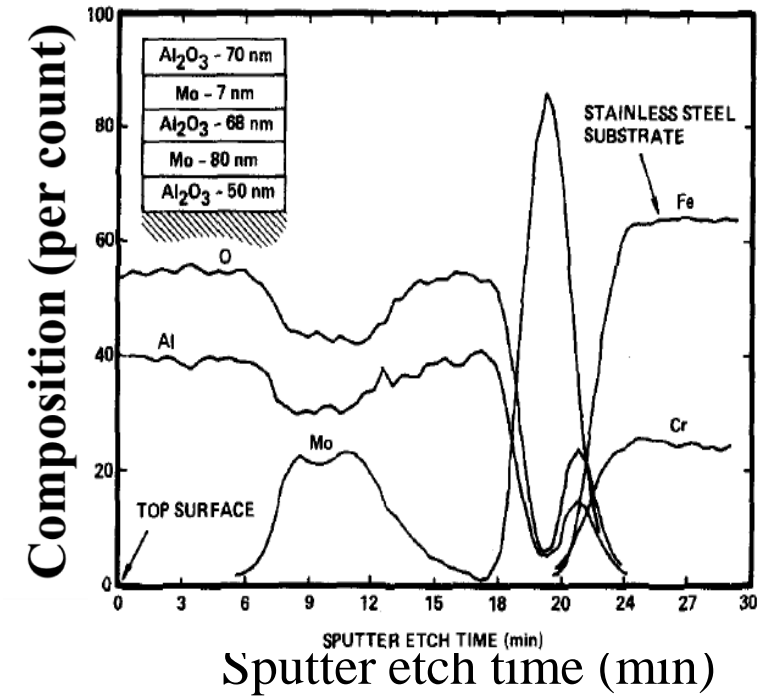
Fig. 11. Spectra reflectance of $\text{Al}_2\text{O}_3/\text{Mo}/\text{Al}_2\text{O}_3$ coating after long term annealing at 920°C [207].



(a)

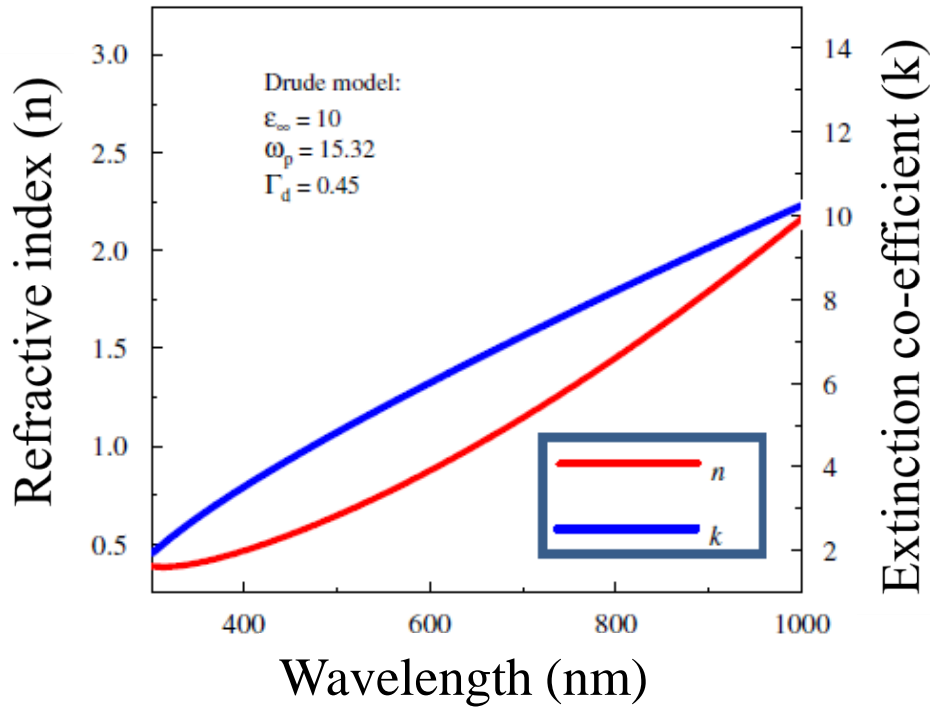


(b)

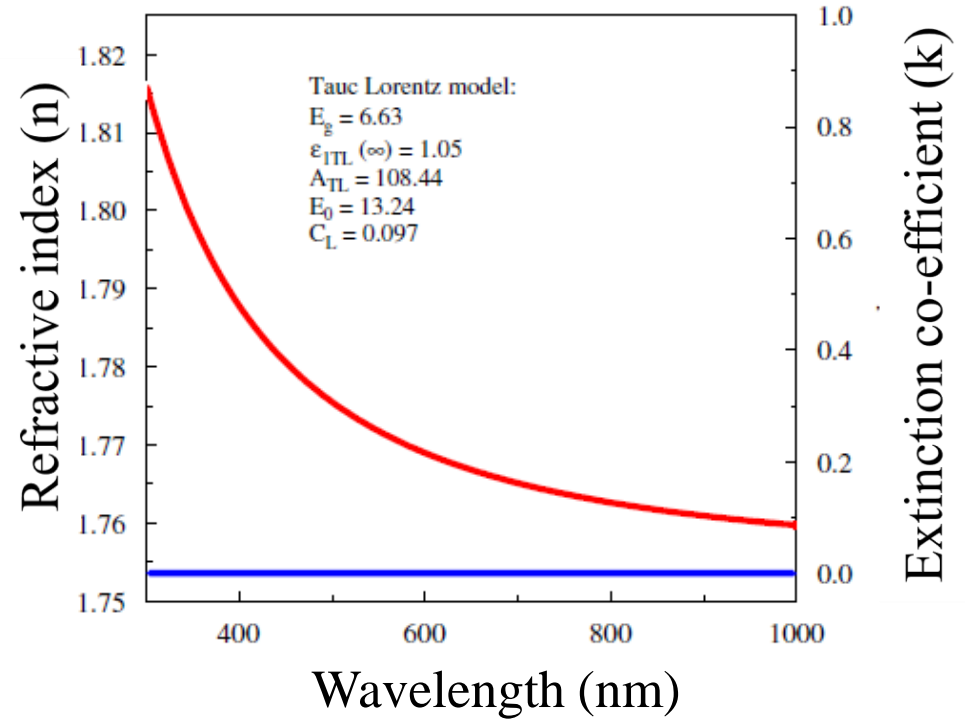


(c)

Fig. 12. The wavelength dependence of refractive index and extinction coefficient of Mo films, sputtered in pure Ar and in an Ar + O₂ mixture; Auger depth profile-composition analysis of heat-treated Al₂O₃/Mo/Al₂O₃ coating in vacuum, deposited on Mo coated stainless steel substrate a) Al₂O₃ layer deposited by reactive sputtering; (b) Al₂O₃ layer deposited by r.f sputtering of alumina [208].



(a)



(b)

Fig. 13. Dependence of experimentally determined n and k values with respect to wavelength for (a) Al_xO_y (layers 1 and 3) (b) Al layer in $Al_xO_y/Al/Al_xO_y$ absorber coating deposited on Cu substrate [149]

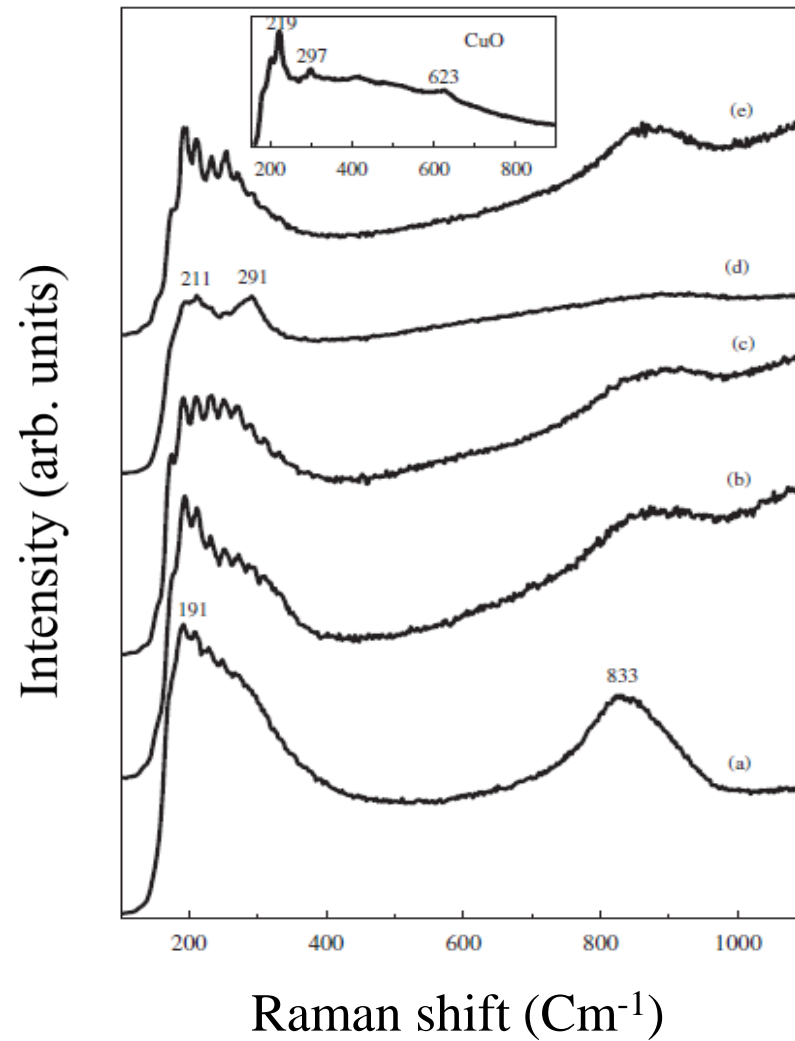


Fig. 14. Raman spectra of (a) as-deposited and heat treated absorbers annealed in air at (b) 250 °C, (c) 350 °C, (d) 450 °C and (e) 500 °C for 2h in vacuum. The Raman spectrum of CuO has been represented in the inset [149].

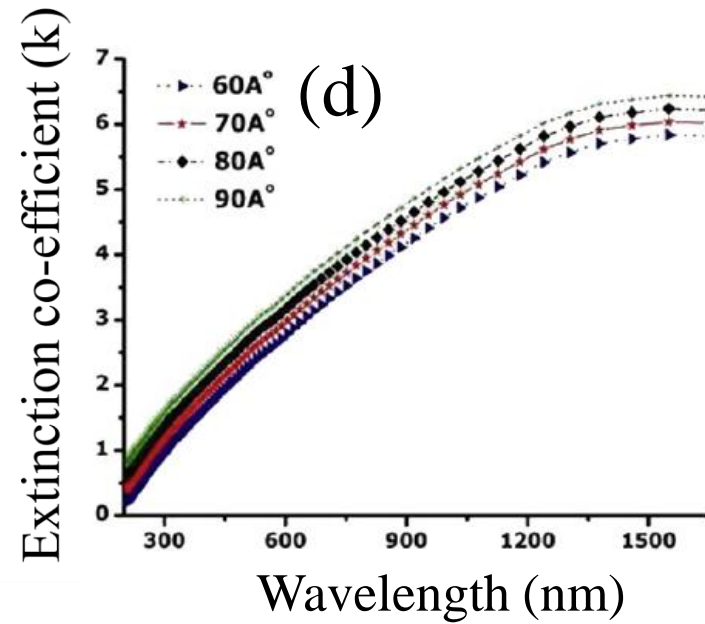
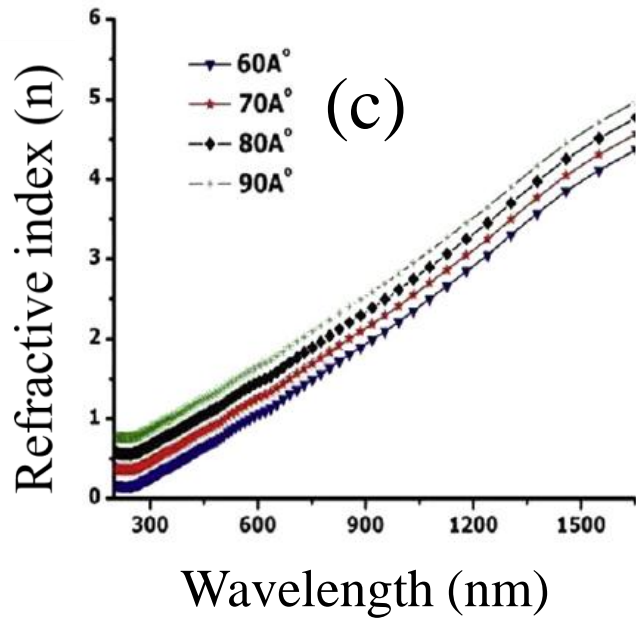
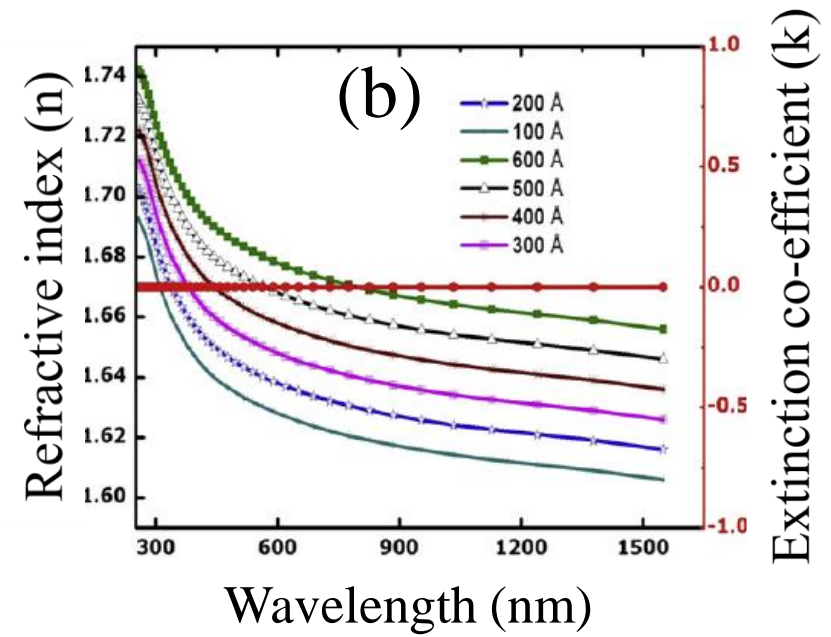
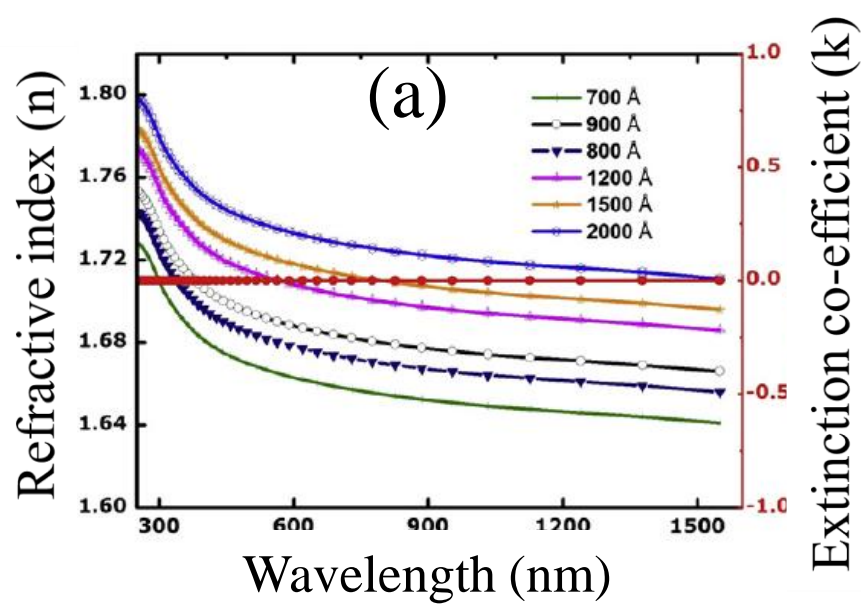
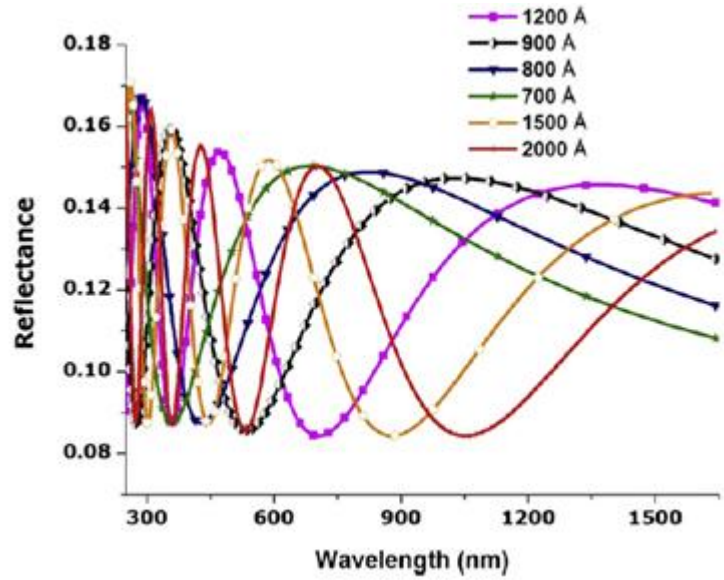
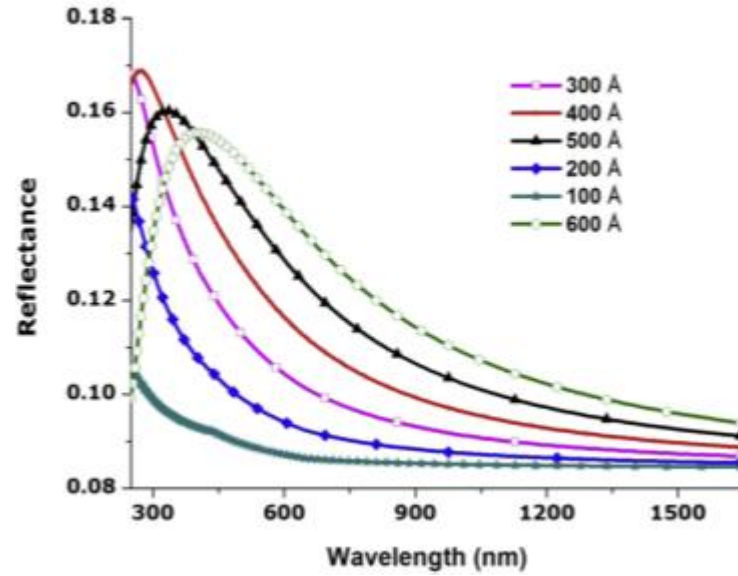


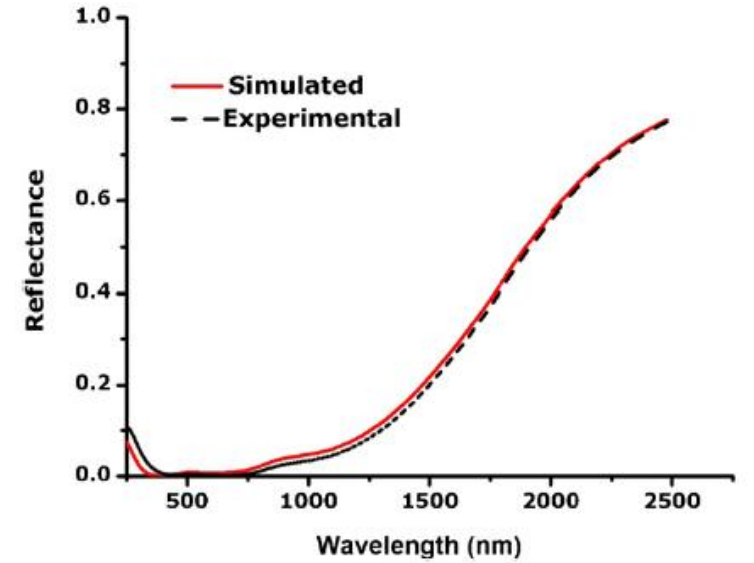
Fig. 15. The variation of optical constants as a function of wavelength in difference thickness of (a) top Al_xO_y layer, (b) base Al_xO_y layer (c) & (d) [212].



(a)



(b)



(c)

Fig. 16. The thickness dependence of reflectance spectra (a) top Al_xO_y layer (b) base Al_xO_y layer and (c) simulated and experimental spectra of $\text{Al}_x\text{O}_y/\text{Pt}/\text{Al}_x\text{O}_y$ absorber coating [212].

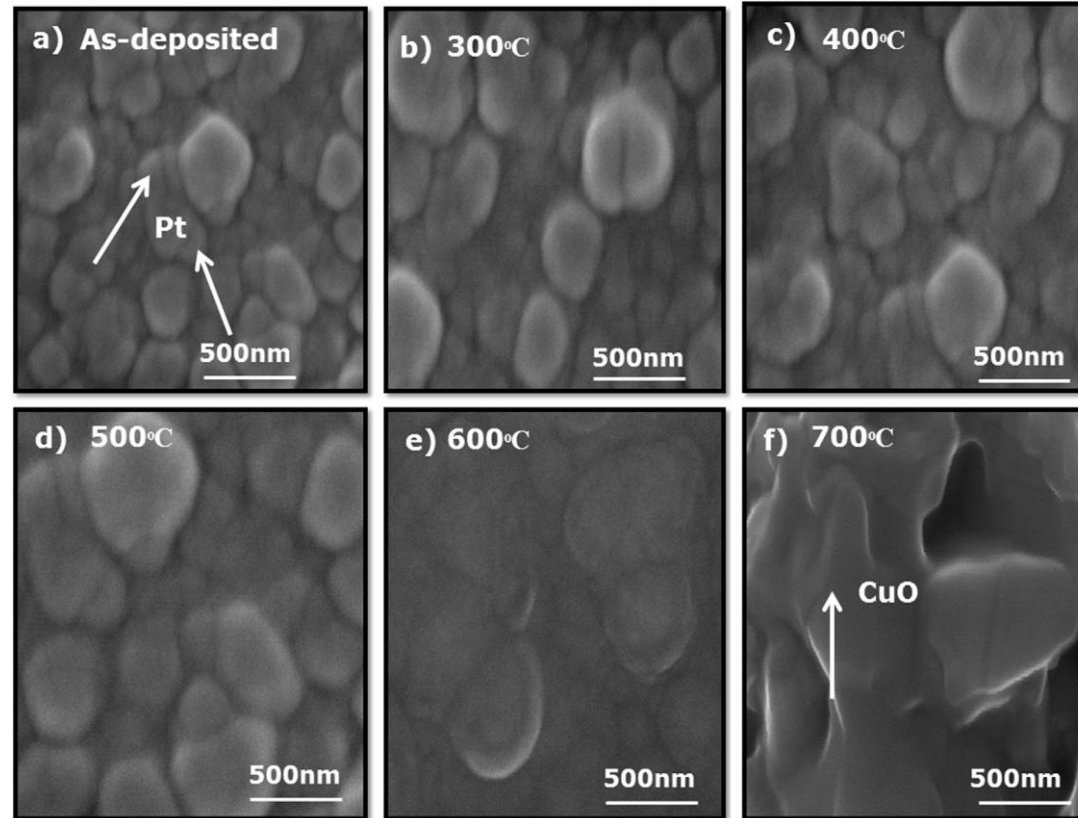
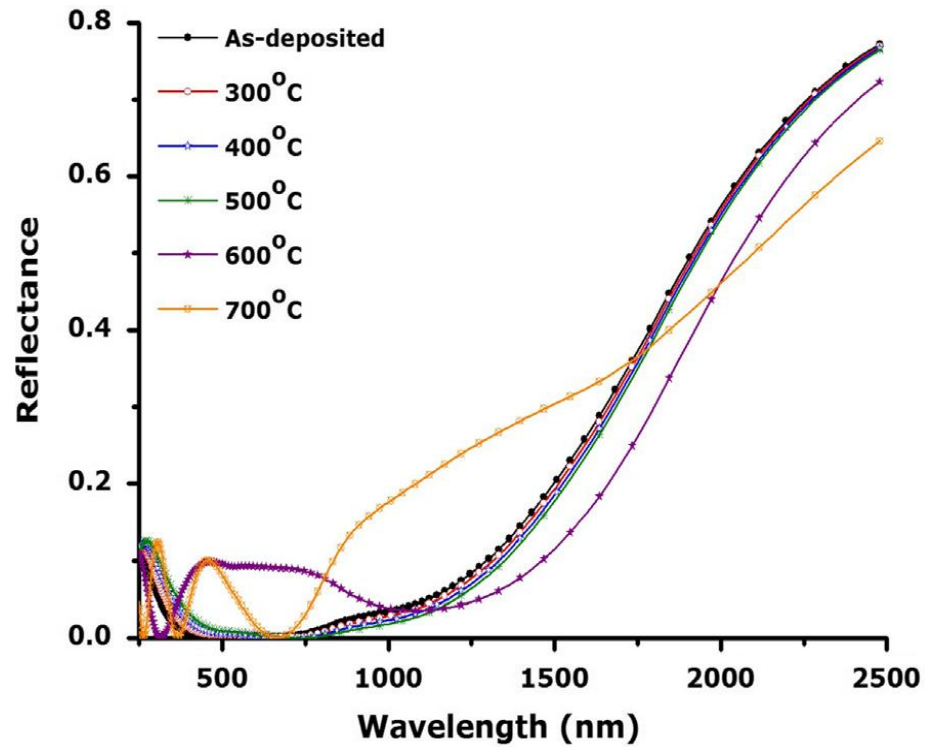
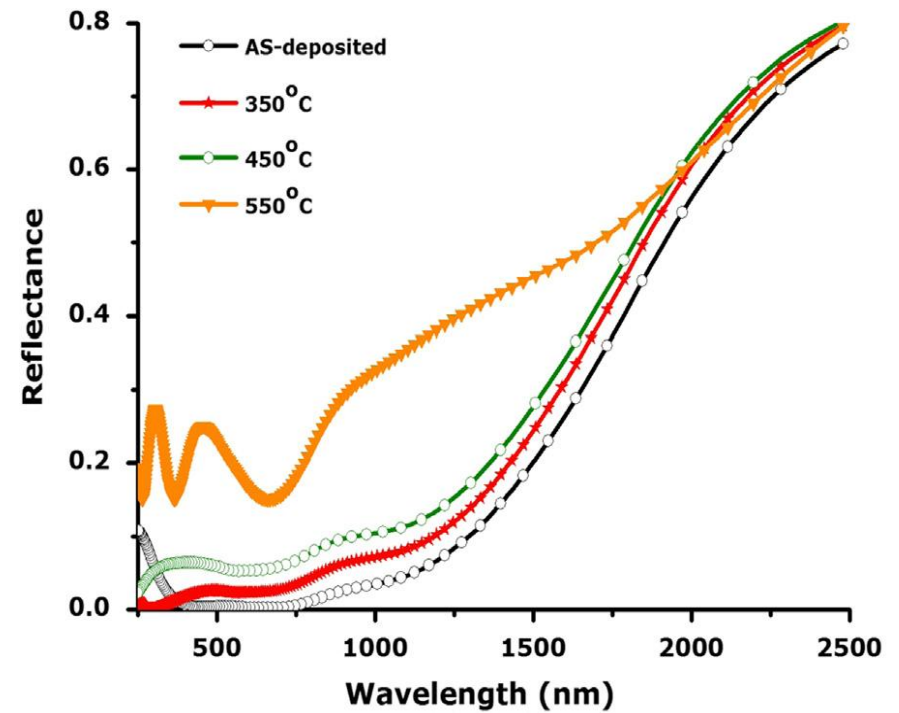


Fig. 17. SEM images of as deposited (a) and heat treated coatings in air at (b) 300 °C (c) 400 °C (d) 500 °C (e) 600 °C and (f) 700 °C of $\text{Al}_x\text{O}_y/\text{Pt}/\text{Al}_x\text{O}_y$ coating on Cu substrates [214].



(a)



(b)

Fig. 18. Thermal stability study of $\text{Al}_x\text{O}_y/\text{Pt}/\text{Al}_x\text{O}_y$ in different temperatures in air for (a) 2 hrs and (b) 24 hrs [214].

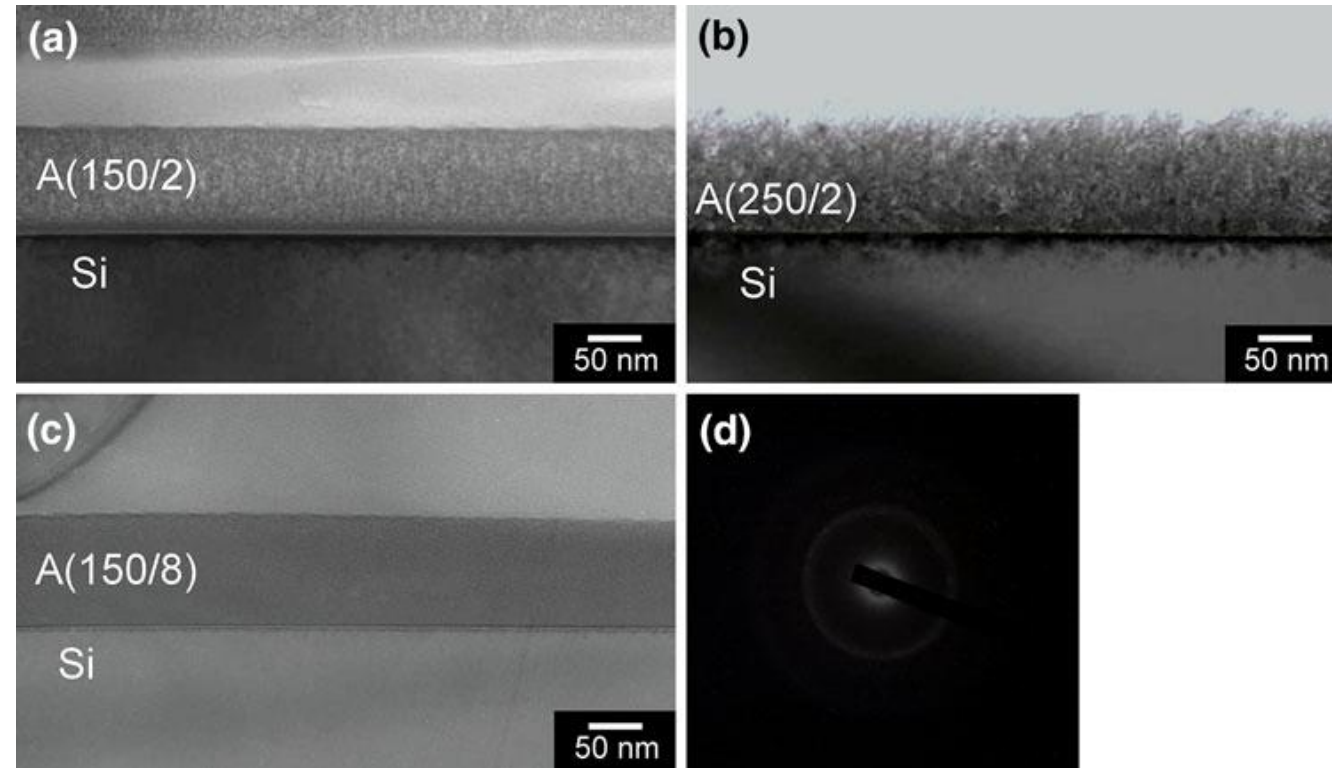


Fig. 19. TEM cross-sectional images of as-deposited coating (a) A(150/2), (b) A (250/2) and (c) A (150/8) (c) films; (d) diffraction pattern of as-deposited A(150/2) [217].

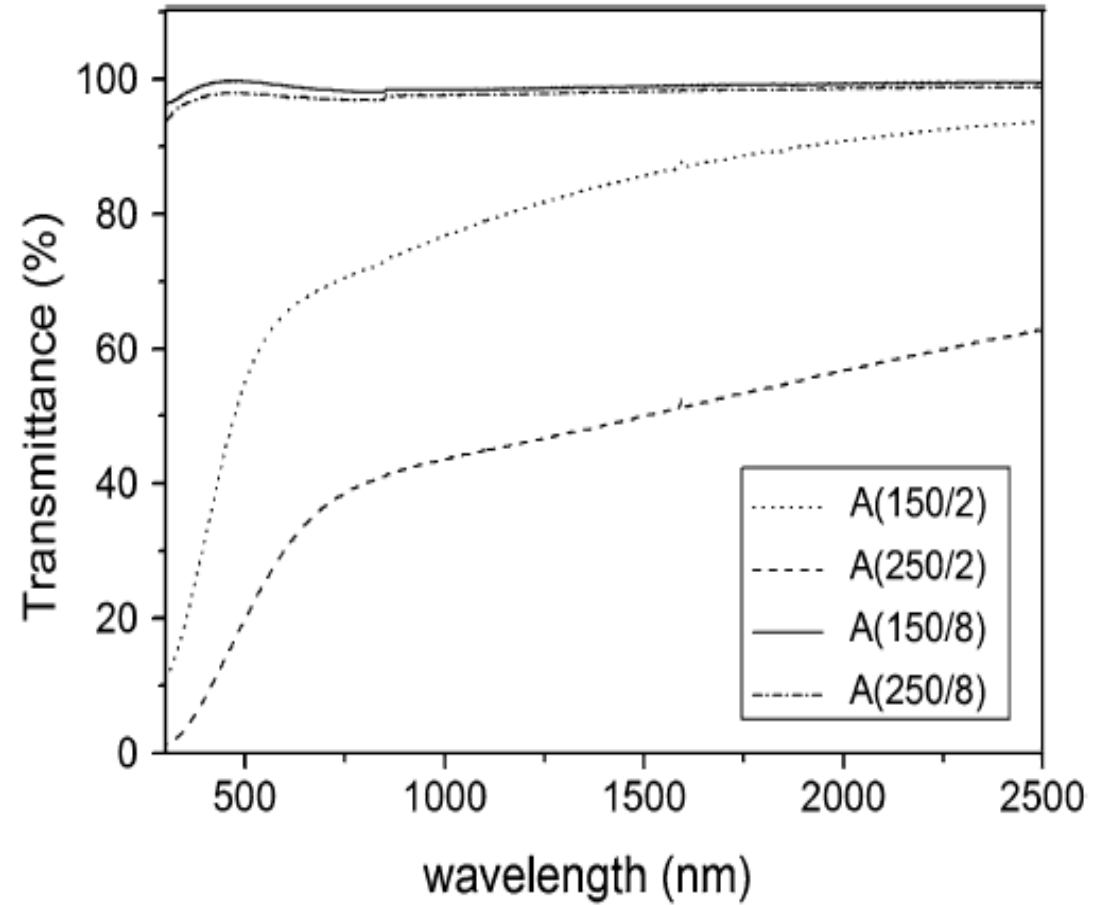


Fig. 20. Transmittance spectra of Al_xO_y in different deposition conditions [217].

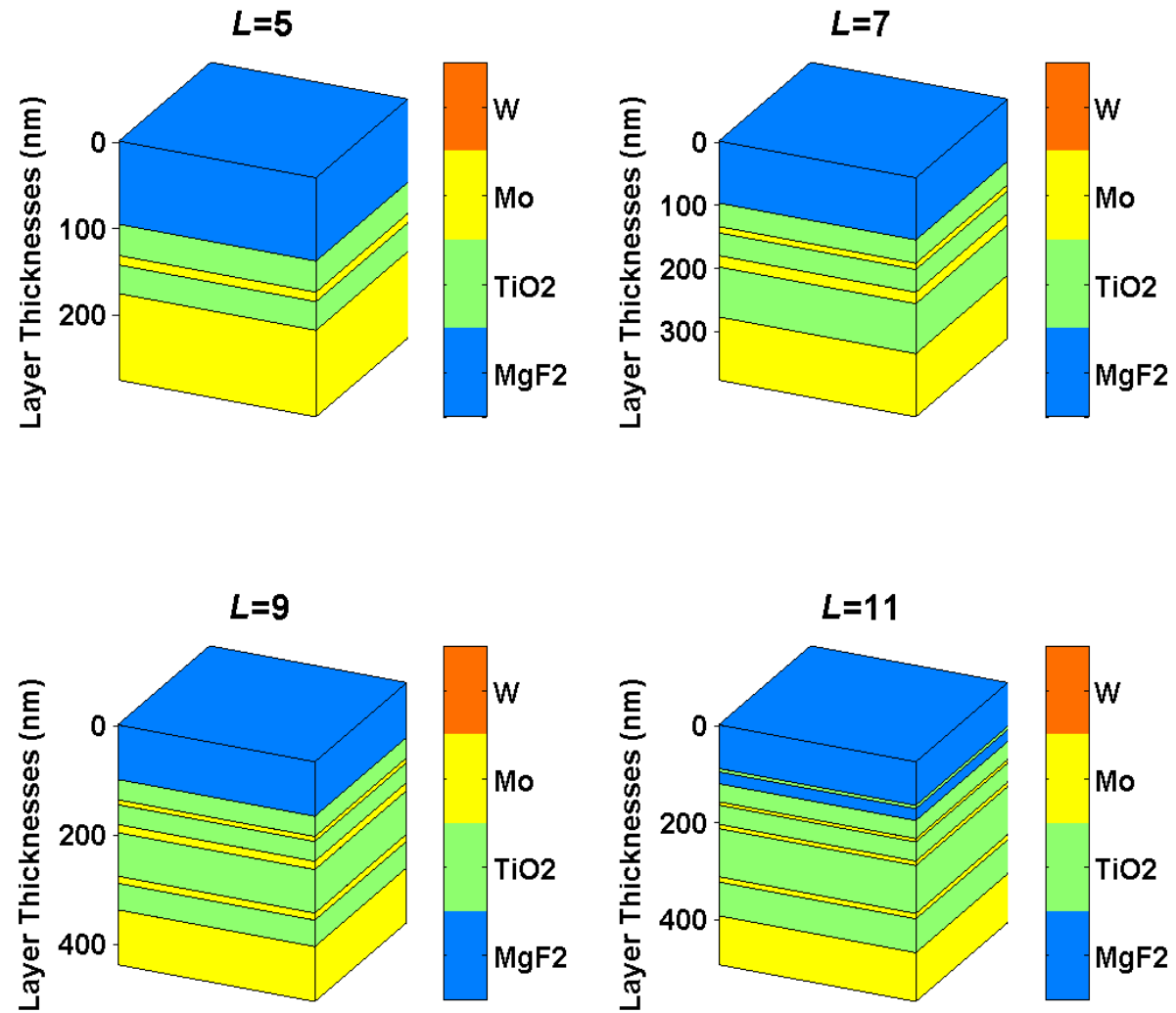


Fig. 21. Schematic of DMD coatings with Mo, MgF₂ and TiO₂ layers. Optimized stacks with no of layers $L = 5, 7, 9$ and 11 are shown [53].

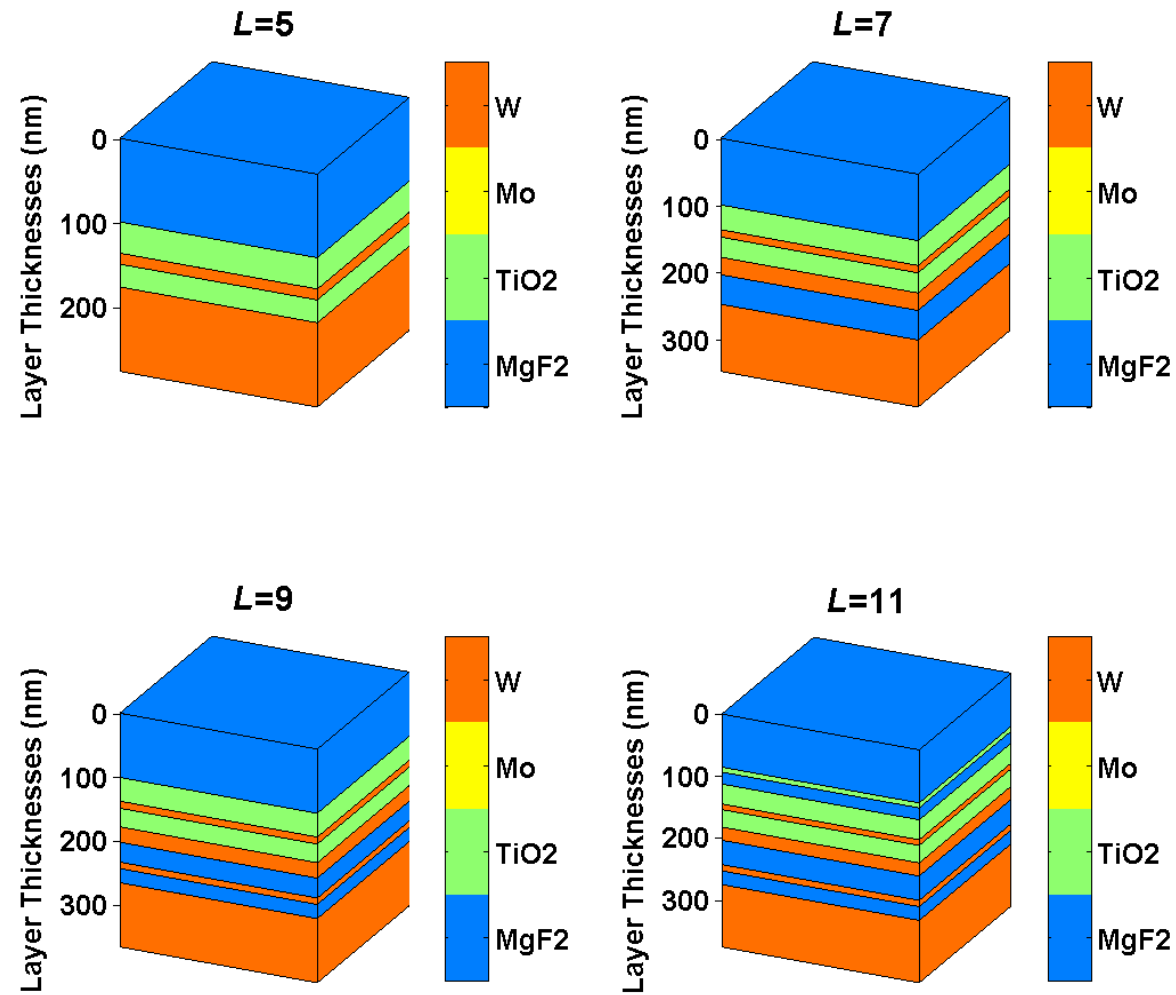
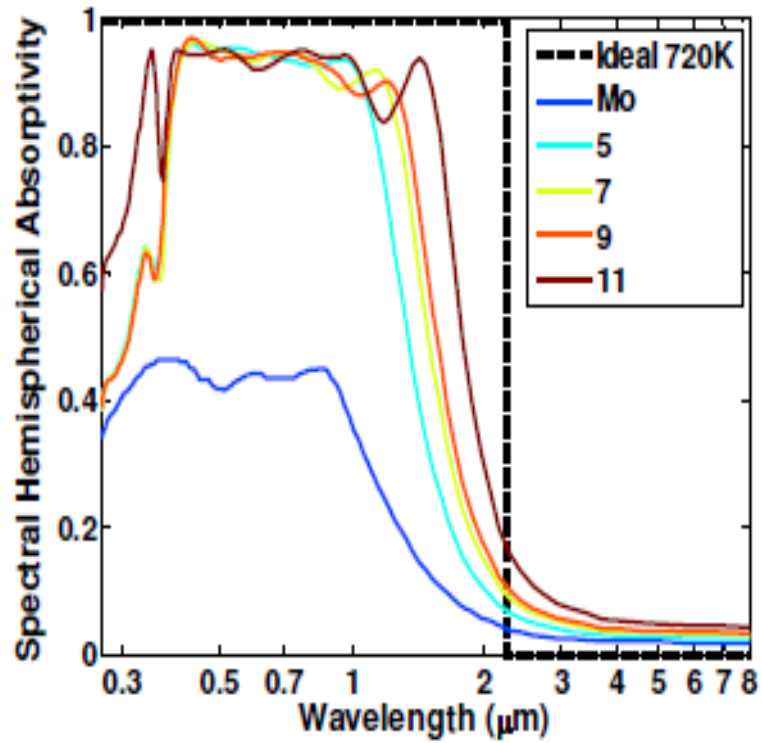
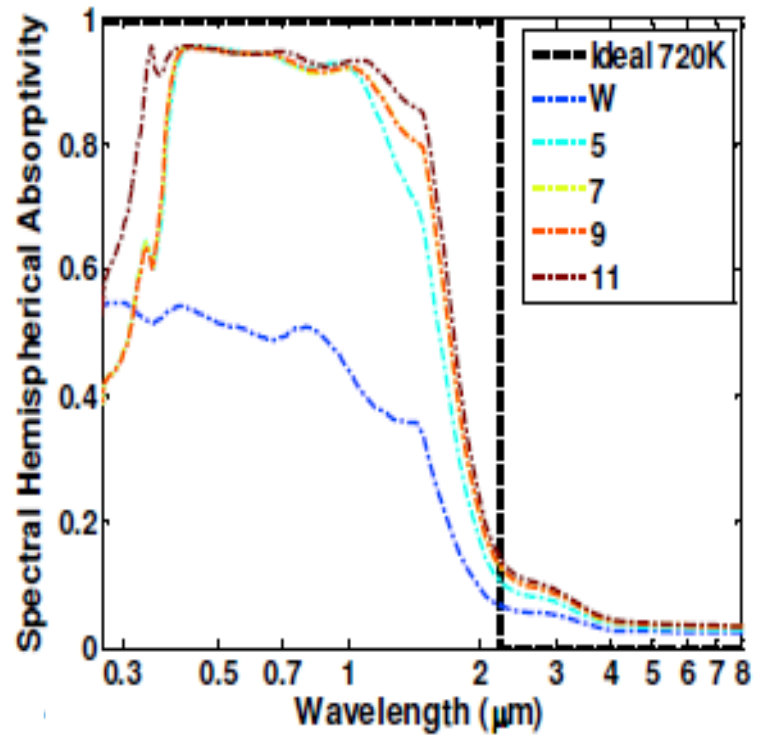


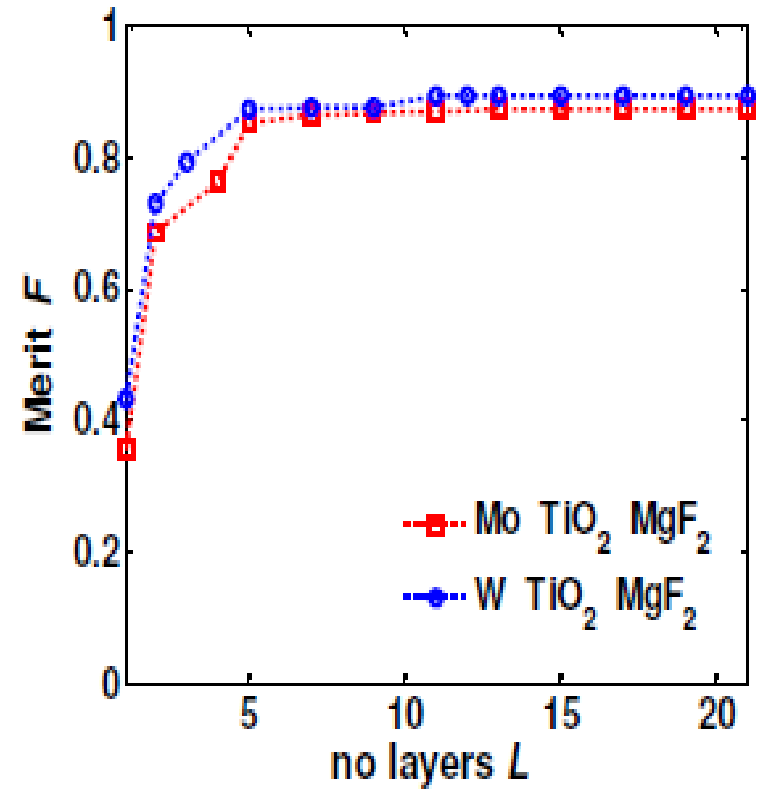
Fig. 22. Schematic of DMD coatings with W, MgF₂ and TiO₂ layers. Optimized stacks with no of layers $L = 5, 7, 9$ and 11 are shown [53].



(a)



(b)



(c)

Fig. 23. Absorption spectra of the metal-dielectric stack composed of (a) Mo, TiO_2 and MgF_2 (b) W, TiO_2 and MgF_2 . The spectra selectivity of ideal selective absorber at 720 K has also been plotted as reference (c) The variation of merit function of the metal-dielectric stack using Mo, TiO_2 , MgF_2 and W, TiO_2 , MgF_2 . The substrate (Mo or W) has been considered as $L = 1$ [53].

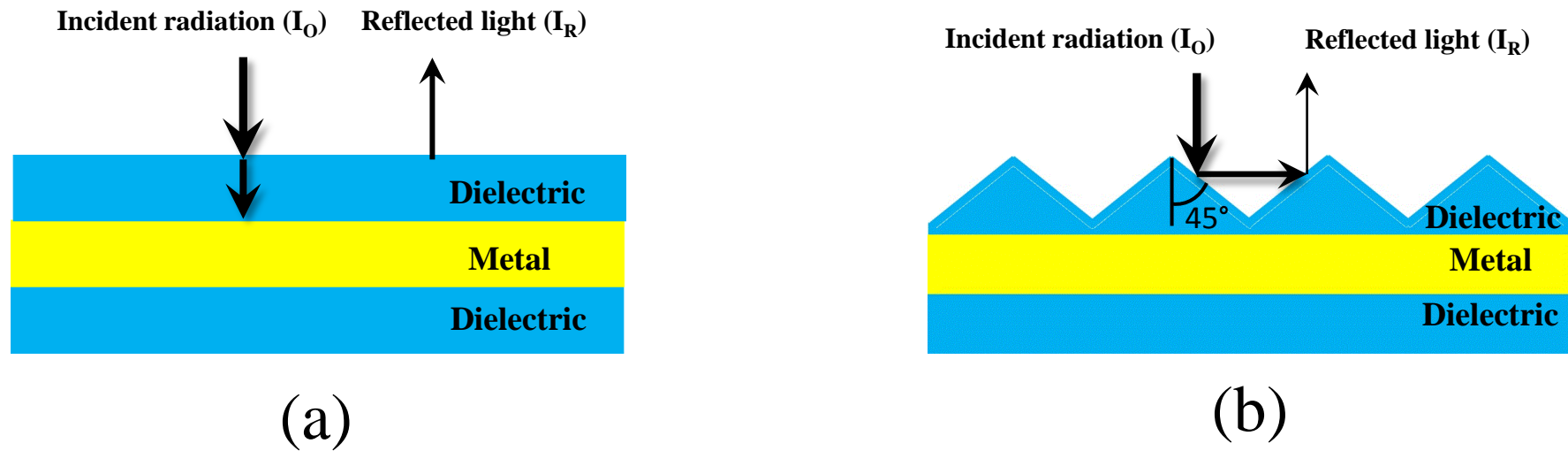


Fig. 24. The interaction of light with (a) flat and (b) textured DMD coatings [237].